INFLUENCE OF RADIOACTIVITY ON PARTICLE-SURFACE INTERACTIONS

A Dissertation
Presented to
The Academic Faculty

by

Yong-ha Kim

In Partial Fulfillment
of the Requirements for the Degree
Doctor of Philosophy in the
School of Civil and Environmental Engineering

Georgia Institute of Technology
May 2016

INFLUENCE OF RADIOACTIVITY ON PARTICLE-SURFACE INTERACTIONS

Approved by:

Dr. Sotira Yiacoumi, Advisor
School of Civil and Environmental Engineering
Georgia Institute of Technology

Dr. Ching-Hua Huang
School of Civil and Environmental Engineering
Georgia Institute of Technology

Dr. Costas Tsouris
School of Civil and Environmental Engineering
Georgia Institute of Technology

Dr. Athanasios Nenes
School of Earth and Atmospheric Science
Georgia Institute of Technology

Dr. Spyros Pavlostathis
School of Civil and Environmental Engineering
Georgia Institute of Technology

Date Approved: December 4, 2015

To my beloved parents, parents-in-law, son, and wife

ACKNOWLEDGEMENTS

First of all, I would like to express my sincere appreciation to my advisor, Dr. Sotira Yiacoumi, for her support, guidance, encouragement, patience, and consideration. I would also like to express my deep gratitude to Dr. Costas Tsouris; his enthusiasm and dedication to our research have been admirable and have always inspired me to study harder. Without their invaluable advice, in-depth discussion, and tremendous help, it would have been impossible for me to successfully complete my Ph.D. thesis. I also wish to sincerely thank my other committee members: Dr. Athanasios Nenes, Dr. Spyros Pavlostathis, and Dr. Ching-Hua Huang. Their advice, comments, and suggestions have always been very helpful.

I would like to thank Dr. Jaehong Kim from Yale University for all the interesting and meaningful conversations. I also wish to thank Dr. Guangxuan Zhu for all his help in the laboratory. I am also grateful to Dr. Joanna McFarlane from Oak Ridge National Laboratory and Dr. Ida Lee from The University of Tennessee for their considerable assistance.

I am indeed indebted to the members of the Colloids and Interfacial Science Group, Dr. Ketki Sharma, Austin, Lydia, Dr. Hyojin Kweon, and Alex for their help, consideration, and friendship. I am deeply grateful to all the friends I have met at Georgia Tech, especially Dr. Sihyun Kim, Dr. Seungjin Lee, Sehoon, and Minjae.

I would like to express my heartfelt gratitude to my former advisor, Professor Mooyoung Han at Seoul National University, South Korea for providing me with this

opportunity to study in the US. I also appreciate Dr. Tschung-il Kim from Seoul National University for his continuous help and valuable advice.

This work was supported by the Defense Threat Reduction Agency under grant number DTRA1-08-10-BRCWMD-BAA.

I can't close the acknowledgements without expressing my deepest appreciation to my family, especially my beloved parents, parents-in-law, brother, son Ji Hoo Matthew, and wife Juyoung. Their endless encouragement and support have led to the successful completion of my thesis. In particular, I would be forever grateful to my wife for her devotion and sacrifice.

TABLE OF CONTENTS

LIST OF TABLES

LIST OF FIGURES

Page

LIST OF SYMBOLS

A	Radioactivity
A_{atom}	Atomic weight
B	Particle mobility
d_k	Particle diameter
d_g	Geometric mean particle size
c	Velocity of light
D_k	Diffusion coefficient of single particles
$D_{\pm}$	Ion diffusivities
$-dE/dx$	Linear energy transfer
e	Electrical charge
E	Electric field created by particle charge and the image charge of ions
$E_{\max}$	Maximum kinetic energy of the beta spectrum
f_i	Mole fraction of a radionuclide i
f_l	Weight fraction of an element l
F	Aggregation frequency
G	Auxiliary function (Chapter 3); Hydrodynamic function (Chapter 4)
h	Thickness
I	Ionization rate coefficient (Number of ion pairs produced per decay)
$I^{\pm}$	Ion currents
$I_{excitation}$	Mean excitation energy of the element
j	Number of elementary charges
J	Mean charge of particles

k_B	Boltzmann constant
L_k	Mean free path
m_e	Rest mass of the electron
m_k	Mass of size k particles
M	Total number of the size bins
n_0	Mean ion concentration
n_c	Decay chain length
$n_\pm$	Ion concentrations
$n\ (\infty)$	Macroscopic density
n	Particle number density
N_A	Avogadro's number
N_k	Number concentration of size k particles
N_{kj}	Number concentration of particles of size k and charge j
N_t	Total number concentration of particles
q	Bipolar ion production rate
$q_{I,i}$	Bipolar ion production rates of beta-emitting radionuclides
q_b	Bipolar ion production rates of other ion sources
r_e	Classical electron radius
r_k	Particle radius
R	Range of electrons
s	Distance between the centers of the particles (Chapters 2,4); Self-charging coefficient (Chapters 6, 7)
SI	Specific ionization
t	Time
T	Temperature
T_k	Kinetic energy

$\bar{v}_k$	Particle thermal speed in air
V	Average volume of particles.
V_t	Total volume concentration of particles
V_A	van der Waals interaction potential
V_R	Electrical potential
u	Atomic mass unit
U	Energy flux of beta particles
U_0	Initial energy flux of beta particles
x	Particle volume
w_{air}	Ionization potential of air
Z_{atom}	Atomic number
y	Dimensionless parameter of particle self-charging
X	Dimensionless parameter of particle diffusion charging
Z	Number of nuclides (Chapters 2, 7); Particle concentration (Chapter 4)
Δ	Cut-off energy
α_{rc}	Recombination rate coefficient of ions
α^{Br}	Brownian collision efficiency
$\bar{\alpha}^{Br}$	Average Brownian collision efficiency
β^{Br}	Brownian collision frequency
$\beta_J^{\pm}$	Ion-particle attachment coefficient
$\beta_{k,j}^{\pm}$	Ion-particle attachment coefficient
β	Ratio of electron velocity to the velocity of light
δ_i	Path length of charged particles such as electrons
δ^{Kr}	Kronecker delta
ε_0	Permittivity of vacuum

ε	Dielectric constant of the air
η_0	Specific radioactivity
$\eta_{l,m}$	A property distribution factor between two size bins
λ	Decay constant
λ_k	Dimensionless parameter of size k particle
$\mu_{\pm}$	Ion mobilities
μ_{air}	Apparent linear absorption coefficient of air
μ_{mean}	Mean atomic weight
ρ	Space charge density
ρ_{air}	Density of air
ρ_p	Particle density
τ	Timescale needed to reach a steady state
σ_{air}	Electrical conductivity
σ_k	Standard deviation
ω	Dimensionless parameter of particle size

LIST OF ABBREVIATIONS

AFM	Atomic force microscopy
AMP	Ammonium molybdophosphate
BL	Beer-Lambert
LET	Linear energy transfer
PBM	Population balance model
SSPM	Scanning surface potential microscopy
ZrHP	Zirconium hydrogen phosphate

SUMMARY

Atmospheric dispersion of particles containing radionuclides can cause severe radioactive contamination over a wide area. In case of a nuclear plant accident or a deliberate explosion of radiological devices, accurate prediction of atmospheric transport of radioactive particles is necessary from the beginning of the nuclear events in order to reduce uncertainty in the assessment of environmental and health risks originated by radiation exposure. Because of large discrepancies between theory and observations after nuclear accidents, however, improving predictive modeling of radioactivity transport is a top priority.

Charge and size are important parameters that can affect any processes involving particles in the atmosphere. In general, it is assumed that, because radionuclides are typically carried by background aerosols, radioactive particles behave similarly to atmospheric particles, whose surface interactions created by electrostatic forces are neglected. However, radioactive decay of radionuclides can induce surface charging of particles. Because of radioactivity-induced charging, the assumption that electrostatic interactions of radioactive particles can be neglected may cause large inaccuracies in predicting dispersion of radionuclides in the atmosphere. Thus, it is essential to evaluate the validity of the assumption and to develop systematic approaches to incorporate charging effects caused by radioactive decay into predictive models of radioactivity transport.

Toward a better understanding of the atmospheric behavior of radioactive particles affected by radioactive decay, this study investigates the influence of radioactivity on particle-surface interactions. The investigations of this study include experimental and modeling parts and focus on radioactivity-induced charging mechanisms and their influence on the microphysics of radioactive particles.

In the experimental part, radioactivity-induced charging mechanisms are investigated using scanning surface potential microscopy. It has been shown that (i) radioactivity induces simultaneous surface charge accumulation through electron emission and ion diffusion and (ii) the charging mechanisms should be interpreted as competing terms in surface charge modeling.

In the modeling part, we present various population balance models, which are employed to combine the knowledge of radiation physics (e.g., ionization and radioactive transformation), surface science (e.g., particle collision and charging), and microphysics (e.g., aggregation and electrostatic dispersion). It has been shown that (i) radioactive particles are strongly charged through charging mechanisms despite the occurrence of ionizing radiation in open air and (ii) the presence of radioactive particles can significantly affect the particle charge distribution in the atmosphere. Because of surface charging caused by radioactive decay, the size growth rates of radioactive particles by aggregation can be significantly different from those of typical atmospheric particles. Thus, electrostatic interactions of radioactive particles can affect the behavior of the particles during short- and long-range transport.

To include mutual effects of radioactivity-induced charging and aggregation (or coagulation) on the microphysical evolution of radioactive particles, three systematic approaches with a wide range of complexity are developed. The approaches can readily be incorporated into microphysical aerosol transport models of any scale. Some examples are provided to show that the approaches developed in this study can also be applied to various investigations including particle measurement systems.

The influence of radioactivity on charge/size distribution dynamics of initially charged radioactive and nonradioactive particles is investigated. It has been found that the charge and size of radioactive particles can evolve dissimilarly over time in comparison with the nonradioactive particles because radioactivity and electrostatic dispersion highly influence the charging and aggregation rates of radioactive particles.

The charging and aggregation of multicomponent radioactive particles were investigated for homogeneous and heterogeneous populations. It has been shown that radioactivity-induced charging can decrease/increase the aggregation rates of multicomponent radioactive particles in homogeneous/heterogeneous populations by generating strong electrostatic repulsive/attractive forces among the particles.

This study contributes toward a better understanding of the microphysical behavior of radioactive particles in environmental systems, and the models developed can be employed to reduce the uncertainty in estimations of local and global radioactivity levels and the corresponding environmental and health risks. The results are useful in atmospheric transport modeling of radioactive plumes released by severe nuclear events, such as the recent accident of the Fukushima nuclear power plant in Japan, as well as investigations in atmospheric systems including radiation sources.

CHAPTER 1

INTRODUCTION

1.1. Use of Radionuclides and Potential Risks

Radionuclides, which are also called radioisotopes, refer to unstable atoms with excess nuclear energy. Radionuclides such as ^{222}Rn and ^{234}Th are naturally generated and widely distributed in the environment (Hoppel, 1985; Burd et al., 2000). Radionuclides such as ^{137}Cs can be artificially created by nuclear reactions. Because of excess nuclear energy, radionuclides are continuously transformed into different nuclides by releasing high energy until the transformed nuclides are stable. Energy released by the transformation of radionuclides can be employed for various purposes such as power generation at nuclear power plants or radiation treatments at medical facilities, indicating the usefulness of radionuclides.

Despite the high utility, substantial risks caused by excessive radiation exposure are always accompanied by the use of radionuclides, which can result in enormous radiation damage to human society and the environment. For example, the recent Fukushima nuclear plant accident released a large amount of radionuclides such as ^{131}I and ^{137}Cs into the atmosphere, which created radioactive contamination locally and globally via short- and long-range transport (Masson et al., 2011; Yoshida and Kanda, 2012). The nuclear plant accident resulted in various types of human radiation exposure such as inhalation exposure, possibly leading to ~ 1,300 cancer mortalities and ~ 2,500 cancer morbidities around the world (Hoeve and Jacobson, 2012). Due to severe radioactive contamination, over a hundred of thousands of local residents lacked access to their home even one year after the Fukushima nuclear plant accident (Yoshida and Kanda, 2012).

There were still 440 nuclear reactors over the world in 2011 (Hoeve and Jacobson, 2012). Historical evidences involving the Fukushima case indicate that a nuclear plant accident can result in rapid and wide dispersion of numerous radionuclides via atmospheric pathways and lead to vast damage to human society and the environment. These facts imply that the public and the environment are still exposed to potential risks of radiation exposure, and in case of nuclear plant accidents, atmospheric transport of radionuclides may be the most important pathway causing radiation exposure. Thus, it is important to secure abilities to accurately predict short- and long-range transport of radionuclides in order to precisely assess human health and environmental risks caused by possible radiation exposure in the future.

1.2. Radioactivity Transport Modeling

Considerable modeling efforts have been made to investigate atmospheric dispersion of radionuclides. Table 1.1 shows some predictive studies of atmospheric transport of radionuclides released by the Chernobyl and Fukushima nuclear plant accidents. Pöllänen et al.(1997) simulated possible trajectories of radioactive particles released during the Chernobyl nuclear plant accident. Adachi et al. (2013) measured the size and activity of single ^{137}Cs particles in the first radioactive plume of the Fukushima nuclear plant accident and then used the particle properties to simulate atmospheric dispersion of ^{137}Cs. These investigations indicated that (i) highly radioactive particles can be transported to a place located hundreds of kilometers from a radioactive source and (ii) understanding of effects of physical and chemical properties (e.g., size and composition) of particles on aerosol microphysics is necessary to accurately forecast atmospheric transport of radionuclides.

Table 1.1. Modeling efforts to predict atmospheric dispersion of radionuclides

Case	Model	Remarks	Reference
Chernobyl nuclear plant accident	TRADOS	○ Understanding the nature of particles is important ○ Highly radioactive particles can be widely dispersed	Pöllänen et al. (1997)
Fukushima nuclear plant accident	RAQM 2	○ Dry deposition of spherical ^{137}Cs particles is important in atmospheric dispersion of radionuclides ○ Chemical and physical properties of radioactive particles can be key parameters for predictive studies	Adachi et al. (2013)
	WRF-Chem	○ Wet deposition can be more important than dry deposition ○ Particle size can be an important parameter, but it is difficult to incorporate its effects into predictive models due to lack of information	Huh et al., (2012, 2013); Hu et al. (2014)
	GATOR-GCMOM	○ Aerosol microphysics models can be used to assess worldwide health effects of nuclear plant accidents	Hoeve and Jacobson (2012)

The Weather Research and Forecasting-Chemistry (WRF-Chem) model can involve the effects of meteorological and chemical parameters on atmospheric transport of radioactivity (Huh et al., 2012, 2013; Hu et al., 2014). Progress has been made to improve the WRF-Chem model by incorporating dry and wet deposition parameterizations (Hu et al., 2014), but discrepancies between the simulation results and measurements still remained. Possible reasons for the discrepancies may involve lack of knowledge of aerosol microphysics affecting size evolution of particles (Hu et al., 2014). However, discrepancies were observed between measurements and simulation results obtained from GATOR-GCMOM, which can comprehensively include the effects of aerosol microphysics on time-evolution of particle size (Hoeve and Jacobson, 2012). Another aerosol microphysics model, GISS-TOMAS has been used to predict global transport of ^{137}Cs particles released during the Fukushima nuclear plant accident, but discrepancies were found between measurements and predictions (Kristiansen et al., 2015). The results of these investigations imply that there are unknown processes affecting transport of radioactivity in the atmosphere.

1.3. Statement of Problem

The aforementioned investigations considered physical and chemical properties of radioactive particles as key parameters affecting short- and long-range transport of radioactivity, as well as taking into account radioactive decay and transformation in simulation. However, the investigations rarely focused on the subsequent effects of radioactive decay and transformation on electrical properties and electrostatic interactions of atmospheric particles carrying radionuclides. Possible reasons for neglecting electrical properties and electrostatic interactions of radioactive particles involve:

- Atmospheric particles may not be highly charged in the atmosphere. Some particles can be charged, but charging effects on particle interactions may be generally negligible (Seinfeld and Pandis, 2006).

- Radioactive particles can be charged because of radioactive decay and transformation. However, radioactive particles can also be easily discharged due to diffusion of ions produced by ionizing radiation. Consequently, only few radioactive particles may be charged (Greenfield, 1956). Thus, it can be assumed that electrostatic particle-surface interactions involving radionuclides [e.g., radioactive particles vs raindrop (Greenfield, 1957); gaseous radionuclides vs atmospheric particle (Craig, 1966)] are neglected.

Although frequently used in atmospheric modeling, the aforementioned assumption that electrostatic interactions are negligible has limitations because radioactive particles can be charged despite ionization of air (Yeh et al. 1976; Clement and Harrison, 1992; Gensdarmes et al., 2001; Walker et al., 2010; Kweon et al., 2014). Yeh et al. (1976) and Clement and Harrison (1992) showed that many positive charges can be accumulated on ^{198}Au particles for 23 seconds. Walker et al. (2010) reported that adhesion forces between radioactive gold and nonradioactive surfaces can be modified due to the surface charging caused by radioactivity. Rosinski et al. (1962) found that ^{198}Au particles aggregate at lower rates than nonradioactive gold particles probably due to the surface charging (Yeh et al., 1976), indicating that deposition rates of radioactive particles may differ from those of nonradioactive particles. These investigations suggest that neglecting the charging of radioactive particles may lead to errors in predictions of radioactivity transport. Thus, the effects of radiological phenomena of radionuclides on the microphysical behavior of radioactive particles should be investigated to more accurately predict the transport of radioactivity in the environment.

1.4. Scopes and Objectives

Toward a better understanding of transport of radioactivity in the atmosphere, the main goal of this effort is to establish a theoretical framework that can couple knowledge of radiation physics and surface science with aerosol microphysics. To construct a solid foundation to bridge the knowledge of radiation physics, surface science, and aerosol microphysics, this study focuses on theoretical and experimental investigations into the influence of radioactivity on particle-surface interactions. To achieve the main goal of this study, the following research objectives are given:

- Evaluate the assumption that electrostatic interactions caused by radioactivity are negligible in open air.
- Investigate the influence of radioactivity on the surface charge of single radioactive particles at the microscopic level and examine the influence of radioactivity-induced charge on aggregation kinetics of radioactive particles.
- Develop a theoretical framework that can incorporate the charging effects caused by radioactivity into microphysical aerosol transport models.
- Assess the influence of radioactivity on the dynamic evolution of the particle charge and size distributions in the atmosphere.
- Study the influence of radioactivity on the dynamic evolution of the activity, charge, and size distributions of multicomponent radioactive particles in homogeneous and heterogeneous populations.

1.5. Organization of Dissertation

This study consists of eight chapters. Five chapters focus on the accomplishment of the aforementioned research objectives. The other three chapters include introduction, background and literature review, and conclusions and recommendations of this study.

The motivation of this study and the significance are given in Chapter 1. In Chapter 2, background and literature review are provided, including basic knowledge of

radiation physics, the charging of radioactive particles, electrostatic interactions of particles and ions, and population balance models.

Chapter 3 is aimed at assessing the assumption that electrostatic interactions induced by radioactivity can be neglected in open air. The assessment is performed by calculating charge accumulation and neutralization rates of atmospheric particles containing radionuclides in open air. Results of this chapter demonstrate that radioactive particles can be highly charged in open air.

In Chapter 4, theoretical and experimental investigations are combined to evaluate the influence of radioactivity on charging and aggregation of radioactive particles in the atmosphere, which are critical processes included in aerosol microphysics models. The charging mechanisms induced by radioactivity are examined at the microscopic level. The effects of radioactivity-induced charging on particle aggregation are investigated using a simple population balance model. Results of this chapter show that radioactivity-induced charging can affect the size growth of radioactive particles by aggregation.

The focus of Chapter 5 is on the development of modeling approaches to couple radioactivity-induced charging with particle aggregation. Three approaches with a wide range of complexity are developed and applied to investigate the charging of radioactive and nonradioactive particles undergoing aggregation. Results of this chapter indicate that the developed approaches can be used for other purposes such as investigations with particle measurement systems, as well as aerosols transport models.

Chapter 6 investigates the effects of radioactivity-induced charging on charge/size distribution dynamics of radioactive and nonradioactive particles. To comprehensively involve the influence of radioactivity, electrostatic dispersion of particles and ions is added to the developed models. Results of this chapter indicate that charge/size distribution dynamics of charged radioactive particles can be highly different from that of nonradioactive particles because of radioactivity-induced charging and electrostatic dispersion.

Chapter 7 focuses on the surface charging and aggregation kinetics of multicomponent radioactive particles in homogeneous and heterogeneous populations. In this chapter, radioactive transformation, charge balance, and population balance are combined to forecast time-dependent changes in the activity, charge, and size distributions, and compositional changes of radioactive particles. Results of this chapter show that the charging and aggregation behavior of radioactive particles can be highly affected by the composition of particles.

Conclusions and recommendations of this study are provided in Chapter 8. Key processes involved in each chapter are given in Table 1.2.

Table 1.2 Key processes considered in Chapters 3-7.

Population	Radioactive composition	Processes	Chapter				
			3	4	5	6	7
Homogeneous population	Single-component radioactive particle	Ionizing radiation	O	O	O	O	
		Charging	O	O	O	O	
		Aggregation		O	O	O	
		Electrostatic dispersion				O	
Homogeneous population	Multicomponent radioactive particle	Ionizing radiation	O				O
		Charging	O				O
		Aggregation					O
		Electrostatic dispersion					
Heterogeneous population	Multicomponent radioactive particle	Ionizing radiation	O				O
		Charging	O				O
		Aggregation					O
		Electrostatic dispersion					

CHAPTER 2

BACKGROUND AND LITERATURE REVIEW

2.1. Radiation Physics

2.1.1. Units

Table 2.1 shows units of radioactivity, radiation energy, and radiation dose. Radioactivity refers to a property of radioactive atoms releasing energetic particles or radiation from unstable nuclei (Sawyer et al., 1994). The SI and non-SI units of radioactivity are the becquerel (Bq) and curie (Ci), respectively. One Bq represents the emission of an energetic particle per second or one disintegration per second, which corresponds to 2.703×10^{-11} Ci. For beta decay, 1 Bq stands for the emission of an energetic electron per decay, which is typically called beta particle.

The SI and non-SI units of energy of energetic particles and radiation are the joule (J) and the electron volt (eV), respectively. The definition of eV is the kinetic energy of an electron accelerated by a potential difference of 1 volt. One eV corresponds to 1.602×10^{-19} J.

Radiation energy can be absorbed by the surrounding molecules. The SI and non-SI units of the radiation dose are the gray (Gy) and the radiation absorbed dose (rad), respectively. The gray is defined as the absorption of energy of 1 J per 100 kg of absorbing medium, which corresponds to 100 rad. The rates of radiation dose can be expressed as gray per second (Gy s^{-1}) or microgray per hour (μGy h^{-1}).

As an example of unit operation, radiation dose rates can be converted to ionization rates of absorbing medium by ionizing radiation (Gensdarmes et al., 1998; Subramanian et al., 2012). For air, 1 μGy h^{-1} may produce 6.1573×10^{7} ions m^{-3} s^{-1} (Gensdarmes et al., 1998; Subramanian et al., 2012).

Table 2.1. Units of radioactivity, radiation energy, and radiation dose

	International System of Units (SI units)	Non-SI units	Unit conversion
Radioactivity	Bq	Ci	1 Bq = 2.703×10^{-11} Ci
Radiation energy	J	eV	1 J = 6.242×10^{18} eV
Radiation dose	Gy	Rad	1 Gy = 100 rad

2.1.2. Radioactive Decay Modes

The modes of radioactive decay include alpha (α), beta (β), and gamma (γ) decay. Alpha decay of a nucleus emits an alpha particle constituting two protons and two neutrons. For example, the alpha decay of ^{238}Pu can be expressed as:

$$^{238}_{94}\mathrm{Pu} \rightarrow {}^{234}_{92}\mathrm{U} + {}^{4}_{2}\alpha^{2+},$$

where α is the alpha particle. Because of the absence of electrons, the alpha particle is positively charged. A neutron of a nucleus can be transformed into a proton by emitting an electron. This transformation is called beta decay and the emitted electron is called a negatron, fast electron, or beta particle, β^-. For instance, the beta decay of ^{198}Au can be given as:

$$^{198}_{79}\mathrm{Au} \rightarrow {}^{198}_{80}\mathrm{Hg} + \beta^- + \bar{\nu},$$

where $\bar{\nu}$ is the antineutrino. Some neutrons and protons in nuclei can be in an excited state. The nuclei emit photons to alter a high energy state to a low one, which are known as gamma decay. In contrast to alpha and beta decays, photons are uncharged. These decay modes are involved in the decay chains of most radionuclides released during nuclear plant accidents.

2.1.3. Interactions of Charged Energetic Particles with Matter

Alpha and beta particles, which are typically called charged particles in nuclear physics and radiation physics (Martin, 2005), can interact with orbital electrons of elements of matter because of Coulombic forces. Alpha particles can interact with the orbital electrons because of electrostatic attraction while beta particles can repel them via electrostatic repulsion. Energy of the energetic particles can be transferred to the orbital electrons via these electrostatic interactions, leading to the ejection of the electrons and

the transformation of the elements to positive ions. The ejected electrons can be rapidly captured by the surrounding uncharged molecules, which become negative ions.

The rate of radioactivity-induced ionization can be given by the specific ionization (*SI*):

$$SI = \frac{-dE}{dx}\frac{1}{w_{air}} \tag{2.1}$$

where (-*dE*/*dx*) is the linear energy transfer (LET), and w_{air} is the ionization potential of air. The specific ionization is defined as the number of ion pairs produced by a charged energetic particle per unit length. Thus, the total number of ion pairs produced per decay, *I* is given as:

$$I = SI\delta \tag{2.2}$$

where δ is the path length of the charged particle. The equations to calculate LET and the path length of the charged particles are available elsewhere (ICRU, 1984; Katz and Penfold, 1952; Tomé and Palta, 1998). For beta particles, the ionization rate of gas molecules can be also estimated using the absorption theory:

$$\frac{dU}{dh} = -\mu_{air}U \tag{2.3}$$

where *U* is the energy flux of beta particles, *h* is the thickness, and μ_{air} is the apparent linear absorption coefficient of air. The energy flux of beta particles can be given by the Beer-Lambert (BL) law (Sharma et al., 2014):

$$U\left(h\right) = U_0 e^{-\mu_{\text{air}}h} \tag{2.4}$$

where, U_0 is the initial energy flux of beta particles. According to the work of Cooper and Reist (1973) and Martin (2005), equations 2.4 and 2.5 can be simplified to:

$$SI = \frac{16\rho_{air}}{3w_{air}} E_{\max} \left(E_{\max} - 0.036\right)^{-1.4} \tag{2.5}$$

where ρ_{air} is the density of air, and $E_{\max}$ is the maximum kinetic energy of the beta spectrum.

2.1.4. Kinetics of Radioactive Decay and Growth

Radioactive decay of radionuclides results in decrease in the concentration of the radionuclides, but increase in the concentration of the progeny. For a serial decay chain, $Z_1 \xrightarrow{\lambda_1} Z_2 \xrightarrow{\lambda_2} \cdots_i \longrightarrow Z_i \xrightarrow{\lambda_i} \cdots \longrightarrow Z_n$, changes in the concentrations of the radionuclides and their progeny can be given by the Bateman equations:

$$\frac{dZ_1}{dt} = -\lambda_1 Z_1, \tag{2.6}$$

$$\frac{dZ_i}{dt} = \lambda_{i-1} Z_{i-1} - \lambda_i Z_i \qquad (i = 2, 3, \cdots, n), \tag{2.7}$$

where Z_i is the number of the nuclide i, λ is the decay constant, n is the decay chain length, and t is the time. For the initial condition: $Z_1 = Z_{1,0}$ and $Z_i = 0$ ($i = 2, 3, \cdots, n$) at $t = 0$ s, the general solution of equations 2.6 and 2.7 is given as (Cetnar, 2006):

$$Z_i = \frac{Z_{1,0}}{\lambda_n} \sum_{i=1}^{n} \lambda_i \phi_i \exp\left(-\lambda_i t\right) \tag{2.8}$$

with

$$\phi_i = \prod_{\substack{i'=1 \\ i' \neq i}}^{n} \frac{\lambda_i}{\left(\lambda_{i'} - \lambda_i\right)}.$$

The solution of equation 2.6 and 2.7 for $n \leq 4$ can be easily obtained using the integrating factor method or an algebraic approach under the same initial condition

(Martin, 2005; Moral and Pacheco, 2003). Changes in radioactivity given by each radionuclide and the total radioactivity can be easily obtained using the analytical solutions of equations 2.6 and 2.7.

2.2. Surface Charging Caused by Radioactivity

Radioactive decay produces alpha and beta particles, which are emitted into the surrounding environment. Emission of such particles can lead to modification of the electrostatic characteristics of radioactive surfaces. Specifically, alpha and beta particles having high kinetic energy can produce two important effects (Yeh et al., 1976; Clement and Harrison, 1992; Clement et al., 1995; Walker et al., 2013; Kweon et al., 2013): (i) electron emission from a radioactive surface and (ii) generation of positive and negative ions that can diffuse onto particles. The first effect leads to accumulation of positive charges on the radioactive surfaces, a charging process that has been named "self-charging mechanism." The second effect has been named "diffusion-charging mechanism" or "ionic-charging mechanism." This mechanism may accumulate positive or negative ions on radioactive and nonradioactive surfaces.

2.3. Surface Interactions

2.3.1. Particle vs Particle

Particle-particle interactions depend on transport mechanisms and surface interactions of particles. Transport mechanisms involve Brownian diffusion, fluid shear, and differential sedimentation. All mechanisms can result in collision of particles. Particles in the nuclei and accumulation modes, however, typically collide with one another only by Brownian diffusion. The collision frequency of particles by Brownian diffusion, β^{Br} is given by (Fuchs, 1989):

$$\beta_{kl}^{Br} = 2\pi\left(d_k + d_l\right)\left(D_k + D_l\right)\left(\frac{d_k + d_l}{d_k + d_l + \sqrt{\delta_k^{\,2} + \delta_l^{\,2}}} + \frac{8\left(D_k + D_l\right)}{(d_k + d_l)\sqrt{\bar{v}_k^{\,2} + \bar{v}_l^{\,2}}}\right)^{-1}, \qquad (2.9)$$

with

$$\delta_k = \frac{1}{3d_k L_k}\left(\left(d_k + L_k\right)^3 - \left(d_k^2 + L_k^2\right)^{\frac{3}{2}}\right) - d_k,$$

where d_k is the particle diameter, D_k is the diffusion coefficient of single particles, $\bar{v}_k$ is the thermal velocity, and L_k is the mean free path.

As one particle approaches the other particle, the colliding particles are influenced by van der Waals and electrostatic forces. The influence of surface forces on particle collision can be quantified using the collision efficiency, α^{Br} (Spielman, 1970; Yiacoumi et al., 1996):

$$\alpha_{k,l}^{Br} = \left[(1 + \frac{r_k}{r_l})\int_2^{\infty} e\exp(\frac{V_A + V_R}{k_B T})s^{-2}ds\right]^{-1} \qquad (2.10)$$

where r_k is a particle radius, V_A is the van der Waals interaction potential, V_R is the electrical potential, k_B is Boltzmann constant, T is temperature, and s is the distance between the centers of the particles. If the effects of van der Waals forces are negligible, equation 2.10 can be easily solved and the following solution is found (Fuchs, 1989):

$$\alpha_{kl}^{Br} = \frac{u}{e^u - 1}, \qquad (2.11)$$

with $u = \dfrac{j_k j_l e^2}{4\pi\varepsilon_0\varepsilon(r_k + r_l)k_B T}$,

where e is the electrical charge, ε_0 is the permittivity of vacuum, and ε is the dielectric constant of the air.

2.3.2. Particle vs Ion

In a system involving particles and ions, an ion can be attached onto a particle surface. The ion-particle attachment coefficient, $\beta_{k,j}^{\pm}$, is given by (Fuchs, 1963; Hoppel and Frick, 1986):

$$\beta_{k,j}^{\pm} = \frac{I^{\pm}}{n(\infty)} \tag{2.12}$$

with $I^{\pm} = 4\pi r_k^2 \left(D_{\pm} \frac{\partial n_{\pm}}{\partial r_k} + \mu_{\pm} E n_{\pm} \right)$

where $I^{\pm}$ represents the ion currents, n (∞) is the macroscopic density, $n_{\pm}$ represents the ion concentrations, $D_{\pm}$ represents the ion diffusivities, $\mu_{\pm}$ represents the ion mobilities, and E is the electric field created by particle charge and the image charge of ions. The numerical solution of equation 2.12 is developed by Fuchs (1963), and Hoppel and Frick (1986) corrected the procedure to use the numerical solution. The ion-particle attachment coefficients given by Fuchs (1963) and Hoppel and Frick (1986) can be used to investigate the attachment between an ion and a particle of any size. In continuum regime, the ion-particle attachment coefficients can be easily obtained using analytical solutions given by Gunn (1954):

$$\beta_{k,j}^{+} = \frac{je\mu_{+}}{\varepsilon_0 \left[\exp(2\lambda_k j) - 1 \right]}, \tag{2.13}$$

$$\beta_{k,j}^{-} = \frac{je\mu_{-}}{\varepsilon_0 \left[1 - \exp(-2\lambda_k j) \right]}, \tag{2.14}$$

with $\lambda_k = \frac{e^2}{8\pi\varepsilon_0 \varepsilon r_k k_B T}$.

The attachment coefficient between an ion and uncharged particles is given as (Harrison and Carslow, 2003):

$$\beta_{k,j}^{\pm} = \frac{4\pi k_B T r_k}{e}, \tag{2.15}$$

2.4. Population Balance Model

Aggregation is an important microphysical process of atmospheric particles. Aggregation rates of particles are obtained from solving the integro-differential equation (Seinfeld and Pandis, 2005):

$$\frac{\partial n(x,t)}{\partial t} = \frac{1}{2}\int_{x0}^{x-x_0} F\left(x', x-x'\right) n\left(x'\right) n\left(x-x'\right) dx' - \int_{x_0}^{\infty} F\left(x, x'\right) n\left(x\right) n\left(x'\right) dx', \tag{2.16}$$

where n is the number density of particles, and F is the aggregation frequency. In equation 2.16, the two terms on the right-hand side (RHS) accounts for the production and loss of particles by aggregation, respectively. The aggregation frequency is computed by multiplying the collision frequency with the collision efficiency. Equation 2.16 can be extended to simulate aggregation of multicomponent particles (Gelbard and Seinfeld, 1978; Vale and McKenna, 2005), bipolarly charged particles (Oron and Seinfeld, 1989a&b; Vemury et al., 1997), and magnetic particles with different magnetic susceptibilities (Tsouris et al., 1995).

CHAPTER 3

SURFACE CHARGE ACCUMULATION OF PARTICLES CONTAINING RADIONUCLIDES IN OPEN AIR

Radioactivity can induce charge accumulation on radioactive particles. However, electrostatic interactions caused by radioactivity are typically neglected in transport modeling of radioactive plumes because it is assumed that ionizing radiation leads to charge neutralization. In this chapter, the assumption that electrostatic interactions caused by radioactivity are negligible is evaluated by examining charge accumulation and neutralization on particles containing radionuclides in open air. A charge-balance model is employed to predict charge accumulation on radioactive particles. It is shown that particles containing short-lived radionuclides can be charged with multiple elementary charges through radioactive decay. The presence of radioactive particles can significantly modify the particle charge distribution in open air and yield an asymmetric bimodal charge distribution, suggesting that strong electrostatic particle interactions may occur during short- and long-range transport of radioactive particles. Possible effects of transported radioactive particles on electrical properties of the local atmosphere are reported.

3.1 Introduction

Atmospheric dispersion of particles containing radionuclides may cause environmental and public health problems. The Chernobyl and Fukushima accidents led to radioactive contamination in many regions through transport and deposition of radionuclides (Chesser et al. 2004, Ooe et al. 1988, Pöllänen et al. 1997, Parache et al.

2011). Some areas may be contaminated for a long period of time due to the presence of long-lived radionuclides [e.g., ^{137}Cs (Yoshenko et al. 2006a, 2006b)]. Thus, accurate prediction of transport of radioactive particles is needed from the beginning of a nuclear event in order to reduce uncertainty in our evaluations of environmental and health risks.

Modeling efforts have been made to predict transport of airborne radionuclides (ApSimon et al. 1989, Lee and Feichter 1995, Rehfeld and Heimann 1995, Pöllänen et al. 1997). However, discrepancies between theory and observations have been reported. For the Chernobyl case, large radioactive particles, which in theory should settle quickly, were transported to areas far away from the site of the accident (Lujanienė et al. 2009, Pöllänen et al. 1997). Predictions that did not follow well the observations were also reported for other cases of radioactivity transport (ApSimon et al. 1989, Lee and Feichter 1995, Rehfeld and Heimann 1995). These discrepancies emphasize the need to improve predictive modeling of radioactivity transport.

The nature of particulates in radioactive plumes plays a major role in radioactivity transport (Pöllänen et al. 1997). So far, it has been assumed that, because radionuclides are typically carried by background aerosols (Kaneyasu et al. 2012), radioactive particles behave similarly to atmospheric particles, whose electrostatic surface interactions are neglected (Seinfeld and Pandis 2006). It has been shown, however, that radioactive particles can be strongly charged (Clement and Harrison 1992, Gensdarmes et al. 2001, Kim et al. 2014, Kweon et al. 2013, Reed et al. 1977, Walker et al. 2010, Yeh et al. 1976); therefore, the assumption of neglecting electrostatic interactions may cause inaccuracies in predicting transport of radioactive particles. Nevertheless, the assumption has been used in many cases with the explanation that the presence of ionizing radiation induces charge neutralization of particles in open air (Greenfield 1956, 1957). For example, Greenfield (1957) employed this assumption and found that the wet scavenging rate of radioactive particles can significantly decrease for a particle size range of 0.1 - 1 μm. This size range is typically called the Greenfield gap (Seinfeld and Pandis 2006, Shaw

1986). To reduce uncertainty in predictive modeling of radioactivity transport, there is a need to investigate whether radioactive particles can be charged in open air in order to evaluate the convenient assumption of negligible electrostatic interactions. In particular, although radioactive particles typically contain mixtures of radionuclides (Cuddihy et al. 1989, Devell et al. 1986, Kaneyasu et al. 2012, Kauppinen et al. 1986, Pöllänen et al. 1997), little information has been reported about ionizing radiation and particle charging under such conditions. Thus, this chapter examines charge accumulation and neutralization on the surface of particles containing various radionuclides in open air, under realistic conditions, to assess the importance of electrostatic interactions caused by radioactivity.

3.2. Methodology

3.2.1. Characteristics of Radioactive Particles

Various radionuclides (e.g., ^{99}Mo, ^{103}Ru, ^{106}Ru, ^{131}I, ^{132}Te, ^{134}Cs, and ^{137}Cs) were found in particles released from the Chernobyl and Fukushima accidents (Cuddihy et al. 1989, Devell et al. 1986, Kaneyasu et al. 2012, Kauppinen et al. 1986, Pöllänen et al. 1997). The radioactivity A of individual particles containing radionuclides can be given by the number of radioactive atoms and decay constant λ:

$$A_k = \sum_i A_{k,i} = \sum_i \frac{m_k N_A f_i}{\mu_{mean}} \lambda_i \tag{3.1}$$

where m_k is the mass of size k particles, N_A is Avogadro's number, f_i is the mole fraction of a radionuclide i and μ_{mean} is the mean atomic weight.

For beta decay, radionuclides emit electrons with kinetic energy T_k. Energy deposition by the emitted electrons causes atomic electron ejection from gas molecules in air, thereby generating ion pairs. The mean number of ion pairs produced per decay I (i.e.,

ionization rate coefficient) can be estimated using the linear energy transfer (LET) equation (Huizenga and Storchi, 1989; ICRU, 1984; Tomé and Palta, 1998) and the additivity rule (Bragg and Kleeman, 1905):

$$I_i = \left[\sum_l f_l \left(\frac{1}{\rho_{air}} \frac{-dE}{dx} \right)_{\Delta,l} \right] \frac{\delta_i}{w_{air}} \tag{3.2}$$

where f_l is the weight fraction of an element l, ρ_{air} is the air density, Δ is the cut-off energy, δ_i is the path length of electrons, and w_{air} is the ionization potential. LET, $(-dE/dx)_{\Delta,l}$, represents the mean energy loss of energetic electrons during their movement and involves energy transfer to air molecules. LET can be given as

$$\left(\frac{1}{\rho_{air}} \frac{-dE}{dx} \right)_{\Delta,l} = \frac{2\pi r_e^2 m_e c^2}{\beta^2} \frac{Z_{atom}}{u_{Aatom}} \left[\ln\left(\frac{T_k}{I_{excitation}} \right)^2 + \ln\left(1 + \frac{\tau}{2} \right) + G(\tau, \eta) \right] \tag{3.3}$$

where r_e is the classical electron radius, m_e is the rest mass of the electron, c is the velocity of light, β is the ratio of electron velocity to the velocity of light, Z_{atom} is the atomic number, u is the atomic mass unit, A_{atom} is the atomic weight, $I_{excitation}$ is the mean excitation energy of the element, G is the auxiliary function (Tomé and Palta, 1998), $\tau = T_k/m_e c^2$ and $\eta = \Delta/T$. In equation 3.3, the sum of the three terms in square brackets on the right-hand side (RHS) represents the dimensionless stopping number for elements (Seltzer and Berger 1982). In particular, the last term restricts the amount of transferred energy up to Δ.

We assumed that air consists of N_2, O_2, CO_2, and Ar and that the weight fraction of N, O, C, and Ar is comparable to the dry air around sea level. To secure validity of equation 3.3, the binding energies of atomic electrons should be smaller than Δ. Similarly to ICRU (1984) and Tomé and Palta (1998), it was assumed that Δ = 1 keV for N, O, and C and Δ = 10 keV for Ar, which can be greater than the binding energies of atomic

electrons in K- and L-shells of the elements. Ionizing radiation caused by beta decay can polarize elements, which can influence LET. However, this effect is negligible for electrons with $T \leq 10$ MeV (ICRU, 1984). $I_{excitation}$ of the elements can be obtained from the empirical formula (Marmier and Sheldon, 1969). For beta decay, $w_{air} = 34$ eV (Whyte, 1963).

The path length of energetic electrons depends on their kinetic energy. Because it is difficult to predict the tortuous path of energetic electrons, the mean path length of the electrons was estimated using the semi-empirical range-energy relationship given by Katz and Penfold (1952):

$$R = 0.412T^{1.265-0.0954\ln T} \qquad \left(0.01 < T \leq 2.5 \text{ MeV}\right) \tag{3.4}$$

where R is the range of electrons in g/cm^2. In contrast to alpha decay, beta decay exhibits a continuous energy distribution because of the creation of antineutrinos. In this study, the ionization coefficients of radionuclides and the mean path length of energetic electrons were estimated using the mean value of the energy distribution, E_{mean}. Equations 3.1 and 3.2 provide the number of electrons emitted and ion pairs produced by beta decay of radionuclides.

3.2.2. Charge Balance Model

Electron emission and diffusion of positive and negative ions induce charge accumulation and neutralization on radioactive particles (Kim et al., 2014). Electron emission refers to the self-charging mechanism, while ion diffusion corresponds to the diffusion-charging mechanism. For beta decay, the net charge accumulation rate on radioactive particles is given by:

$$\frac{dJ}{dt} = A + \beta_J^+ n_+ - \beta_J^- n_- \tag{3.5}$$

where J is the charge number, $\beta_J^{\pm}$ is the ion-particle attachment coefficient, $n_{\pm}$ is the ion concentration, and t is time. Clement and Harrison (1992) extended equation 3.5 to investigate the charging of monodispersed particles containing single radionuclides. Based on the work of Clement and Harrison, a sectional approach can give the charge distribution of polydispersed particles containing various radionuclides as:

$$\frac{dN_{kj}}{dt} = A_{k,j-1}N_{k,j-1} - A_{k,j}N_{k,j} + \beta_{k,j-1}^{+}n_{+}N_{k,j-1} - \beta_{k,j}^{+}n_{+}N_{k,j} + \beta_{k,j+1}^{-}n_{-}N_{k,j+1} - \beta_{k,j}^{-}n_{-}N_{k,j} \tag{3.6}$$

where N_{kj} is the number concentration of radioactive particles of size k and charge j. In equation 3.6, the first two terms on the RHS represent the charge accumulation rate by the self-charging mechanism and the remaining terms account for the charge accumulation rate by the diffusion-charging mechanism. The ion-particle attachment, ion-ion recombination, ionization, and electron emission can influence the ion concentration (Clement and Harrison, 1992; Renard et al., 2013), through the following equations:

$$\frac{dn_{+}}{dt} = -n_{+}\sum_{k}\sum_{j}\beta_{k,j}^{+}N_{k,j} - \alpha_{rc}n_{+}n_{-} + q\,, \tag{3.7}$$

$$\frac{dn_{-}}{dt} = -n_{-}\sum_{k}\sum_{j}\beta_{k,j}^{-}N_{k,j} - \alpha_{rc}n_{+}n_{-} + q + \sum_{k}\sum_{j}N_{k,j}A_{k,j}\,, \tag{3.8}$$

where α_{rc} is the recombination coefficient and q is the bipolar ion production rate. In equations 3.7 and 3.8, the first two terms on the RHS represent ion loss through ion-particle attachment and ion-ion recombination. The third term represents ion production by beta radiation, as well as other ion sources, and can be obtained using

$$q = \sum_{i} q_{I,i} + q_b \tag{3.9}$$

where $q_{I,i}$ and q_b are the bipolar ion production rates of beta-emitting radionuclides and other ion sources, respectively. $q_{I,i}$ can be calculated by multiplying the number of electrons emitted per unit time with their ionization rate coefficient. The last term of equation 3.8 accounts for the emitted electrons. Effects of each radionuclide on charge accumulation are included using η and $q_{I,i}$. Equations 3.6-3.8, without radioactivity terms, can be valid in predicting electrification phenomena of aerosols in the upper troposphere and stratosphere (Renard et al., 2013). In this study, the ion-particle attachment coefficient in the charge balance equation was estimated according to Harrison and Carslaw (2003).

3.2.3. Experimental Data

Experimental data from the literature were used to validate the charge balance model and ionization rate coefficient (Table 3.1). The charge distribution of ^{137}Cs particles was measured as a function of A and I. The charge accumulation of ^{198}Au particles was investigated as a function of A. The experiments were carried out in cylindrical tubes. Under such condition, the mean path length of electrons can be estimated as a function of the tube diameter, d_{tube} on the basis of the criteria of Clement and Harrison (1992) and Gensdarmes et al. (2001): if $\delta_{i,mean} < d_{tube}$, $\delta_i = (\pi/4)d_{tube}$, while $\delta_i = d_{tube}$ if $\delta_{i,mean} > d_{tube}$.

3.3. Results and Discussion

3.3.1. Ionization Rate Coefficient

The ionization rate coefficient I of radionuclides was estimated using LET (eq 3.2) and evaluated employing the charge balance model and experimental data (Cases 1-7). For comparison, I was also estimated from a typical approach using the Beer-Lambert (BL) law (Clement and Harrison, 1992; Cooper and Reist, 1973;

Table 3.1. Experimental observations on charging of beta-emitting radioactive particles.

Radionuclide		^{137}Cs				^{198}Au		
Case number		1	2	3	4	5	6	7
Radioactivity η (mBq)		12.8	3.2	12.8	3.2	470	210	77
Ionization rate coefficient I		52	4,395	52	4,395	-	-	-
Particle diameter (μm)		0.82	0.82	1.05	1.05	0.53	0.53	0.53
Tube diameter (cm)		0.6	40	0.6	40	1.5	1.5	1.5
Ion mobility: ($cm^2\ V^{-1}\ s^{-1}$)	Positive ion	1.19				1.2		
	Negative ion	1.54				1.2		
References		*Gensdarmes et al.* (2001)				*Clement and Harrison* (1992) *Yeh et al.* (1976)		

mBq: milliBecquerels

Gensdarmes et al., 2001). Hereafter, we refer to estimation by the LET or BL approach, respectively. Note that the BL approach employed in this study includes the empirical formula for air (Martin, 2000), while previous studies have used that obtained for aluminium (Clement and Harrison, 1992; Cooper and Reist, 1973; Gensdarmes et al., 2001).

Figure 3.1(a) shows the charge accumulation rates for Case 1. The ionization rate coefficient was estimated as I_{LET} = 29 by the LET approach and I_{BL} = 126 by the BL approach. Both approaches predicted that ^{137}Cs particles initially accumulated positive charge, which neutralized the negative surface charge assumed initially based on the experiments by Gensdarmes et al. (2001). However, the results with I_{LET} were closer to the experimental data than those with I_{BL}. The discrepancy resulted from the difference in the ion concentration caused by ionization. For the case with I_{LET}, the ion concentration in the system increased more slowly and was lower than that estimated by I_{BL}, causing the particles to accumulate more positive charges through the self-charging mechanism until the diffusion-charging mechanism was strong enough to counterbalance the surface charge. As shown in Table 3.1, the mobility of negative ions is greater than that of positive ions, and this is the reason that the diffusion-charging mechanism neutralizes positive charge added by the self-charging mechanism.

The I_{LET} value of this study was different than that of Gensdarmes et al. (2001) due to the differences in determining (1) the mean kinetic energy of electrons and (2) the estimation method to obtain LET. To compute the amount of energy transferred to air molecules, we employed the mean kinetic energy obtained from the beta spectrum of ^{137}Cs [E_{mean} = 0.192 MeV (Mantel, 1972)], while Gensdarmes et al. (2001) assumed that the mean kinetic energy is one fourth of the maximum kinetic energy (E_{mean} = 0.128 MeV). For ^{137}Cs, a lower E_{mean} provides a higher value for LET, thereby increasing its ionization rate coefficient. In this study, LET was estimated using the restricted LET formula with the cut-off energy, while Gensdarmes et al. (2001) obtained LET from a

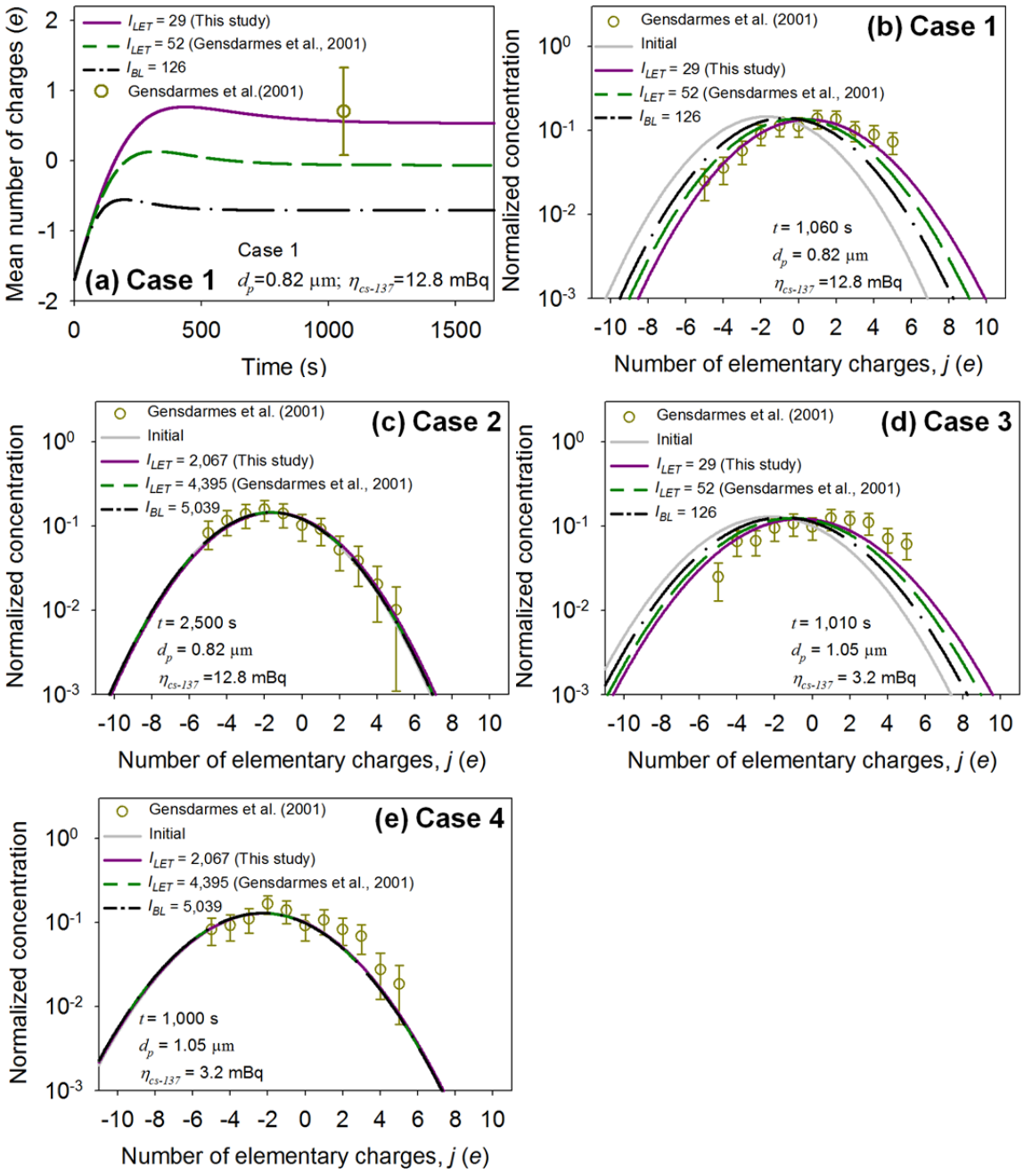

Figure 3.1. Charge accumulation for Case 1 (a) and charge distribution for Cases 1-4 (b-e).

chart in Joffre (1963) without providing specific assumptions. Nevertheless, the LET approach of this study predicted the charge accumulation rates for Cases 1 and 3 more accurately than the LET approach described in Gensdarmes et al. (2001) [Figure 3.1(b) and 1(d)].

For Cases 2 and 4, the results of both approaches agreed well with the measurements [Figure 3.1(c) and (e)], but the LET approach forecasted more precisely the charge accumulation behavior of the ^{198}Au particles (Cases 5 to 7) (Figure 3.2). Compared to Reed et al. (1977) and Clement and Harrison (1992), the discrepancy in the predictions for Cases 5 - 7 results mainly from employing different ion mobilities and ionization rate coefficients. These results suggest that the LET approach employed in this study can reliably estimate ionization rate coefficients of radionuclides to predict charge accumulation on radioactive particles.

3.3.2. Charge Accumulation on Particles Containing Radionuclides

Charge accumulation on particles containing radionuclides was investigated using the charge balance model with eqs 3.1-3.4 under the experimental conditions of Cases 1-4. The mole fraction of ^{137}Cs contained in the particles was estimated using eq 3.1. It was assumed that (i) various short-lived and long-lived radionuclides are added to the ^{137}Cs particles, (ii) the mole fraction of added radionuclides equals that of ^{137}Cs, and (iii) their radioactivity is constant because of short charge accumulation time.

Figure 3.3 shows charge distributions of ^{137}Cs particles containing other radionuclides under the experimental conditions of Cases 1 and 2. The relative difference of charge distributions represents the effects of each radionuclide on charge accumulation rates. The charge distributions of ^{137}Cs particles became quite different as short-lived radionuclides were added. The contained short-lived radionuclides increased the self-charging rates of the particles, thus accumulating more positive charges. Despite

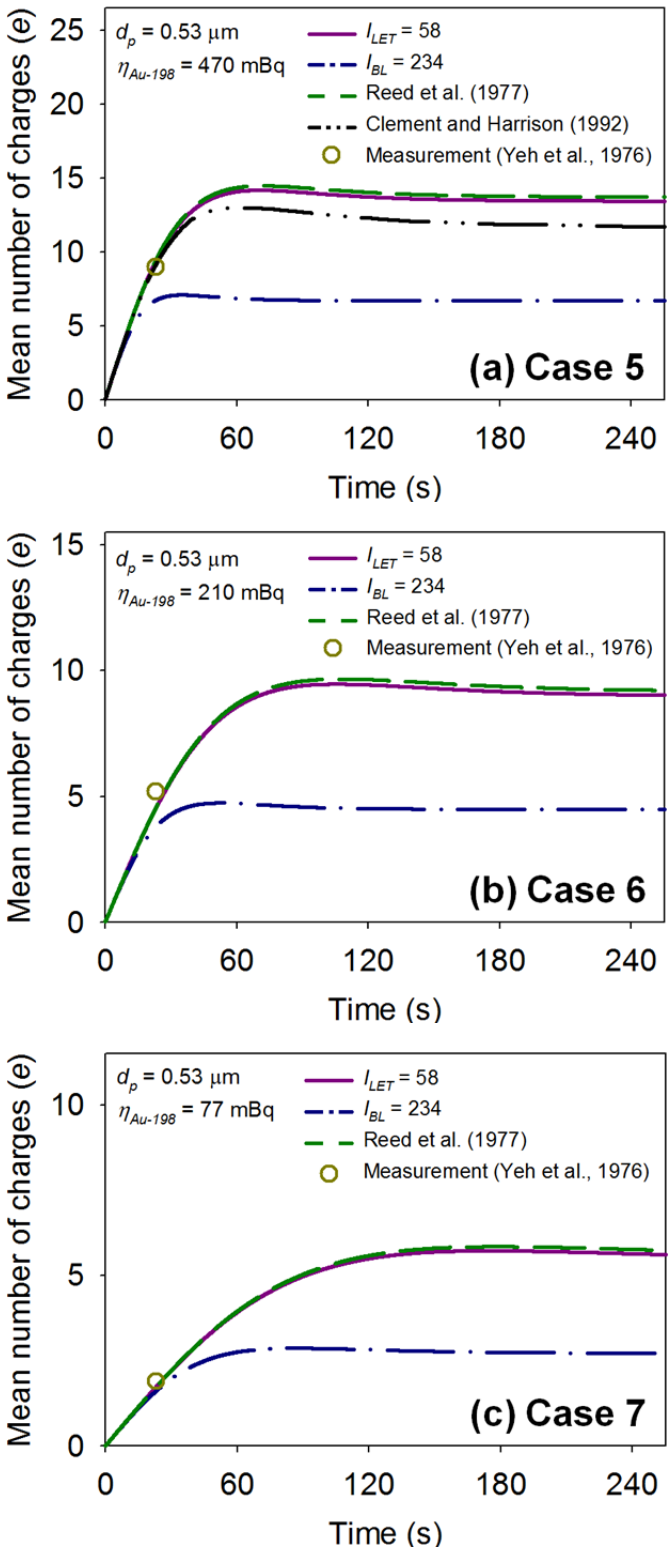

Figure 3.2. Charge accumulation rate for Cases 5-7: (a) Case 5, (b) Case 6, and (c) Case 7.

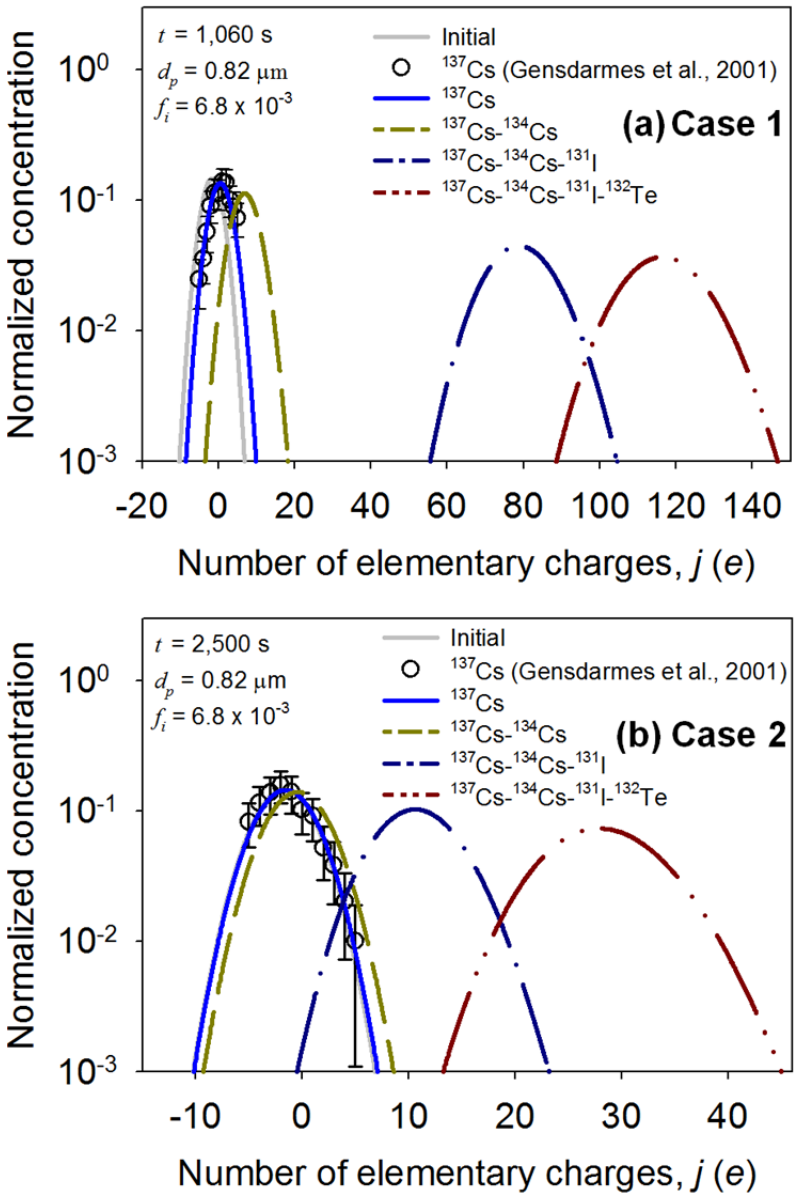

Figure 3.3. Charge distributions of particles containing short- and long-lived radionuclides: (a) Case 1 and (b) Case 2.

differences in ionization rate coefficients, the ^{137}Cs particles accumulated more positive charges as the half-life of the added radionuclides was much shorter ($^{132}Te > ^{131}I > ^{134}Cs$). As more ion pairs were created, the positively charged radioactive particles were effectively neutralized due to the diffusion of more negative ions (Cases 1 vs. 2). Particles of lower mole fraction of radioactive elements accumulated fewer positive charges, but the effects of the contained short-lived radionuclides persisted (Cases 1 vs. 3 and 2 vs. 4; data not shown). These results suggest that the type, amount, and ionization rate coefficient of radionuclides contained in particles influence significantly charge accumulation on radioactive particles.

3.3.3. Charge Accumulation on Particles Containing Radionuclides in Open Air

3.3.3.1. Ionization Rate Coefficient of Beta-emitting Radionuclides in Dry Air

The ionization rate coefficient of various beta-emitting radionuclides in dry air was estimated using the LET approach. Energetic electrons can freely travel until their energy is completely dissipated. Compared to confined spaces (e.g., Case 1), the path length of energetic electrons can be maximized in open spaces, which can affect results of the LET approach (eq 3.2). Thus, the validity of the Katz and Penfold relationship (eq 3.4) was evaluated using the generalized semi-empirical range–energy relationship for monoenergetic electrons (Tabata et al., 1972) and the continuous-slowing-down approximation (CSDA) (ICRU, 1984) which can compute the mean path length of electrons in dry air. For various radionuclides released from the Chernobyl and Fukushima accidents, the range of energetic electrons given by eq 3.4 was similar to that by CSDA as well as that by the relationship for monoenergetic electrons (Figure 3.4), suggesting that the Katz and Penfold relationship can be used to approximate the mean path length of electrons in dry air. Table 3.2 shows the ionization rate coefficient of various beta-emitting radionuclides estimated using the LET approach with the Katz and Penfold relationship.

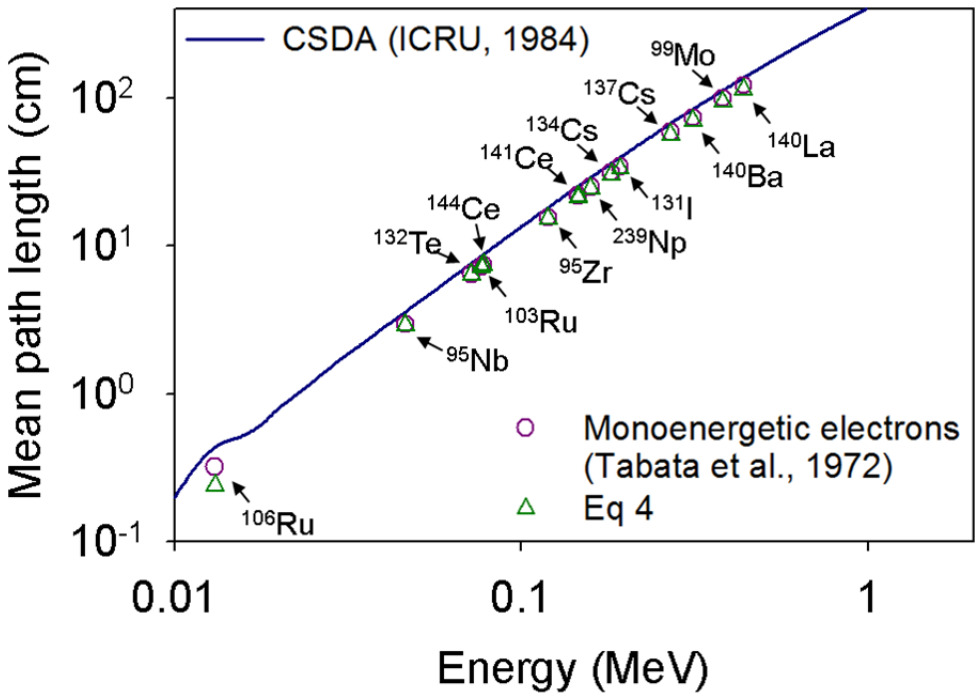

Figure 3.4. Mean path length of electrons emitted during beta decay of various radionuclides in dry air.

Table 3.2. Ionization rate coefficient of various beta-emitting radionuclides in dry air (Temperature = 295 K; Pressure = 100 kPa).

Radionuclide	Half-life	Energy of electrons (MeV)		Mean path length of electrons (cm)	Ionization rate coefficient, I
		E_{max} [a]	E_{mean} [b]		
^{95}Zr	64.032 d	0.3960	0.1191	15.35	1,261
^{95}Nb	34.991 d	0.1600	0.0463	2.91	472
^{99}Mo	2.7489 d	1.1800	0.3803	93.93	4,323
^{103}Ru	39.26 d	0.2294	0.0765 [c]	7.19	800
^{106}Ru	373.59 d	0.0394	0.0131 [c]	0.24	110
^{132}Te	3.204 d	0.2150	0.0717 [c]	6.41	748
^{131}I	8.01 d	0.6080	0.1812	30.43	1,945
^{134}Cs	2.0652 yr	0.6620	0.1581	24.45	1,688
^{137}Cs	30.16 yr	0.5140	0.1921	33.39	2,067
^{140}Ba	12.752 d	1.0200	0.2690	56.22	2,956
^{140}La	1.6781 d	1.3600	0.4360	114.30	5,041
^{141}Ce	2.508 d	0.4350	0.1453	21.32	1,547
^{144}Ce	284.91 d	0.3200	0.0778	7.41	814
^{239}Np	2.356 d	0.4380	0.1460[c]	21.49	1,554

[a] Mantel (1972) and Martin (2000).

[b] E_{mean} of radionuclides was obtained via Mantel (1972) except for ^{103}Ru, ^{106}Ru, ^{132}Te, and ^{239}Np.

[c] It was assumed that $E_{mean} = 1/3E_{max}$ (Cooper and Reist, 1973).

3.3.3.2. Charge Distribution of Radioactive Particles in Open Air

3.3.3.2.1. Testing the Validity of the Assumption of Greenfield (1956)

Charge accumulation on particles containing radionuclides was investigated under the ionization condition of Greenfield (1956), who showed that up to 75% of monodispersed radioactive particles ($\eta \approx 0.118$ Bq, $I = 15{,}000$, $N_t = 3.55 \times 10^{10}$ particles m^{-3}) are neutralized due to beta radiation. Figure 3.5 shows the steady-state number fraction of the charged and uncharged radioactive particles under the ionization condition of Greenfield (1956): $q_I = \eta I N_t = 6.3 \times 10^{13}$ ion pairs m^{-3} s^{-1}. The numbers of the positively and negatively charged particles were similar because of the symmetric particle charge distribution. Despite surface charge neutralization caused by beta radiation, more charged radioactive particles were generated at 250 K than estimated by Greenfield (1956). A similar result was obtained for 295 K. These discrepancies mainly resulted from the ion-particle attachment coefficient in eqs 3.6-3.8. We used the typical values of the ion-particle attachment coefficient in the lower atmosphere (e.g., $\beta_{-1}^{+} = \beta_{+1}^{-}$ = 2.7×10^{-12} m^3 s^{-1} and $\beta_0^{\pm} = 1.5\times10^{-12}$ m^3 s^{-1} at 250 K; $\beta_{-1}^{+} = \beta_{+1}^{-} = 3.2\times10^{-12}$ m^3 s^{-1} and $\beta_0^{\pm} = 1.9\times10^{-12}$ m^3 s^{-1} at 295 K), while Greenfield assumed that $\beta_{-1}^{+} = \beta_{+1}^{-} = 6\times10^{-12}$ m^3 s^{-1} and $\beta_0^{\pm} = 10^{-12}$ m^3 s^{-1} at 250 K. The values of the attachment coefficient estimated by Greenfield are beyond the typical range of values suggested more recently by many researchers (Harrison and Carslaw, 2003; Hoppel and Frick, 1986). The difference in the values of the ion-particle attachment coefficient resulted in dissimilar charge accumulation and neutralization rates of the radioactive particles, leading to the discrepancies mentioned above. The results of this study suggest that many radioactive particles can be charged despite the occurrence of charge neutralization induced by beta radiation in open air.

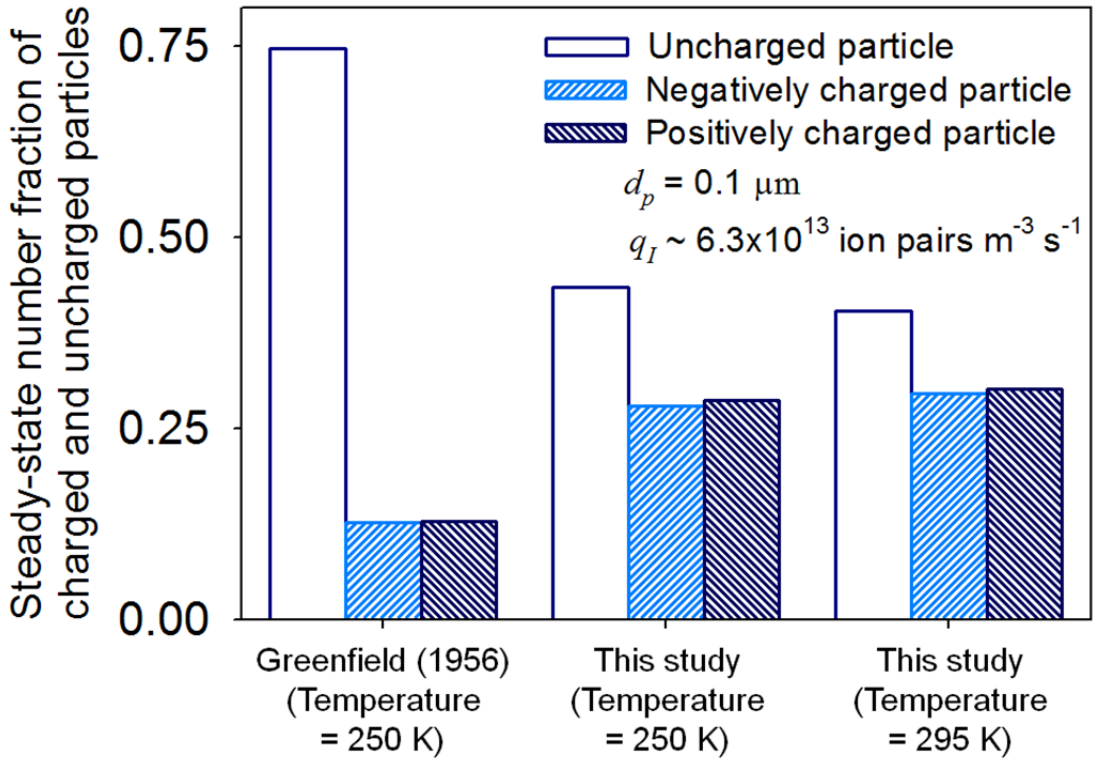

Figure 3.5. Steady-state number fraction of charged and uncharged radioactive particles under the ionization condition of Greenfield (1956).

3.3.3.2.2. Effects of Radioactive Particles on Particle Charge Distribution in the Atmosphere

The Chernobyl accident released many particles containing beta-emitting radionuclides into the atmosphere. During short- and long-range transport, the radioactive particles became charged and ionized air molecules, thereby affecting the particle charge distribution in the atmosphere. Thus, effects of the Chernobyl radioactive particles on the particle charge distribution in the atmosphere were investigated here, using the charge balance model.

For single particle composition, we used observations of Devell et al. (1986) who measured properties of individual Chernobyl radioactive particles. Hereafter, we refer to the radioactive particles by Ch1, Ch2, and Ch3: Ch1 contained ^{103}Ru, ^{99}Mo, ^{106}Ru, ^{132}Te, and ^{131}I; Ch2 involved ^{103}Ru, ^{106}Ru, ^{132}Te, and ^{131}I; Ch3 consisted of ^{106}Ru, ^{131}I, ^{140}Ba, ^{140}La, ^{95}Zr, ^{95}Nb, ^{141}Ce, ^{144}Ce, and ^{239}Np. The radioactivity of each radionuclide was given by Devell et al. (1986). The total radioactivity of Ch1, Ch2, and Ch3 was 15,280 Bq, 8,780 Bq, and 2,740 Bq, respectively. The size distribution of background aerosols (BA) was obtained from Trier (1997). It was assumed that (i) the monodispersed Chernobyl radioactive particles were mixed with BA, (ii) their total particle number concentrations were similar, and (iii) all particles were initially neutralized. The charge balance equation was defined for each particle group and all equations were solved simultaneously. The ionization rate coefficients shown on Table 3.2 were used to calculate $q_{I,i}$ in eqs 3.7 and 3.8. Some typical values used in simulation were obtained from Harrison and Carslaw (2003) by assuming the fair-weather atmosphere (e.g., q_b = 10^7 ion pairs m^{-3} s^{-1} and $\alpha_{rc} = 1.6\times10^{-12}$ m^3 s^{-1}.)

Figure 3.6 shows the steady-state particle charge distributions in fair-weather atmosphere involving various Chernobyl radioactive particles. Beta radiation caused by the radioactive particles generated numerous ion pairs in the atmosphere. The ions were rapidly captured by the background aerosols and the particles quickly obtained a

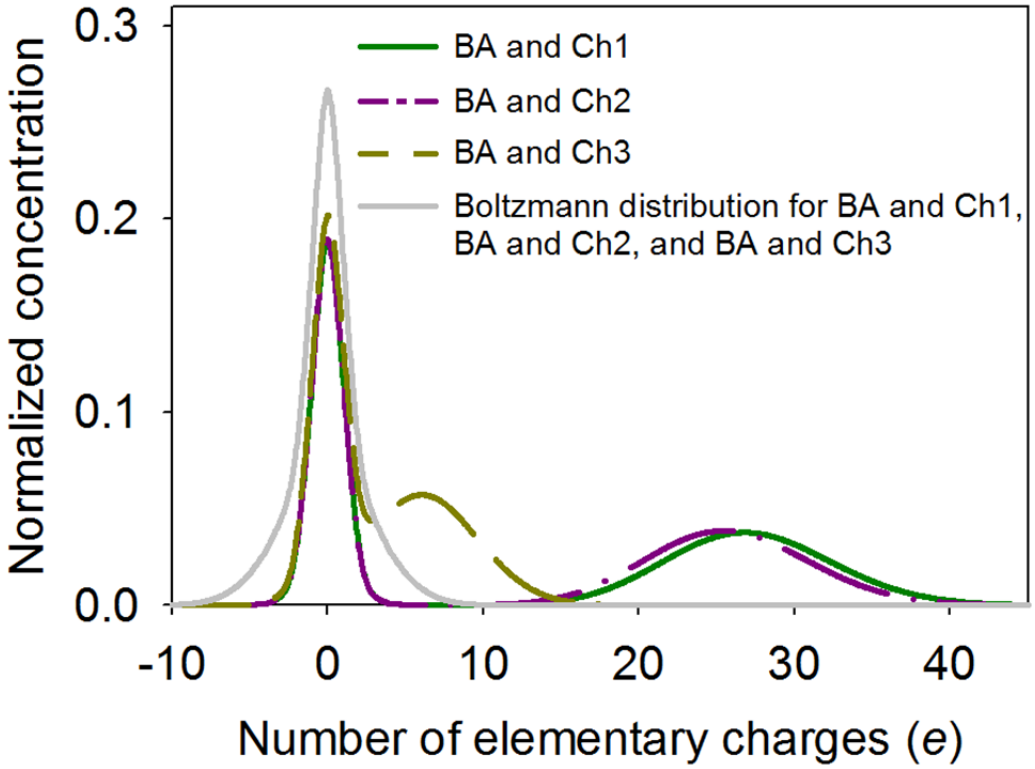

Figure 3.6. Particle charge distributions in fair-weather atmosphere containing various Chernobyl radioactive particles (Ch1, Ch2, and Ch3; d_p = 1 μm). The geometric mean diameter, d_g and geometric standard deviation σ_g of the background aerosols (BA) are 0.116 μm and 1.46, respectively (Trier, 1997). $N_{BA} = N_{Ch1} = N_{Ch2} = N_{Ch3} = 6.718 \times 10^9$ particles m^{-3}.

unimodal symmetrical charge distribution (i.e., the Boltzmann distribution). However, despite ionization induced by beta radiation, most Chernobyl radioactive particles accumulated more positive than negative charges because of the self-charging mechanism. The presence of the positively charged particles produced asymmetric bimodal particle charge distributions in the atmosphere. When the self-charging mechanism was neglected, all particle charge distributions became Boltzmann distributions.

The particle charge distributions in fair-weather atmosphere involving radioactive particles were investigated using polydispersed conditions. We assumed ammonium sulfate particles carrying ^{103}Ru, ^{99}Mo, ^{106}Ru, ^{132}Te, and ^{131}I which correspond to the radioactive composition of Ch1. Radioactivity of single particles was calculated using eq 1. The initial size distribution of polydispersed radioactive particles was obtained from Tripathi and Harrison (2001).

Figure 3.7 shows the steady-state particle charge distributions in the atmosphere containing the polydispersed radioactive particles. For all cases, the particle charge distribution was different from the Boltzmann distribution. Some particles were highly radioactive and accumulated many positive charges until reaching steady state. As the mole fraction of the radionuclides increased, the number of highly radioactive particles increased and thus, more positively charged particles were generated. If the mole fraction of the radionuclides is similar, large particles can contain more radionuclides than small particles (eq 1). Thus, the self-charging rate of single radioactive particles was dissimilar for different-size particles, and this led to the creation of the asymmetric multimodal particle charge distributions in the atmosphere.

In the simulations, we assumed similar ion mobilities for positive and negative ions, which correspond to those in fair-weather atmosphere (Harrison and Carslaw, 2003), but positive ions are typically less mobile than negative ions (Clement and Harrison, 1992; Hoppel and Frick, 1986; Gensdarmes et al., 2001). However, the asymmetric bi- and multi-modal charge distributions created by the Chernobyl radioactive particles were

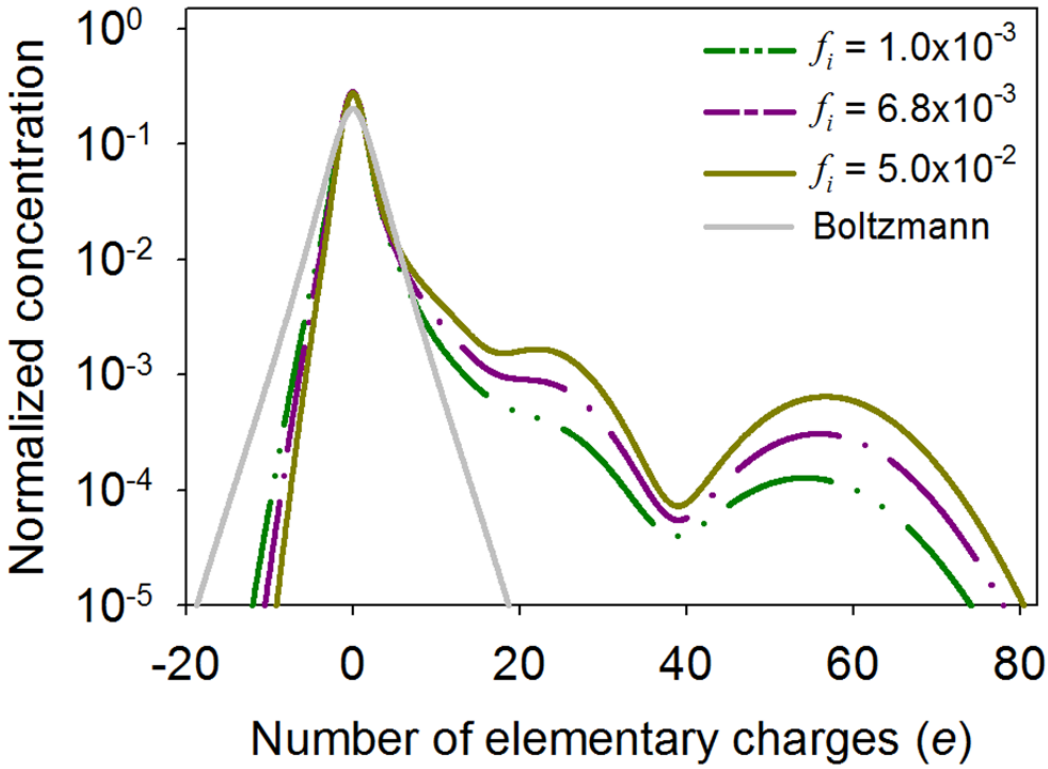

Figure 3.7. Particle charge distributions in fair-weather atmosphere containing background aerosols and particles containing ^{103}Ru, ^{99}Mo, ^{106}Ru, ^{132}Te, and ^{131}I. $d_{g,BA}$ = 0.116 μm, $\sigma_{g,BA}$ = 1.46, $d_{g,Ch1}$ = 0.52 μm, $\sigma_{g,Ch1}$ = 2.4, and $N_{BA} = N_{Ch1} = 6.718 \times 10^{9}$ particles m^{-3}.

maintained for both equal and unequal ion mobilities of positive and negative ions (data not shown).

In fair-weather atmosphere, where cosmic ray and natural radioactivity are major ionization sources, the time needed to reach a steady-state charge distribution can be delayed due to low ion concentrations (Yair and Levin, 1995), but for all cases, the steady-state particle charge distribution was attained within a few seconds due to the rapid ionization by beta radiation. Thus, other processes, such as aggregation, may not affect the steady-state charge distributions caused by the Chernobyl radioactive particles because of the short simulation time, as well as the low particle concentrations. Effects of aggregation on the particle charge distributions should be evaluated if timescale to reach the steady-state particle charge distributions is long or particle concentrations are high. These results suggest that radioactive particles can significantly influence the particle charge distributions in the atmosphere during short- and long-range transport.

3.3.2.3. Possible Effects of Radioactive Particles on Transport of Radioactivity and Atmospheric Electricity

Charge accumulation on radioactive particles can significantly influence short- and long-range transport of radioactivity because it induces strong electrostatic interactions. The generation of an asymmetric bimodal particle charge distribution would produce strong electrostatic particle-particle interactions, which would greatly affect particle growth (Matsoukas, 1997; Oron and Seinfeld, 1989a, 1989b). For example, positively charged radioactive particles may attract negatively charged background aerosols. Additionally, radioactive particles can favorably interact with raindrops due to the electrostatic image force generated between them. Recent experiments of Walker et al. (2010) suggested that radioactivity increased the adhesion force between a charged particle and a conductive surface through the generation of the attractive image force. Radioactive surfaces can be charged at humid conditions (Kweon et al., 2013) and the

surface charge of the particles in the proximity of raindrops can generate an attractive electrostatic image force (Tripathi and Harrison, 2001). Thus, the scavenging rate of charged radioactive particles may be enhanced by radioactivity-induced electrostatic interactions. Hence, the dry and wet deposition rates of radioactive particles may be significantly affected by electrostatic interactions caused by radioactivity.

During atmospheric transport, radioactive particles can significantly influence the electrical properties of the local atmosphere because they can ionize air molecules. Table 3.3 shows changes in electrical properties of the local atmosphere by radioactive particles measured after nuclear events, including the Chernobyl accident. During short- and long-range transport, radioactive particles were accumulated on ground surfaces via various mechanisms, such as thundershower, and dry and wet deposition. For example, radioactive particles flying at 5-km altitude were carried to ground surfaces by thundershower (Harris, 1955). Ionization induced by the radioactive particles increased ion concentrations near ground surfaces and this led to changes in electrical properties of the local atmosphere. High ion concentrations increased the electrical conductivity of the local atmosphere to much higher than normal levels. This could result in short-circuiting of the electric field (Israelsson and Knudsen, 1986; Israelsson et al.,1987), thereby decreasing potential gradient and space charge in the local atmosphere. The duration time of these effects may depend on radioactivity in air and on ground surfaces because radioactive particles can be transported to other places by various processes, such as runoff (Israelsson and Knudsen, 1986) and wind-driven resuspension (Yamauchi et al., 2012).

Table 3.3. Changes in electrical properties of the local atmosphere by transported radionuclides.

Nuclear events	Emission sources	Observations	Distance from emission sources	Major transport mechanisms (from the local atmosphere to ground level)	Electrical conductivity [a]	Potential gradient [a]	Space charge [a]	Reference
Weapon tests	Nevada, USA	Tucson, USA	850 km	Thundershower	10 times increase	6 times decrease	-	Harris (1955)
Nuclear plant accidents	Chernobyl, Ukraine	Uppsala, Sweden	1,300 km	Wet deposition	11 times increase	10 times decrease	10 times decrease	Israelsson and Knudsen (1986)
		Athens, Greece	1,500 km	Dry deposition	7 times increase	2 times decrease	-	Retalis and Pitta (1989)
		Vantaa, Finland	1,050 km	Dry and wet deposition	10 times increase	10 times decrease	-	Tuomi (1989)
	Fukushima, Japan	Kakioka, Japan	150 km	Dry and wet deposition	-	10 times decrease	-	Takeda et al. (2011)
		Kakioka, Japan	150 km	Dry and wet deposition Resuspension	-	10 times decrease	-	Yamauchi et al. (2012)

[a] Changes in electrical properties were obtained by comparing maximum or average values for observations with normal levels of observation locations.

After the Chernobyl accident, abnormal lightning activity was observed at contaminated radioactive sites in Sweden (Israelsson et al., 1987). Lightning flashes of the contaminated sites significantly increased for a few months after the accident. The average lightning frequency of the contaminated sites was up to five times higher than that of low-radioactivity sites. Israelsson et al.(1987) suggested that the observations of lightning activity enhancement may be attributed to ionization caused by radioactivity.

3.4. Summary

In case of a nuclear plant accident, accurate prediction of radioactivity transport is crucial in evaluating environmental and health risks caused by radioactive contamination. Electrostatic interactions can be important in simulating various atmospheric processes, but they are typically neglected in modeling studies of radioactivity transport. This study has shown that radioactivity can induce surface charge accumulation of radioactive particles and background aerosols, significantly influence the particle charge distribution in open air, and change the electrical properties of the local atmosphere. Based on the charging behavior of radioactive particles and the expected influence of radioactivity-induced charge on particle interactions with other particles, raindrops, and other environmental surfaces, electrostatic interactions should be considered in predictive studies of short- and long-range radioactivity transport.

3.5. Acknowledgements

This chapter involves contributions from coauthors and was published in: Kim, Y-H., Yiacoumi, S., Tsouris, C. 2015a. Surface charge accumulation of particles containing radionuclides in open air. *J. Environ. Radioactivity*, 143, 91-99.

CHAPTER 4

INFLUENCE OF RADIOACTIVITY ON SURFACE CHARGING AND AGGREGATION KINETICS OF PARTICLES IN THE ATMOSPHERE

Radioactivity can influence surface interactions, but its effects on particle aggregation kinetics have not been included in transport modeling of radioactive particles. In this chapter, experimental and theoretical studies have been performed to investigate the influence of radioactivity on surface charging and aggregation kinetics of radioactive particles in the atmosphere. Radioactivity-induced charging mechanisms have been investigated at the microscopic level, and heterogeneous surface potential caused by radioactivity is reported. The radioactivity-induced surface charging is highly influenced by several parameters, such as rate and type of radioactivity decay. A population balance model, including interparticle forces, has been employed to study the effects of radioactivity on particle aggregation kinetics in air. It has been found that radioactivity can hinder aggregation of particles because of similar surface charging caused by the decay process. Experimental and theoretical studies provide useful insights into the understanding of transport characteristics of radioactive particles emitted from severe nuclear events, such as the recent accident of Fukushima, or deliberate explosions of radiological devices.

4.1. Introduction

Radioactive particles can be generated by either natural or anthropogenic sources in the atmosphere. Anthropogenic sources, such as nuclear plant accidents or explosions

of radiological dispersal devices, can be more harmful to humans and the environment because of potentially high concentrations and radioactivity levels of the resulting particle plumes. Serious human exposure to radioactive particles from the Chernobyl and Fukushima nuclear accidents occurred both locally and globally through dry deposition and inhalation (Levi, 1991; Hoeve and Jacobson, 2012). For example, small radioactive particles, including ^{131}I and ^{137}Cs, released from the Fukushima nuclear accident, were spread throughout the world within a few weeks (Masson et al., 2011), threatening the health and safety of both local and global populations and environment systems (Hoeve and Jacobson, 2012; Yoshida and Kanda, 2012; Parache et al., 2011; Manley et al., 2012). Thus, understanding radioactive particle transport in the atmosphere is needed to predict particle distribution in the environment and to minimize the risk of human and animal exposure to radioactivity.

Predicting changes in the size distribution of radioactive particles is essential to understanding their transport characteristics in the atmosphere (Kaneyasu et al., 2012). Particularly, aggregation of particles is important because it leads to radioactivity transport at shorter rather than longer distances. Theoretical studies have been conducted to calculate aggregation rates of radioactive particles (Simons, 1981; Park and Lee, 1988; Alipchenkov et al., 2009). The basic assumption in those studies was that effects of radioactivity on the interaction of particles are insignificant because the particles can be neutralized in a high radiation field (Cooper and Reist, 1973; Walker et al., 2010). This assumption arises from consideration of the source term in a reactor accident where the radiation fields are high. Thus, the effects of radioactivity on interparticle forces among radioactive particles or between radioactive and nonradioactive particles have not been taken into account in modeling (Hoeve and Jacobson, 2012; Dvorzhak et al., 2012). However, particles containing radionuclides interact with each other and with surfaces during transport and deposition, phenomena that are not accurately predicted by conventional plume transport modeling (e.g., Kashparov et al., 2000). The assumption

that the particles do not change during deposition can add to the uncertainty of predicting the effect of radioactivity on the charging of environmental surfaces.

Although ignored in source term calculations, effects of radioactivity on surface charging have been studied for several decades (Kweon et al., 2013; Yeh et al., 1976; Gensdarmes et al., 2001; Subramanian et al., 2012). Measurement methods to study particle size and charge, such as cascade impactors and electrostatic separators, have been employed to investigate the distribution or the mean number of charges of a radioactive particle population. These studies have indicated that the radioactive particles can be negatively or positively charged by radioactivity through such mechanisms as electron emission or ion diffusion according to their decay pathways. Few studies have been performed, however, to verify such mechanisms of a single radioactive particle at the micron-scale where the influence of electrostatic forces on surface interactions becomes important.

The hypothesis motivating this study is that aggregation kinetics of radioactive particles can differ from those of nonradioactive particles in the atmosphere due to radioactivity-induced surface charging. Microscopic measurements using scanning surface potential microscopy (SSPM) were performed to investigate radioactivity-induced surface charging of a single radioactive particle. A population balance model was subsequently employed to predict aggregation rates of radioactive particles in the atmosphere.

4.2. Materials and Methods

4.2.1. Experimental Section

4.2.1.1. SSPM measurements

SSPM was employed to analyze the surface charging caused by radioactivity because of the high sensitivity of this technique to changes of surface potential or surface

charge (Bhushan and Goldade, 2000; Lee, 2007). The experimental setup for SSPM measurements was introduced into a radioactive control area at the Oak Ridge National Laboratory. A surface topography trace was followed immediately by a second, spatially elevated, trace for measurements of the electrical potential at a height of 50 nm above the sample surface. The surface topography trace along with the corresponding SSPM map was recorded on a raster-by-raster basis to form three-dimensional maps. Various DC step voltages of 10-mV interval provided a constant voltage source correlated with the electrical-potential image map of the structures obtained with SSPM. The SSPM was calibrated with specially prepared surface structures. The standard deviation from the calibration data and the minimum detection limit were 0.79 mV and 1 mV, respectively.

4.2.1.2. SSPM Measurements of Nonradioactive Materials Irradiated by ^{210}Po

Polonium-210 (^{210}Po), whose half-life is 138 days, was used in this part of the study because it is readily available in a commercial device. Two Au substrates were used to measure changes in the surface potential of nonradioactive materials irradiated by ^{210}Po. The substrate Au{111} is epitaxially grown on mica, while amorphous Au film was deposited on a glass slide using Cr as an intermediate adhesive layer. Surface potential measurements of the Au substrates were performed under constant ^{210}Po irradiation at various locations ranging from approximately 4 to 7 cm from the substrate (Figure A.1). The ^{210}Po source was protected by a metal grid located approximately 0.5 cm from the source. Because of geometrical constraints, namely the protective encapsulation of the polonium source and the restricting geometry of the SSPM head, the shortest possible distance between the ^{210}Po source and the substrate was approximately 4 cm. Both Au substrates were characterized by SSPM before and after the radiation treatment. The irradiation experiments for Au/Cr were repeated after 98 days and for Au{111} were repeated after 96 days, to obtain data related to the influence of the source strength.

4.2.1.3. SSPM Measurements of Radioactive Materials

SSPM measurements of radioactive particles were obtained using cesium-137 (^{137}Cs). To minimize the contamination in the laboratory, particles of ammonium molybdophosphate (AMP), mixed with zirconium hydrogen phosphate (ZrHP) at 50/50 wt%, were chosen as a Cs sorbent. AMP/ZrHP particles were prepared by using a sol gel method (ORNL, 2001). Multiple AMP/ZrHP particles were then mounted in Crystalbond^{TM} (Ted Pella. Inc., Redding, CA) on an AFM coupon and polished to a surface finish of 1 to 3 μm to secure them in place for dosing with ^{137}Cs and for surface analysis (Figure 4.1). The sample was layered with the metal base covered with a quartz coupon to ensure electrical isolation. ^{137}Cs uptake of AMP/ZrHP particles was accomplished by contact with dilutions of a 1-μCi/mL spiked solution. The uptake appeared to reach steady state after 48 hours of contact at 25°C and averaged approximately 8±1% (Table A1). The average uptake for these particles appears to be much lower than reported in the literature (ORNL, 2001*)*, but the radioactivity of the prepared samples was found to provide sufficient signal for the SSPM measurements. ^{133}Cs was used with ^{137}Cs to control the radioactivity level of the particles. A blank was prepared that had not been contacted with the ^{137}Cs spiked solution, but all other steps of sample preparation were the same.

4.2.2. Theoretical Section

4.2.2.1. Charging of Radioactive Particles

Charging of the radioactive particles is mainly caused by different decay types emitting alpha and beta particles and positive and negative ions which cause self-charging and diffusion charging (Yeh et al., 1976; Reed et al., 1977; Clement and Harrison, 1992; Clement et al., 1995; Gensdarmes et al., 2001; Subramanian et al., 2012). Based on the charging mechanisms, the mean number of charges *J* carried by a radioactive particle can be obtained by using the charge balance equation

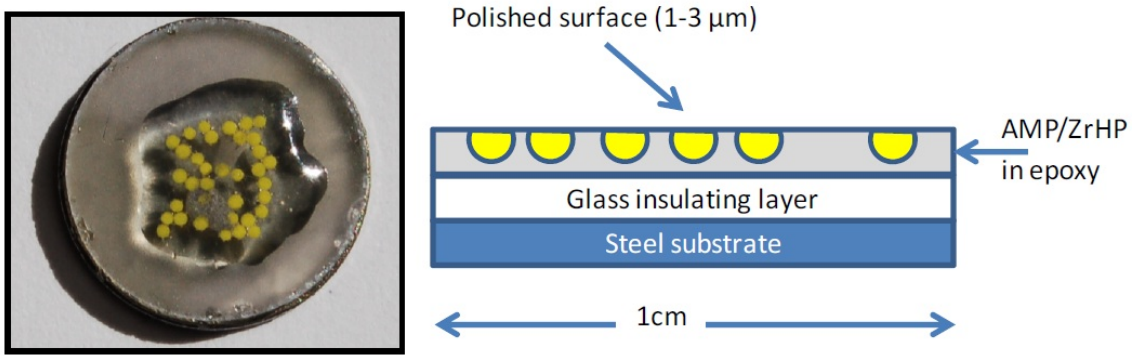

Figure 4.1. AMP/ZrHP microspheres mounted in Crystalbond™ and polished to a 1-micron surface finish. The spheres are 300-800 microns in diameter, and the sample assembly is 1-cm diameter.

(Reed et al.,1977; Clement and Harrison, 1992; Clement et al., 1995):

$$\frac{dJ_k}{dt} = sA_k + \beta^+_{k,J} n_+ - \beta^-_{k,J} n_- \tag{4.1}$$

where $\beta^+_{k,J}$ represents the ion-particle attachment coefficients, $n_\pm$ is the ion concentration, s is the number of residual charges left on a particle per decay, and A is radioactivity.

The first and second terms on the right-hand side represent the net capture rates of positive and negative ions. The third term represents the number of positive charges left on the radioactive particle during the decay process. The emitted beta particles are considered as negative ions. Equation 4.1 can apply for both alpha and beta decay (Reed et al., 1977; Clement and Harrison, 1992).

Equation 4.1 can be solved by using numerical or iterative methods, but such solutions are computationally intensive. To reduce the computational time, an approximate solution of the charging equation (Clement et al., 1995), derived for the beta decay at steady state, was given as:

$$J_k = \begin{cases} y - \left(\dfrac{y(X-1)}{\exp(2\omega y) - 1} \right) & \omega y > 0.22 \quad (4.2a) \\ y + \dfrac{X-1}{2\omega} & \omega y \le 0.22 \quad (4.2b) \end{cases}, \tag{4.2}$$

with $\omega = \dfrac{e^2}{8\pi\varepsilon_0 \varepsilon r_k k_B T}$, $y = \dfrac{\varepsilon_0 A}{e\mu_- n_0}$, $A = \eta_0 r_k^3$, $n_0 = \left(\dfrac{IAZ + q}{\alpha} \right)^{0.5}$, $X = \dfrac{\mu_+ n_+}{\mu_- n_-}$,

where e is the eletrical charge, ε_0 is the permittivity of vacuum, r_k is the particle radius, k_B is the Boltzmann constant, T is the temperature, $\mu_\pm$ is the ion mobility, n_0 is the mean ion concentration, η_0 is the specific radioactivity, I is the number of ion pairs produced per

decay, Z is the particle concentration, q is the bipolar ion production rate, and α is the recombination rate.

In equation 4.2, the mean number of charges is mainly determined by three parameters: the parameter ω that is inversely proportional to size, the ion asymmetric parameter X between the negative and positive ion flux, and the self-charging parameter y. It should be noted that the calculation of y is based upon the charges left on the particle surface per decay and the negative ion concentration. Equation 4.2 can apply for both radioactive and nonradioactive particles (Clement et al., 1995).

4.2.2.2. Population balance model

A population balance model in its discrete form was employed to predict changes in the size distribution of radioactive particles as a function of time t. A simple population balance model can be formulated in the following form:

$$\frac{dN_k}{dt} = \frac{1}{2}\sum_{i+j=k} F(i,j)N_i N_j - \sum_{j=1}^{\infty} F(k,j)N_k N_j \,, \tag{4.3}$$

where N_k represents the number concentration of size k particles and F is the aggregation frequency of two colliding particles. The first term on the right-hand side represents the production of size k particles by aggregation of smaller particles i and j. A factor of 1/2 corrects for the double counting of the aggregation of particles i and j. The second term represents the loss of particles k due to aggregation of particles k with any size particles. Changes in the particle size distribution are mainly governed by the aggregation frequency given by multiplying the collision frequency by the collision efficiency.

4.2.2.3. Collision Frequency and Collision Efficiency

The collision frequency and collision efficiency of two colliding particles are determined by transport mechanisms and interparticle forces (Taboada-Serrano et al.,

2005; Chin et al., 1998; Tsouris et al., 1995). For smaller particles under laminar flow, the collision frequency is mainly determined by Brownian motion (Friedlander, 2000), and can be calculated by using equation 4.4:

$$\beta_{Br}(i,j) = \frac{2k_B T}{3\mu_{air}}\left(\frac{1}{r_i} + \frac{1}{r_j}\right)(r_i + r_j) \tag{4.4}$$

where μ_{air} is the fluid viscosity.

Under such conditions, the collision efficiency can be calculated by using equation 4.5 (Spielman, 1970).

$$\alpha_{Br}(i,j) = \left[(1 + \frac{r_j}{r_i}) \int_2^\infty e \exp\left(\frac{V_A + V_R}{k_B T}\right) G^{-1} s^{-2} ds \right]^{-1}, \tag{4.5}$$

where V_A and V_R are Van der Waals and electrostatic potential energy, G is hydrodynamic function, and s is the distance between the centers of the particles.

The London-van der Waals attraction was assumed to compute V_A (equation A1). Particularly, changes in the number and sign of charges are considered in calculating V_R (equation A2) to investigate the radioactivity effects on the aggregation rate of radioactive particles. An analytical solution, derived for air, is employed to estimate G (equation A3) (Alam, 1987).

4.2.2.4. Simulation Scenario and Assumptions

Cesium and iodine are radionuclides emitted into air during nuclear plant accidents (Levi, 1991; Hoeve and Jacobson, 2012; Masson et al., 2011; Yoshida and Kanda, 2012; Parache et al., 2011; Manley et al., 2012; Kaneyasu et al., 2012). We assumed that a plume of CsI particles is released into air, and that the initial particle size distribution may be either monodispersed or log-normal. CsI particles may contain various radioactive isotopes such as ^{131}I, ^{135}I, ^{134}Cs, and ^{137}Cs (Clement and Harrison,

1992). Properties of the radioactive isotopes, initial size of monodispersed radioactive particles, and geometric mean size of log-normal distributed radioactive particles used in this study are shown in Table 4.1.

Lay et al. (*1972*) studied Brownian aggregation of particles with two log-normal initial size distributions having geometric standard deviation (s_g) values of 1.1 and 1.3. The case of s_g = 1.1 was used for all cases in this study to exclude effects of other aggregation mechanisms and reduce the number of discrete size bins and, thus, the computational time. Although the number concentration of emitted radioactive particles may vary in air, a particle concentration of 10^{11} m^{-3} was used as a standard value (See Text A1). For such conditions, steady-state aggregation rates can be accomplished within a few hours (Clement et al., 1995). Other input constants are shown in Table A2.
The level of radioactivity (e.g., decay rate) is determined by the number of active atoms and the isotope half-life. According to Clement et al. (1995), the decay rates of single radioactive particles were calculated by using the specific radioactivity, and were assumed constant for all cases investigating the influence of radioactivity levels on aggregation kinetics. We assumed that during particle emission, charging of radioactive particles occurs rapidly and the particle charge readily reaches steady state because the characteristic time-scale for particle charging is much shorter than that for particle aggregation (Clement et al., 1995). It was also assumed that: (i) beta decay is the dominant charging mechanism, (ii) no breakage of aggregates occurs, (iii) particle aggregates are of spherical shape, and (iv) the ion recombination is the dominant ion removal mechanism.

Table 4.1. Properties of CsI particles.

Isotope	^{131}I	^{135}I	^{134}Cs	^{137}Cs
Half-life (Clement and Harrison, 1992)	8.1 d	6.7 h	2.1 yr	30 yr
Specific radioactivity, η_0 (Bq μm^{-3}) (Clement and Harrison, 1992)	4.4×10^{4}	1.3×10^{6}	9.3×10^{2}	6.4×10^{1}
I *(Ion pairs per decay)* (Clement and Harrison, 1992)	7.7×10^{3}	1.3×10^{4}	6.3×10^{3}	1.1×10^{3}
Initial particle size, d_k (μm) (Initially monodispersed distribution) (Mulpuru et al., 1992)	0.3		0.3	
Geometric mean particle size, d_g (μm) (Initially log-normal distribution) (Kauppinen et al., 1986; Kaneyasu et al., 2012)	0.33		0.63	

4.3. Results and Discussion

4.3.1. Surface Charging by Diffusion of Positive and Negative Ions

The surface potential of both Au{111} and amorphous Au film irradiated by ^{210}Po at various distances and time intervals was measured through SSPM (Figure 4.2). The surface potential of Au{111} irradiated at the nearest location had the highest value, which is also higher than that of amorphous Au irradiated at the same location. The surface potential decreased significantly when the radiation source ^{210}Po moved away, becoming insignificant at 7 cm from the source. Approximately, the surface potential of both Au substrates decreased by 40% as time elapsed up to 98 days. No surface potential changes were measured in control experiments.

The surface potential of both Au substrates was high at 4 cm, but rapidly declined at 5 cm away from the ^{210}Po source. The observations can be attributed mainly to the behavior of the emitted alpha particles, decay products of ^{210}Po, with approximately 5.3 MeV initial kinetic energy. The emitted alpha particles of ^{210}Po collide frequently with gas molecules along their path. These collisions can create 7.6×10^4 ion pairs per decay of ^{210}Po (Table A3). The estimated effective range of the alpha particles was 3.95 cm (Table A3). According to (Holloway and Livingston, 1938; Feather and Nimmo, 1928; Schulze, 1935; Stetter and Jentschke, 1935), at this range, the ionization capability of alpha particles was at a maximum compared to farther distances (Figure 4.2), because most of their kinetic energy was consumed by the ionization around 4 cm (Holloway and Livingston, 1938; Friedlander and Kennedy, 1955). The produced positive and negative ions can be diffused onto the particle surface causing charging. Because beyond this range, the ion concentration might be significantly reduced, the surface potential could be high at 4 cm and then rapidly decreased.

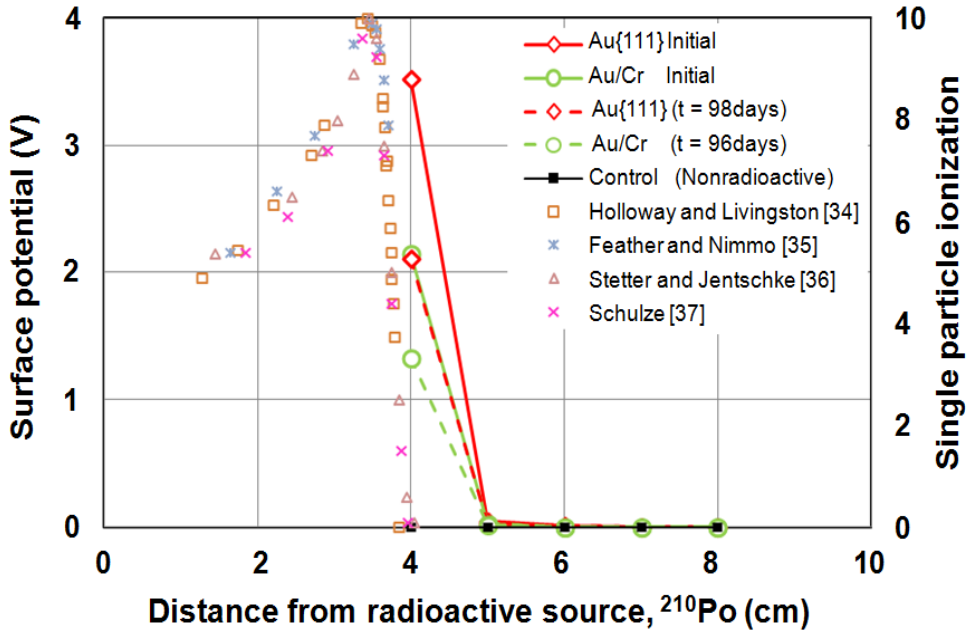

Figure 4.2. Surface potential and single particle ionization in terms of distance from radioactive source. Measurements below 4 cm were not possible with our SSPM setup because of geometrical constraints. Lines with symbols denote surface potential; symbols denote single particle ionization.

The diffusion charging was also influenced by several experimental parameters. The different surface potential of two Au substrates indicates that the structure and ion affinity of the surface may affect the diffusion charging. Moreover, the extent of the surface potential changed by the radioactivity of the system. Because radioactivity-induced ionization becomes weaker as the decay rate decreases, the surface potential of both Au substrates decreased with time. Changes in the surface potential as a function of time were very similar to changes in radioactivity predicted by first-order decay (Figure A.2), indicating that surface charging may be governed by the radioactivity of the system.

These results suggest that emission of radiological debris into air can produce positive and negative ions, causing the charging of nearby suspended particles and thus radioactivity may influence the interaction between particles in air.

4.3.2. Self-charging and Diffusion Charging of Surfaces.

The surface potential of AMP/ZrHP particles loaded with varying levels of ^{137}Cs has been measured to investigate the effects of different decay products on surface charging. Figure 4.3 shows surface potential images and the cross section analysis of a nonradioactive control AMP/ZrHP particle (loaded with ^{133}Cs) obtained by SSPM as discussed in section 4.2.1.3.SSPM measurements of radioactive materials under Materials and Methods. No surface potential changes were measured for the nonradioactive particle, while the potential measurements reached saturation (±10V) for the radioactive particle. The bright and dark colors of the radioactive particle image indicate positively and negatively charged regions, respectively.

The surface potential data were converted to charge density according to (Chung et al., 2010). As can be seen in Figure 4.3, the charge density of the radioactive particle changes dramatically, probably due to surface heterogeneity and localized charging. The locus of the measurements is shown with arrows on the image. Most of the area showed a negative charge density. This heterogeneous charge distribution is the result of the

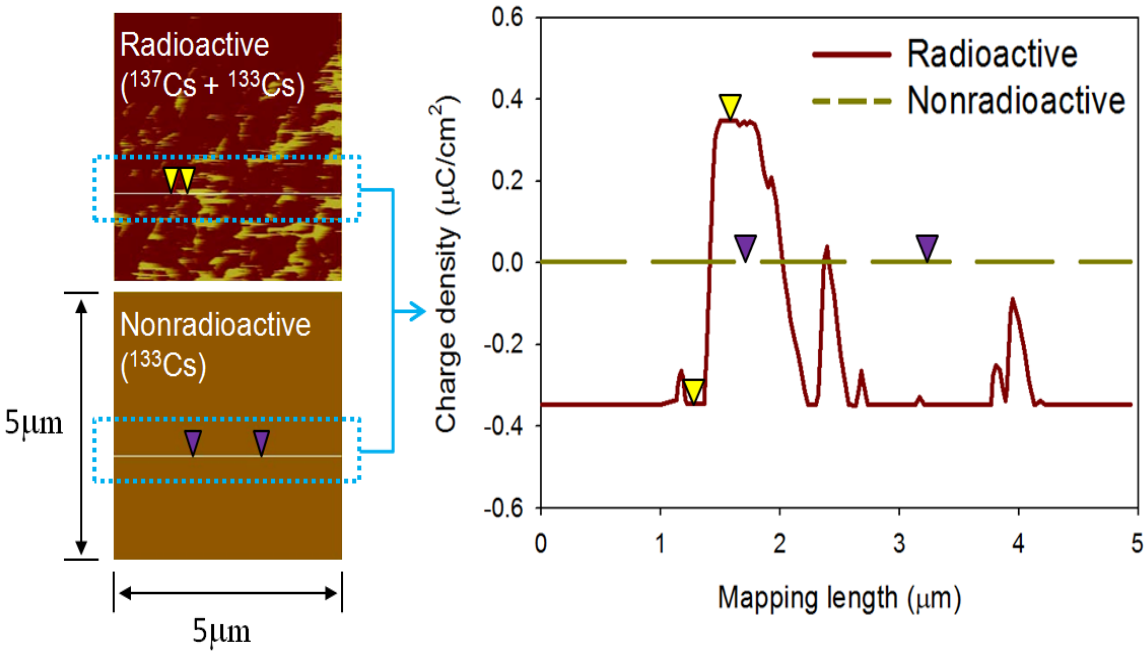

Figure 4.3. Surface charge density of AMP/ZrHP particle loaded with ^{137}Cs and ^{133}Cs (left: surface potential images, right: converted charge density): For the radioactive particle, beta and gamma dose rates were 2.26×10^{-3} Gray hr^{-1} and 5.0×10^{-6} Gray hr^{-1}, respectively. The SSPM limit is ±10 V, corresponding to ±0.35 μC cm^{-2}.

competition of self-charging and diffusion charging caused by the beta and gamma decays of ^{137}Cs (beta dose rate = 2.26×10^{-3} Gray/hr, gamma dose rate = 5.0×10^{-6} Gray/hr).

The surface potential data were converted to charge density according to (Chung et al., 2010). As can be seen in Figure 4.3, the charge density of the radioactive particle changes dramatically, probably due to surface heterogeneity and localized charging. The locus of the measurements is shown with arrows on the image. Most of the area showed a negative charge density. This heterogeneous charge distribution is the result of the competition of self-charging and diffusion charging caused by the beta and gamma decays of ^{137}Cs (beta dose rate = 2.26×10^{-3} Gray/hr, gamma dose rate = 5.0×10^{-6} Gray/hr).

Beta decay of ^{137}Cs emitted electrons leaving behind positive charge. The beta and gamma decays of ^{137}Cs can produce 5.0×10^{3} ion pairs per decay (Table A3) and 275 ion pairs/cm^3/s, respectively (Subramanian et al., 2012). The produced positive and negative ions may simultaneously diffuse onto the surface being self-charged. However, the mobility of negative ions is slightly greater than that of positive ions under standard conditions (Gensdarmes et al., 2001; Subramanian et al., 2012; Clement and Harrison, 1992; Clement et al., 1995; Adachi et al., 1985). Thus, more negative ions diffuse onto the particle surface being positively charged, causing heterogeneity of the surface charge density. A similar behavior was observed during experiments by Gensdarmes and coworkers who reported charge heterogeneity of radioactive particle populations and a higher number of negative ions accumulating on the ^{137}Cs particle surface in air (Gensdarmes et al., 2001).

Since the surface potential of the radioactive particle reached the instrument's measurement limit, a sample with a much lower dose rate (3.8×10^{-5} Gray/hr beta; < 5.0×10^{-6} Gray/hr gamma) was prepared for additional measurements. Using this dose rate, we observed again heterogeneous charge distribution with mostly negative potential and zones of positive potential. However, even at this low decay rate, the surface-potential values were still over the measurement limit of the SSPM instrument. Since the

radioactive particles used in this study were insulators, attached to a dielectric substrate and confined in a matrix, the generated charges would have been trapped in the substrate and accumulated over time. This may be the reason for exceeding the measurement limit of the instrument despite the weak ionization conditions. Studies with materials of lower activity are possible, but may cause difficulties in quantifying ^{137}Cs uptake.

The radioactivity-induced charge can be quantified by solving equation 4.1, which is based on the charging mechanisms. There have been several experimental investigations to verify equation 4.1 by analyzing the mean charge or charge distribution of radioactive particle populations (Yeh et al., 1976; Gensdarmes et al., 2001; Subramanian et al., 2012). Microscopic investigations in this study provide experimental indication of the simultaneous occurrence of the charging mechanisms of individual radioactive particles, which appear as competing terms in equation 4.1.

4.3.3. Model Validation

4.3.3.1. Mean number of charges

The accuracy of the approximate solution was evaluated by using the iterative solution (Clement and Harrison, 1992) and recent experiments (Gensdarmes et al., 2001). All input values for the calculations were set based on the experiments to avoid modification of the experimental data and to minimize the error. Estimated through the approximate solution and Gaussian distribution (equation A8), the charge distribution of the radioactive particles was found in close agreement with the charge distribution obtained experimentally and through the iterative solution (Figure 4.4). Root mean square errors of both solutions were also similar (Table A4).

4.3.3.2. Population balance model

The accuracy of the numerical solution of the population balance model was evaluated for a monodispersed initial distribution by using the Smoluchowski solution

(equation A10). It was assumed that the collision frequency function was constant and that other basic assumptions were similar to those for the simulation scenario discussed earlier in this study. The numerical solution was shown to conserve the mass of the particles. Changes in the cumulative volume fraction predicted by the numerical solution were in good agreement with those predicted by the Smoluchowski solution (Figure A3).

4.3.4. Mean Number of Charges

The mean number of charges carried by a particle was calculated by equation 4.2 (Figure 4.5). The change in the slopes of some of the lines was attributed to using two different solutions for different regimes (equation 4.2). The number of positive charges of all radioactive particles increases as the particle size increases due to the size-dependent decay rate. Particles with a higher level of radioactivity tend to acquire a higher number of positive charges due to the self-charging effect (Yeh et al., 1976), indicating that larger particles can have many charges. Thus, highly radioactive particles may acquire many positive charges (e.g., $^{135}I > ^{131}I > ^{134}Cs > ^{137}Cs$). At a higher particle concentration or highly ionizing conditions, the number of positive charges tends to decrease because of the increased number of negative ions, which can neutralize the positive charge through diffusion charging, as shown in Figure 4.3. Therefore, the determination of the mean number of charges can be significantly influenced by the level of radioactivity and the ion concentration.

In a radiation field generated by highly radioactive particles, the local concentrations of negative and positive ions increase and become similar (Clement et al., 1995). However, negative charge can be added to nonradioactive particles due to different physical properties of ions. Therefore, nonradioactive particles near a radioactive source, such as radioactive particles, may become slightly negatively charged due to diffusion of negative ions (Figure 4.5). Simulation results show that radioactivity causes both

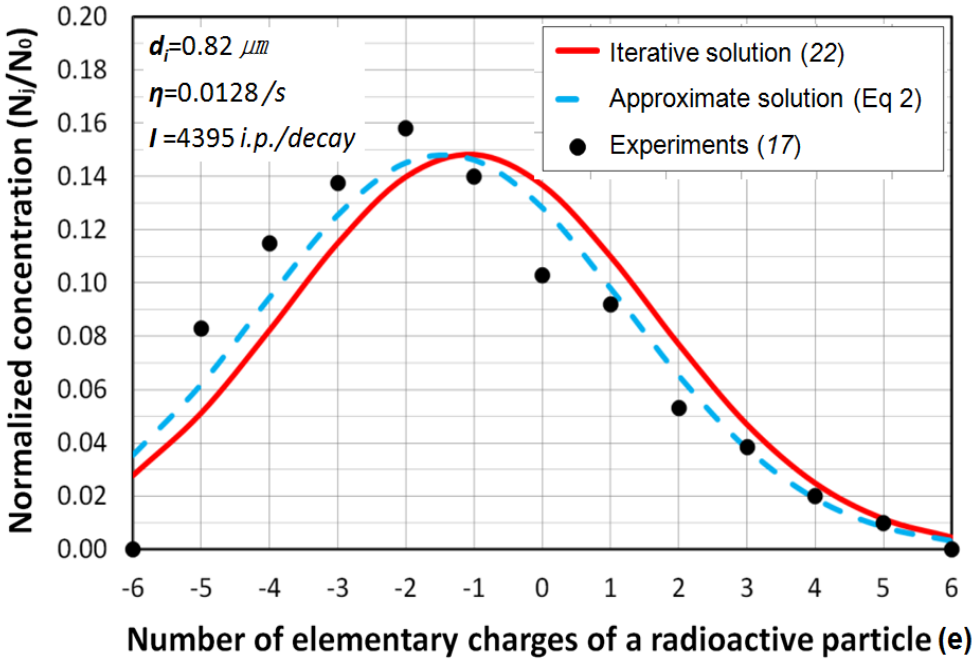

Figure 4.4. Comparison of the charge distribution of radioactive particles obtained from the approximate solution (equation 4.2), the iterative solution (Clement and Harrison, 1992), and experimental data (Gensdarmes et al., 2001).

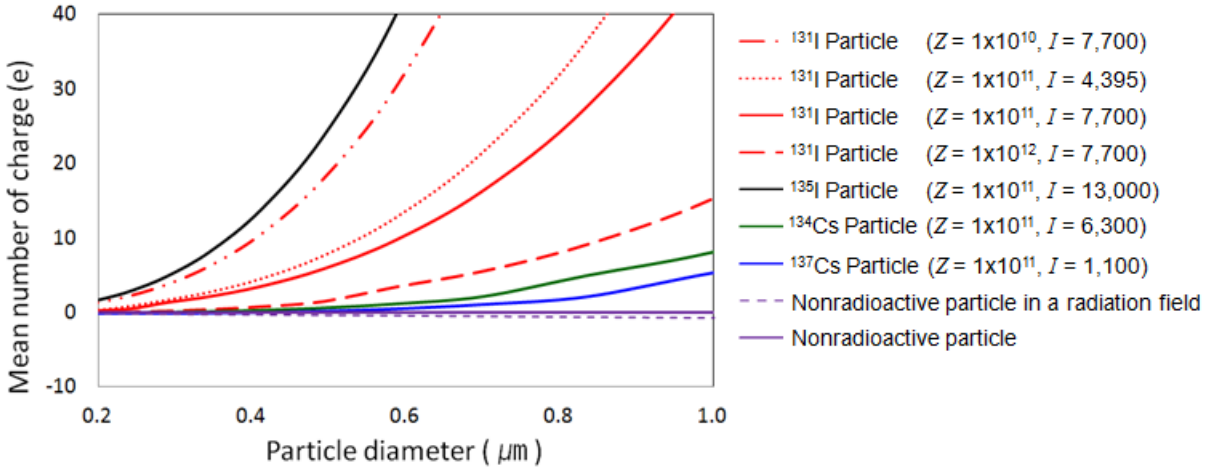

Figure 4.5. The mean number and sign of particle charges as a function of size, radioactivity, and number concentration (the ion concentration of a radiation field was assumed to be 5×10^{13} m^{-3}, corresponding to that produced by ^{131}I with $d_k = 0.1$ μm, $Z = 10^{11}$ m^{-3}, and $I = 7{,}700$).

radioactive particles and neighboring nonradioactive particles to be charged.

4.3.5. Aggregation Frequency of Radioactive Particles

The aggregation frequency of two radioactive particles is calculated by using equations 4.2, 4.4 and 4.5. The surface charge of radioactive particles causes their aggregation frequency to be different from that of nonradioactive particles since the charging level is significant as shown in Figure 4.5. Since the number of positive charges on a radioactive particle increases as the particle size increases, due to the self-charging effect, the repulsive forces between two radioactive particles increase due to the interaction of similar charge. Thus, the relatively lower values of the aggregation frequency of radioactive particles (e.g., Figure A4) are attributed to the high charging levels of the particles, which generate strong repulsive forces of electrostatic origin.

4.3.6. Aggregation of Radioactive Particles

Changes in the size distribution of radioactive particles were predicted by the population balance model. Figure 4.6 shows the changes in the number concentration for various radioactive particles under a monodispersed initial condition. Particles with a lower level of radioactivity (e.g., ^{137}Cs) aggregate at a similar rate as the nonradioactive particles because the generated repulsive electrostatic forces among the particles are relatively weak. However, as the level of radioactivity increases, the radioactive particles aggregate less frequently since radioactivity causes the generation of strong repulsive electrostatic forces produced by like charges due to the self-charging effect. A similar aggregation behavior was observed during experiments by Rosinski et al. (1962). In the experiment, the specific charging levels of the radioactive particles were not investigated, but the aggregation rates of slightly radioactive gold particles were up to five times lower than those of nonradioactive gold particles. Based on their own experiments, Yeh et al. (1976) reported that the lower aggregation rates of Rosinski et al.(1962) might be the

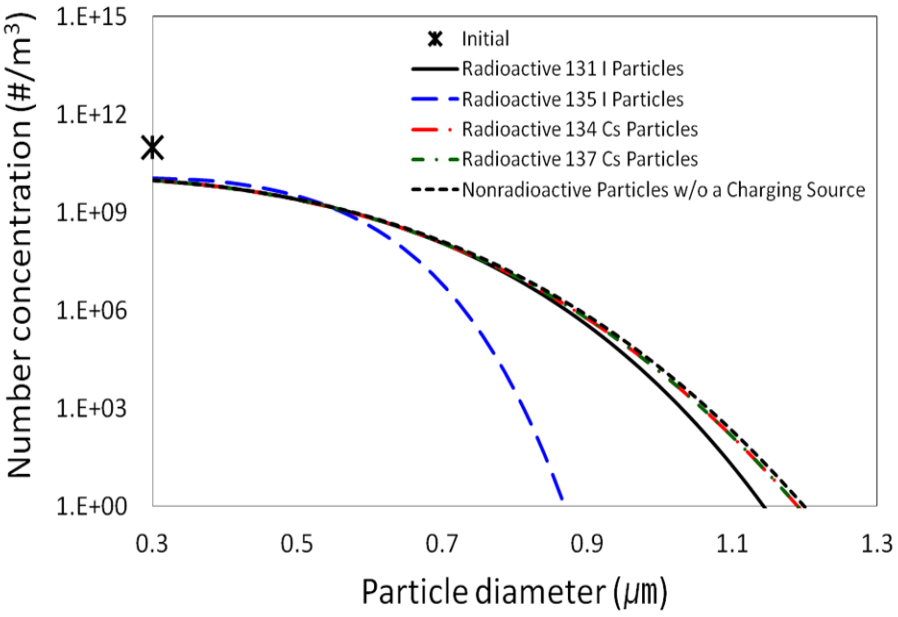

Figure 4.6. Aggregation of various radioactive particles and nonradioactive particles under a monodispersed initial condition (t = 24 hrs; $N_t = 10^{11}$ m^{-3}; d_k = 0.3μm).

result of the repulsive electrostatic forces caused by the self-charging effect.
The aggregation behavior of the radioactive particles is similar for either monodispersed or log-normal initial distribution. For example, aggregation rates of highly radioactive particles (e.g. ^{135}I) are significantly lower than for other cases due to high radioactivity-induced repulsive forces (Figure A5). The hindering effects of a high level of radioactivity on the aggregation rate may become more significant as time elapses because smaller particles will agglomerate until strong repulsive forces between large particles hinder further growth. Aggregation rates of nonradioactive particles inside and outside a radiation field can be also slightly different due to diffusion-charging effects.

4.3.7. Sensitivity Analysis

A sensitivity analysis for radioactive ^{131}I particles was conducted to investigate the effects of charging parameter values on particle aggregation. There are three main charging parameters: ω, y, and X. These parameters can be determined by I, Z, X, and the particle size as shown in equation 4.2. The ranges of variables for the sensitivity analysis are obtained from (Yeh et al., 1976; Gensdarmes et al., 2001; Subramanian et al., 2012; Clement and Harrison, 1992; Clement et al., 1995; Adachi et al., 1985) (See Text A1 and Table A5).

Effects of the charging parameters on aggregation were evaluated. Since the mean number of charges is changed with the parameter values, all parameters were found to influence the aggregation rate of radioactive particles. Particularly, the particle concentration, initial particle size, and number of ion-pairs produced per decay can be important parameters in the aggregation of radioactive particles in air since the particle charging level is highly influenced by these charging parameters, as well as the decay rate. For example, Figure 4.7 shows the effects of I on the radioactive particle aggregation. As I increases, the concentration of ions produced by radioactive particles increases. At a higher ion concentration, the self-charging effect is suppressed due to the

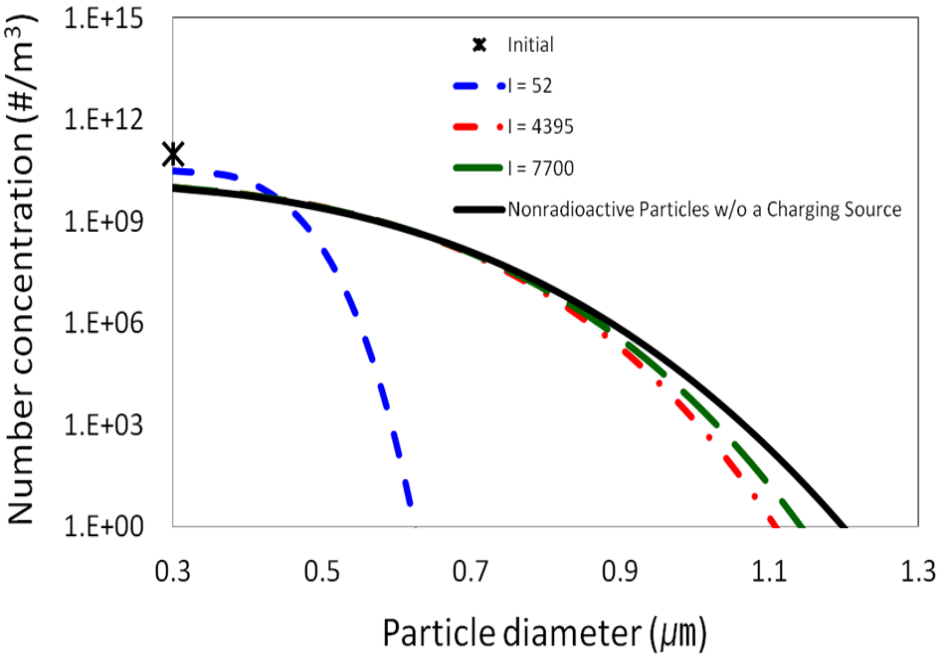

Figure 4.7. Effects of the number of ion pairs produced per decay on the aggregation of radioactive iodine particles under a monodispersed initial condition (t = 24 hrs; $N_t = 10^{11}$ m^{-3})

enhancement of the diffusion charging effect (equation 4.2 and Figure 4.5). In contrast, at a lower ion concentration, the effects of diffusion charging on self-charging is insignificant and thus, the aggregation rate for $I = 52$ was much lower than $I = 7{,}700$. Results of other cases are given in Figure A6.

4.4. Summary

Uncertainty in predictive transport modeling of radioactive particles includes the assumption that radioactivity effects are negligible on particle agglomeration. It has been shown that radioactivity affects significantly the surface potential of radioactive particles or nonradioactive objects near a radioactive source and that high radioactivity hinders the aggregation of radioactive particles since it generates repulsive electrostatic forces caused by similar charges in atmospheric radioactive particle plumes. Radioactivity-induced charging can play a significant role in the behavior of particles in air and thus should be included in predictive models of radioactivity transport. This study has shown a systematic approach of including radioactivity-charging effects in particle aggregation and population dynamics modeling, which can be incorporated into radioactivity transport models to predict the transport and distribution of radioactivity in the environment.

4.5. Acknowledgements

This chapter involves contributions from coauthors and was published in: Kim, Y-H., Yiacoumi, S., Lee, I., McFarlane, J., Tsouris, C. 2014. Influence of Radioactivity on Surface Charging and Aggregation Kinetics of Particles in the Atmosphere. *Environ. Sci. Technol.*, 48, 182-189.

CHAPTER 5

COUPLING CHARGING EFFECTS WITH AGGREGATION OF RADIOACTIVE AND NONRADIOACTIVE PARTICLES

Charging and coagulation influence one another and impact the particle charge and size distributions in the atmosphere. However, few investigations to date have focused on the coagulation kinetics of atmospheric particles accumulating charge. This chapter presents three approaches to include mutual effects of charging and coagulation on the microphysical evolution of atmospheric particles such as radioactive particles. The first approach employs ion balance, charge balance, and a bivariate population balance model (PBM) to comprehensively calculate both charge accumulation and coagulation rates of particles. The second approach involves a much simpler description of charging, and uses a monovariate PBM and subsequent effects of charge on particle coagulation. The third approach is further simplified assuming that particles instantaneously reach their steady-state charge distributions. It is found that compared to the other two approaches, the first approach can accurately predict time-dependent changes in the size and charge distributions of particles over a wide size range covering from the free molecule to continuum regimes. The other two approaches can reliably predict both charge accumulation and coagulation rates for particles larger than about 40 nanometers and atmospherically relevant conditions. These approaches are applied to investigate coagulation kinetics of particles accumulating charge in a radioactive neutralizer, the urban atmosphere, and a radioactive plume. Limitations of the approaches are discussed.

5.1. Introduction

Atmospheric particles play an important role in airborne transport of contaminants, such as radionuclides. Contaminants emitted from anthropogenic sources (e.g., nuclear plant accidents) can be captured by background aerosols and then are transported together with pre-existing particles. Contaminant-laden particles can be deposited onto the ground by dry and wet deposition (primary contamination) and subsequently resuspended by wind or heat-driven convection and moved to other areas (secondary contamination). Due to atmospheric dispersion, radioactive particles (e.g., ^{137}Cs) released during the Fukushima accident were sampled in situ 150 km away from the emission site (Yamauchi et al., 2012). Similar dispersion patterns of radioactive particles were observed after the Chernobyl accident (Yoshenko et al., 2006a, 2006b). Accurate understanding of the behavior of atmospheric particles is necessary to precisely predict transport of contaminants (especially long-lived ones, such as ^{137}Cs), as well as their potential environmental impacts.

The behavior of atmospheric particles is driven by such properties as charge and size that can affect particle deposition and other microphysical processes (Fuchs, 1989; Pruppacher and Klett, 1997). Atmospheric particles can acquire charge via self-charging and diffusion charging; radioactive particles can be charged through these two charging mechanisms (Greenfield, 1956; Yeh et al., 1976; Clement and Harrison, 1992; Clement et al., 1995; Gensdarmes et al., 2001; Walker et al., 2010; Kweon et al., 2013; Kim et al., 2014; 2015) while natural atmospheric particles are typically charged by diffusion charging (Hoppel, 1985; Yair and Levin, 1989; Renard et al., 2013). Particle charging can modify not only the charge but also the size distribution because charge on the particles generates electrostatic surface interactions that facilitate or hinder particle coagulation (Fuchs, 1989; Tsouris et al., 1995; Chin et al., 1998). Coagulation of atmospheric particles can influence their charging because the particle size distribution can highly

affect the time-evolution of ion concentrations (Yair and Levin, 1989). Also, particle coagulation can result in charge neutralization or accumulation on atmospheric particles (Alonso et al., 1998). Particle charging and coagulation can mutually affect each other and simultaneously affect both charge and size distributions in the atmosphere.

Theoretical and experimental investigations have been performed to examine the charging of radioactive particles and background aerosols in the atmosphere. However, the effects of coagulation of particles on the charge distribution have been frequently neglected by assuming that the size distribution is constant while they are charged (Greenfield, 1956; Hoppel, 1985; Yair and Levin, 1989). The assumption may be valid if the particle concentration is low or the steady-state charge distribution is instantaneously attained (Hoppel, 1985; Renard et al., 2013; Kim et al., 2015). If the timescale for particle charging is longer than that for particle coagulation, the assumption may no longer be valid (Yair and Levin, 1989). Also, the effects of charging on the particle size distribution are frequently neglected in aerosol transport models involving microphysics of atmospheric particles. A possible reason for neglecting the charging effects may be that the steady-state mean charge of atmospheric particles rarely may affect their coagulation rates (Seinfeld and Pandis, 2006). However, neglecting electrostatic particle-particle interactions may increase uncertainty of prediction results if particles can acquire multiple elementary charges (e.g., radioactive particles). The simplified assumption of omitting electrostatic particle interactions may create uncertainty in transport predictions of radioactive particles. Hence, it may be necessary to take into account the mutual effects of particle charging and coagulation processes in predicting the behavior of atmospheric particles carrying radioactive contaminants.

Previous attempts to consider charging effects include Oron and Seinfeld (1989a, 1989b), who developed sectional approaches to simultaneously predict the behavior of charged and uncharged atmospheric particles. Laakso et al. (2002) developed a general dynamic equation, including charging and coagulation kinetics of atmospheric particles.

However, the validity of these approaches was not evaluated using analytical solutions. Alonso (1999) and Alonso et al. (1998) developed analytical and numerical approaches to estimate time-dependent changes in the size distributions of singly charged and neutral particles; thus, these approaches cannot be used to investigate the coagulation kinetics of particles acquiring multiple elementary charges. Also, none of these approaches considered self-charging; therefore, the aforementioned approaches may be subject to error when they are used to simulate atmospheric dispersion of radioactive plumes.

Our chapter presents three approaches to simultaneously predict time-dependent changes of the charge and size distributions of radioactive and nonradioactive particles over a wide size range. Development, validity, application, and limitations of these approaches are discussed.

5.2. Model Development

5.2.1. Ion Balance Model

Many atmospheric processes can generate and remove ions in air. Typical ion sources in the atmosphere involve natural and artificial radioactivity, as well as cosmic rays. Ions are generally removed by ion-ion recombination and ion-particle attachment. Changes in ion concentrations by these processes can be given by (Kim et al., 2015):

$$\frac{dn_+}{dt} = -n_+ \sum_k \sum_j \beta_{k,j}^+ N_{k,j} - \alpha_{rc} n_+ n_- + q \,, \tag{5.1}$$

$$\frac{dn_-}{dt} = -n_- \sum_k \sum_j \beta_{k,j}^- N_{k,j} - \alpha_{rc} n_+ n_- + q + q_e \,, \tag{5.2}$$

where $n_\pm$ refers to the number concentrations of positive or negative ions, the indices k and j represent the size and number of elementary charges of particles, respectively, $\beta_{k,j}^\pm$ is the attachment coefficient between a particle and an ion, $N_{k,j}$ is the number

concentration of particles, α_{rc} is the recombination coefficient of ions, and t is time. The first two terms of the right-hand-side (RHS) of equations 5.1 and 5.2 represent the loss rate of ions due to ion-particle attachment and ion-ion recombination, respectively. The third term denotes the production rate of ion pairs, q:

$$q = q_b + q_I , \tag{5.3}$$

where q_b is the ion production rate by cosmic rays and natural radioactivity, and q_I is the ion production rate by radionuclides released by nuclear events. Electrons released by radioactive decay are taken into account via the last term of equation 5.2. Changes in the ion concentrations may affect the electrical conductivity of the atmosphere, σ_{air} (Harrison and Carslaw, 2003):

$$\sigma_{\text{air}} = e\left(\mu_+ n_+ + \mu_- n_-\right), \tag{5.4}$$

where e is the electrical charge and $\mu_{\pm}$ is the mobility of positive or negative ions. In equation 5.4, the terms in the parentheses of the RHS represent polar air conductivities.

5.2.2. Charge Balance Models

Self-charging refers to charge accumulation caused by radioactive decay which typically leads to emission of electrons from particle surfaces. Diffusion charging is attributed to diffusion of ions from the surrounding atmosphere onto the surface of particles. Self-charging generally accumulates positive charge on the surface of particles, while diffusion charging adds both positive and negative charges, indicating that the charging mechanisms can compete with one another. For radioactive particles involved in beta decay, time-dependent changes in their charge distributions due to competition of the charging mechanisms can be expressed by (Clement and Harrison, 1992; Kim et al., 2015):

$$\frac{dN_{kj}}{dt} = A_{k,j-1}N_{k,j-1} - A_{k,j}N_{k,j} + \beta^{+}_{k,j-1}n_{+}N_{k,j-1} - \beta^{+}_{k,j}n_{+}N_{k,j} + \beta^{-}_{k,j+1}n_{-}N_{k,j+1} - \beta^{-}_{k,j}n_{-}N_{k,j} \quad (5.5)$$

where A is the decay rate of the radioactive particles. In equation 5.5, self-charging is represented by terms that include A, while diffusion charging is represented by terms with $\beta^{\pm}_{k,j}$. If the terms for self-charging are removed, equation 5.5 becomes identical to the charge balance model presented by Renard et al. (2013) who predicted electrification phenomena of aerosols in the real atmosphere. The mean value of the particle charge distributions can be given by:

$$\frac{dJ_k}{dt} = \frac{d}{dt}\left(\frac{\sum jN_{kj}}{\sum N_{kj}}\right). \quad (5.6)$$

The mean charge J of the radioactive particles of size k can also be approximated using a simple charge balance equation (Kim et al., 2015):

$$\frac{dJ_k}{dt} = A_k + \beta^{+}_{k,J}n_{+} - \beta^{-}_{k,J}n_{-}. \quad (5.7)$$

Similarly to equation 5.5, the mean charge accumulation rate of the radioactive particles (equation 5.7) depends on the competition between self- and diffusion charging. Equations 5.5 and 5.7 indicate that the net charge of beta-emitting radioactive particles converges to a steady state where self-charging balances diffusion charging. The timescale, τ, needed to reach a steady state can be given by (Clement and Harrison, 1992):

$$\tau = \frac{1}{\beta^{-}n_{-}}. \quad (5.8)$$

At steady state, the mean charge of the radioactive particles can be approximated using (Clement et al., 1995):

$$J_k = \begin{cases} y - \left(\dfrac{y(X-1)}{\exp(2\omega y) - 1} \right) & \omega y > 0.22 \quad (5.9a) \\ y + \dfrac{X-1}{2\omega} & \omega y \le 0.22 \quad (5.9b) \end{cases}, \tag{5.9}$$

with $\omega = \dfrac{e^2}{8\pi\varepsilon_0 \varepsilon r_k k_B T}$, $y = \dfrac{\varepsilon_0 A_k}{e\mu_- n_0}$, $n_0 = \sqrt{\dfrac{q}{\alpha_{rc}}}$, $X = \dfrac{\mu_+ n_+}{\mu_- n_-}$,

where ε_0 is the vacuum permittivity, ε is the dielectric constant of the air, r is the radius of particles, k_B is the Boltzmann constant, T is the temperature, n_0 is the mean ion concentration, and I is the ionization rate coefficient of beta-emitting radionuclides. Equation 5.9 suggests that the steady-state mean charge of beta-emitting radioactive particles is highly influenced by their size and decay rates, as well as the concentrations and mobilities of ions in air. The second term of the RHS of eq 5.9(b) represents charge accumulated only by diffusion charging; thus, it can be used to approximate the steady-state mean charge of nonradioactive particles, such as background aerosols that are externally mixed with radionuclides.

5.2.3. Population Balance Models

5.2.3.1. Bivariate population balance model

A bivariate population balance model, expressed in terms of particle volume x and charge j, can be used to predict effects of coagulation on time-dependent changes in the particle size and charge distributions. In the bivariate population balance model, the time-evolution of the number densities of charged and uncharged particles, n, due to coagulation, can be given by (Zebel, 1958; Oron and Seinfeld, 1989a&b):

$$\frac{\partial n(x,j)}{\partial t} = \frac{1}{2}\sum_{j'=-\infty}^{\infty}\int_0^x F_{j',j-j'}\left(x',x-x'\right)n\left(x',j'\right)n\left(x-x',j-j'\right)dx' - \sum_{j'=-\infty}^{\infty}\int_0^{\infty} F_{j,j'}\left(x,x'\right)n\left(x,j\right)n\left(x',j'\right)dx' \quad (5.10)$$

where F is the coagulation frequency, which can be obtained by multiplying the collision frequency and the collision efficiency. The two terms on the RHS of equation 5.10 represent the production and loss rates of charged and uncharged particles by coagulation, respectively. A numerical solution of equation 5.10 can be obtained through the discretization of the integral terms, respectively (Oron and Seinfeld, 1989a&b). Vanni (2000) tested several sectional approaches and showed that the approach of Kumar and Ramkrishna (1996) is simpler and more accurate than other tested approaches, and also preserves mass and number of particles. Thus, the sectional approach of Kumar and Ramkrishna (1996) was used in this study to discretize the integral terms of equation 5.10, leading to the following discretized form:

$$\frac{dN_{kj}}{dt} = \sum_{j'=-\infty}^{\infty}\sum_{\substack{l,m \\ x_{k-1}\le x_l+x_m\le x_{k+1}}}^{l\ge m}\left(1-\frac{1}{2}\delta_{l,m}^{Kr}\right)\eta_{l,m}F_{l,m,j-j',j'}N_{l,j-j'}N_{m,j'} - \sum_{j'=-\infty}^{\infty}\sum_{l=1}^{M}F_{k,l,j,j'}N_{k,j}N_{l,j'} \quad (5.11)$$

where indices l and m refer to the size bins, δ^{Kr} is the Kronecker delta, $\eta_{l,m}$ is a property distribution factor between two size bins (Kumar and Ramkrishna, 1996), and M is the total number of the size bins. If coagulation is induced by thermal energy (i.e., Brownian coagulation), the collision frequency β^{Br} is given by (Fuchs, 1989):

$$\beta_{kl}^{Br} = 4\pi\left(r_k+r_l\right)\left(D_{p,k}+D_{p,l}\right)\left(\frac{r_k+r_l}{r_k+r_l+\sqrt{g_k^{\,2}+g_l^{\,2}}}+\frac{4\left(D_{p,k}+D_{p,l}\right)}{\left(r_k+r_l\right)\sqrt{\bar{v}_{p,k}^{\,2}+\bar{v}_{p,l}^{\,2}}}\right)^{-1} \quad (5.12)$$

where D_p is the particle diffusion coefficient, g is the particle mean traveling distance, and $\bar{v}_p$ is the particle thermal speed in air. Coagulation of charged particles is influenced

by electrostatic particle-particle interactions. This effect can be accounted for by multiplying the collision frequency with the collision efficiency, α^{Br} (Fuchs, 1989; Seinfeld and Pandis, 2006):

$$\alpha_{kl}^{Br} = \frac{u}{e^{u} - 1} \tag{5.13}$$

with $u = \dfrac{j_k j_l e^2}{4\pi\varepsilon_0 \varepsilon (r_k + r_l) k_B T}$

In equation 5.13, u indicates the relative importance between electrostatic potential energy and thermal energy in coagulation.

5.2.3.2. Monovariate population balance model

The time-evolution of the size distribution of particles can be estimated using a monovariate population balance model, with only the particle volume as the variable (Kumar and Ramkrishna, 1996):

$$\frac{dN_k}{dt} = \sum_{\substack{l,m \\ x_{k-1} \le x_l + x_m \le x_{k+1}}}^{l \ge m} \left(1 - \frac{1}{2}\delta_{l,m}^{Kr}\right) \eta_{l,m} F_{l,m} N_l N_m - \sum_{l=1}^{M} F_{k,l} N_k N_l \,. \tag{5.14}$$

The coagulation frequency can be simply corrected using the mean charge of particles. However, the collision efficiency computed with the mean charge can be different from that with the particle charge distributions (Matsoukas, 1997). To include effects of the particle charge distributions on the coagulation frequency, equation 5.13 can be replaced by the average collision efficiency $\bar{\alpha}$ (Clement et al., 1995), which involves interaction of all charged particles of size k with any charged particles of size l.

$$\bar{\alpha}_{kl}^{Br} = 1 + \frac{\sum_{j_k j_l \neq 0} N_{k,j_k} N_{l,j_l} \left(\alpha_{kl}^{Br} - 1\right)}{\sum_{j_k} N_{k,j_k} \sum_{j_l} N_{l,j_l}} \,. \tag{5.15}$$

The particle charge distributions needed to calculate $\bar{\alpha}^{Br}$ can be obtained by assuming a Gaussian distribution:

$$N_{kj} = \frac{\sum_j N_{k,j}}{\sqrt{2\pi}\sigma_k} \exp\left(-\frac{(j-J_k)^2}{2\sigma_k^2}\right) \tag{5.16}$$

with $\sigma^2 = y + \frac{1}{2\lambda}$.

5.2.4. Approaches to Couple Particle Charging with Coagulation Kinetics

Figure 5.1 shows three approaches which can be used to predict the time-evolution of the charge and size distributions of particles in the atmosphere. All the approaches can be used to simulate charging and coagulation kinetics of atmospheric particles carrying contaminants, including radioactive particles. Approach 1 is a rigorous scheme that simultaneously computes both charge accumulation and coagulation rates of particles using the ion balance model (equations 5.1 and 5.2), the charge balance model (equation 5.5), and the bivariate population balance model (equation 5.11). Approach 2 is a simplified scheme of Approach 1, which can be used to predict the particle charge distribution using the mean charge of particles (equation 5.7) and the Gaussian distribution (equation 5.16). In order to easily simulate the coagulation of charged particles, Approach 2 employs the monovariate population balance model (equation 5.14) that corrects the collision frequency using the average collision efficiency (equation 5.15). Approach 2 can be simplified to Approach 3 by assuming that charge accumulation rates of particles instantaneously reach a steady state, with a timescale based on 5 times larger than τ from equation 5.8. The steady-state particle charge distribution can be approximated by equations 5.9 and 5.16. In Approach 3, the collision frequency is multiplied by the average collision efficiency to include the influence of electrostatic forces on coagulation.

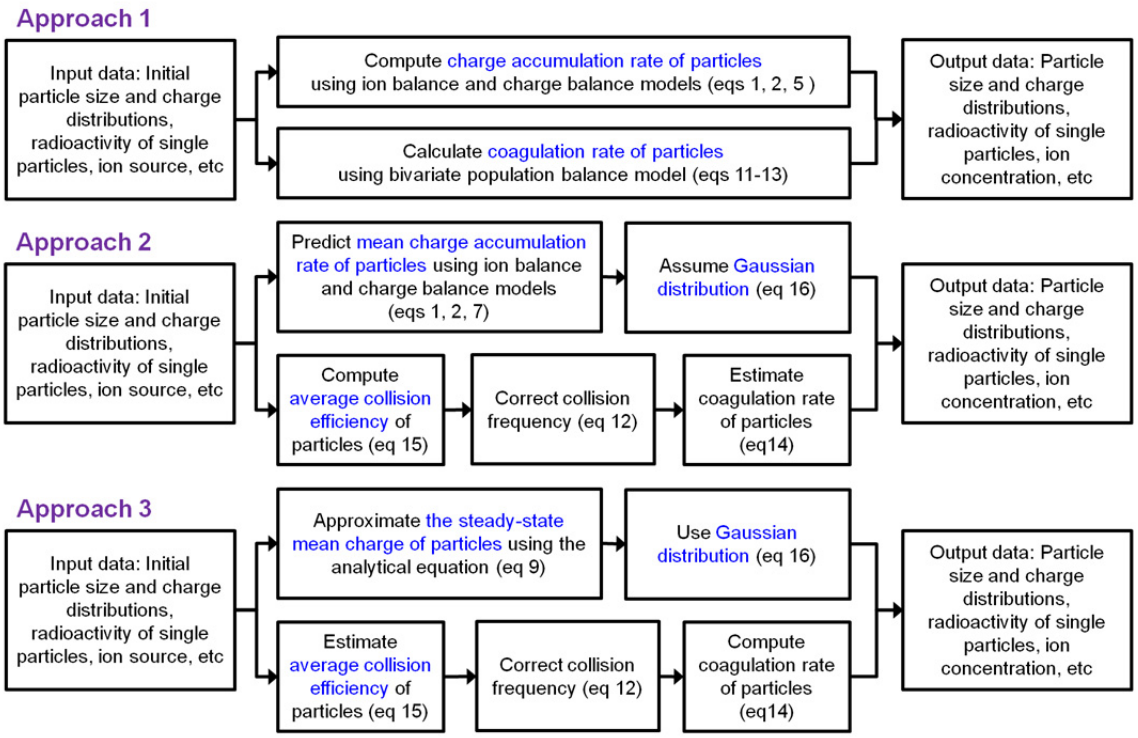

Figure 5.1. Three approaches to predict time-dependent changes in the particle size and charge distributions in the atmosphere.

5.3. Results and Discussion

5.3.1. Methods to Simulate Particle Charging

The three approaches attained above employ different methods to simulate charging of particles. These methods (equation 5.5 in Approach 1, equations 5.7 and 5.16 in Approach 2, and equations 5.9 and 5.16 in Approach 3) were evaluated by comparing their prediction results with measurements obtained using radioactive charge neutralizers (Liu and Pui, 1974; Wiedensohler and Fissan, 1991; Alonso et al., 1997) and radioactive particles (Gensdarmes et al., 2001). Initial conditions for the simulations were determined from the measurements. The properties of ions observed during the measurements are shown in Table 5.1. For the measurements providing the values of ion mass, $\beta_{k,j}^{\pm}$ was calculated using Fuchs (1963) and Hoppel and Frick (1986). However, the mass of ions was not measured during the experiments performed by Gensdarmes et al. (2001). In these experiments, $\beta_{k,j}^{\pm}$ was estimated using analytical equations given by Gunn (1954) and Harrison and Carslaw (2003).

5.3.1.1. Diffusion-charging mechanism

Figure 5.2 shows the steady-state charge distributions of nonradioactive particles over a wide size range. Here, the particles were charged by the diffusion charging mechanism. For particles larger than approximately 40 nm in diameter, the prediction results of all approaches were in good agreement with the measurements [Figures 5.2 (a) and (b)]. Below 40-nm particle size, Approach 1 accurately forecasted the particle charge distributions, but Approaches 2 and 3 underestimated the number concentrations of the negatively charged particles [Figure 5.2 (a)] although the mean charge values of the particles given by all approaches were comparable. Similar discrepancies were observed for the number concentrations of the positively charged particles smaller than about 25

Table 5.1. Properties of ions used for experimental observations.

References	Positive ions		Negative ions	
	Mass (AMU)	Mobility ($cm^2\ V^{-1}\ s^{-1}$)	Mass (AMU)	Mobility ($cm^2\ V^{-1}\ s^{-1}$)
Alonso et al. (1997)	150	1.15	80	1.65
Liu and Pui (1974) [a]	140	1.4	101	1.6
Wiedensohler and Fissan (1991)	140	1.4	101	1.6
Gensdarmes et al. (2001)	-	1.19	-	1.54

[a] The properties of ions were obtained from Wiedensohler and Fissan (1991), who used a radioactive neutralizer similar to that employed by Liu and Pui (1974).

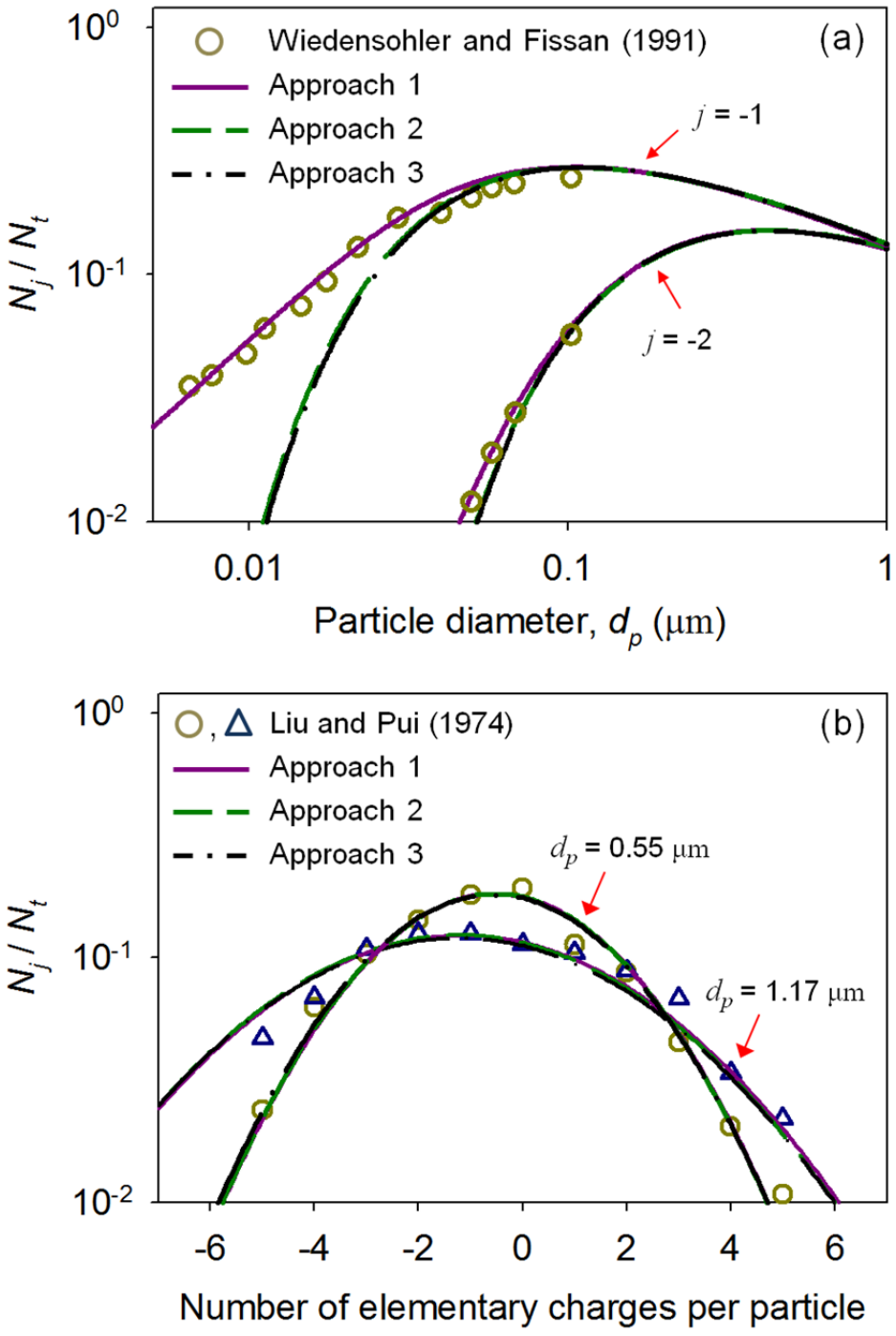

Figure 5.2. Steady-state charge distributions of particles capturing positive and negative ions. The symbols represent the measurements of the charge distributions of particles.

nm (not shown).

Analysis of the discrepancies suggests that they originate from the standard deviation involved in the Gaussian distribution (equation 5.16). At a given temperature, the width of the particle charge distributions can be significantly influenced by three parameters: the particle size, ion mass, and ion mobility (Wiedensohler and Fissan, 1991). In Approaches 2 and 3, however, the effects of the ion properties are not involved, so particle size primarily drives the standard deviation, which can differ from what Approach 1 gives. When Approaches 2 and 3 used the standard deviation values obtained by Approach 1, their simulation results became closer to the measurements, although the discrepancies are still seen for negatively and positively charged particles smaller than about 20 nm.

5.3.1.2. Competition of self-charging and diffusion-charging mechanisms

In our previous work (Kim et al., 2014; 2015), it has been shown that Approaches 1 and 3 can reliably simulate charging of radioactive particles. Thus, in this study, we focused on evaluating the validity of Approach 2 with the experiments of Gensdarmes et al. (2001) who measured the charge distributions of ^{137}Cs particles under various ionizing conditions. Ionizing rates of air molecules were estimated using a linear energy transfer equation for energetic electrons emitted by beta decay (Kim et al., 2015). Results of Approach 1 were included as a reference.

Figure 5.3 shows the charge accumulation on radioactive particles under two ionizing conditions: $q_I = 3.7\times10^8$ m^{-3} s^{-1} and $q_I = 7.1\times10^6$ m^{-3} s^{-1}. Approach 2 predictions are in good agreement with observations and Approach 1 values. During the measurements, the self-charging rate of the radioactive particles was constant because of the long half-life of ^{137}Cs (approximately 30 years), suggesting that changes in their charge accumulation rates may be dominated by diffusion charging rates. The ion concentrations in air can rapidly increase at the high ionizing rate considered,

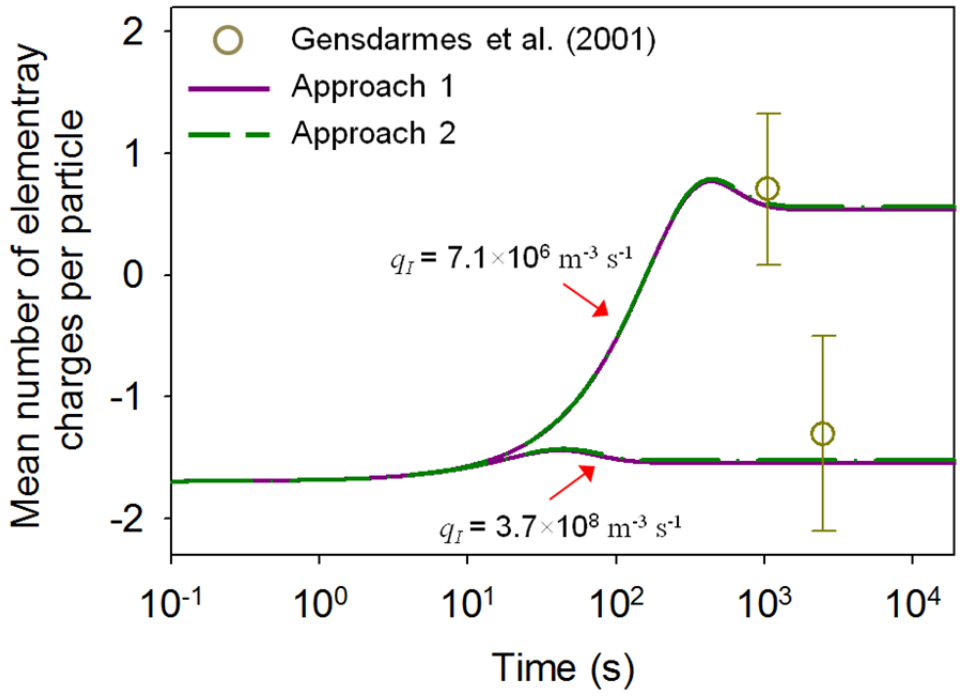

Figure 5.3. Charge accumulation on ^{137}Cs particles under two ionizing conditions: q_I = 7.1×10^{6} m^{-3} s^{-1} and q_I = 3.7×10^{8} m^{-3} s^{-1} (d_k = 0.82 µm; $A_{Cs\text{-}137}$ = 12.8 mBq). The symbols represent the mean value of the particle charge distributions measured by Gensdarmes et al.(2001).

suggesting that the diffusion charging rate of the ^{137}Cs particles quickly increased and then became comparable to their self-charging rate (equation 5.7). The charge accumulation on the radioactive particles promptly reached a steady-state value, and the particle charge distribution was similar to the initial condition (Figure 5.4). In contrast, the time required to reach the steady-state value was much longer at the low ionizing rate considered; hence, the particle charge distribution shifted to the right in Figure 5.4, i.e., more positive charge. The agreement observed in Figure 5.4 between simulation results by Approach 2 and experimental data by Gensdarmes et al. (2001) suggests that Approach 2 can accurately forecast the competition between self- and diffusion charging on submicron particles carrying radionuclides, and precisely predict the particle charge distributions.

5.3.1.3. Timescale to reach steady-state charge accumulation rate

To evaluate the steady-state assumption of particle charging for atmospheric conditions, the timescale for reaching steady-state (equation 5.8) is evaluated with Approaches 1 and 2. Figure 5.5 shows time-dependent changes in the concentrations of negatively charged particles under two different initial conditions of Alonso et al. (1997) who measured the charge distributions of particles of a few nanometers. All particles were initially uncharged or negatively charged. Because the particle size was very small, Approach 1 was used to predict the time-evolution of the particle concentrations. As time elapsed, the initially uncharged particles became negatively charged by capturing negative ions. The diffusion of positive ions led to the discharging of the initially negatively charged particles. For the initial conditions used, the charging and discharging rates of the particles reached a steady state after approximately 0.2 s, respectively. This charging/discharging behavior predicted by Approach 1 is in good agreement with the measurements of Alonso et al.(1997). However, the timescales obtained from equation 5.8 are shorter than the prediction results, as well as the measurements, because

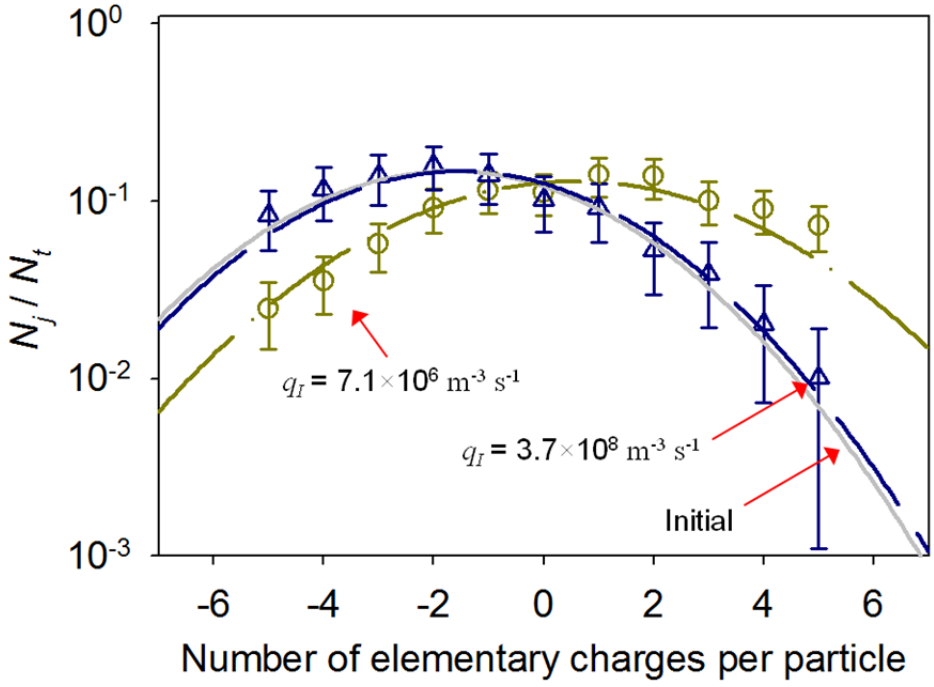

Figure 5.4. Charge distributions of ^{137}Cs particles under two ionizing conditions: q_I = 7.1×10^6 m^{-3} s^{-1} and $q_I = 3.7\times10^8$ m^{-3} s^{-1} (d_k = 0.82 μm; $A_{\text{Cs-137}}$ = 12.8 mBq). The prediction results of Approach 2 were compared with the measurements of Gensdarmes et al.(2001).

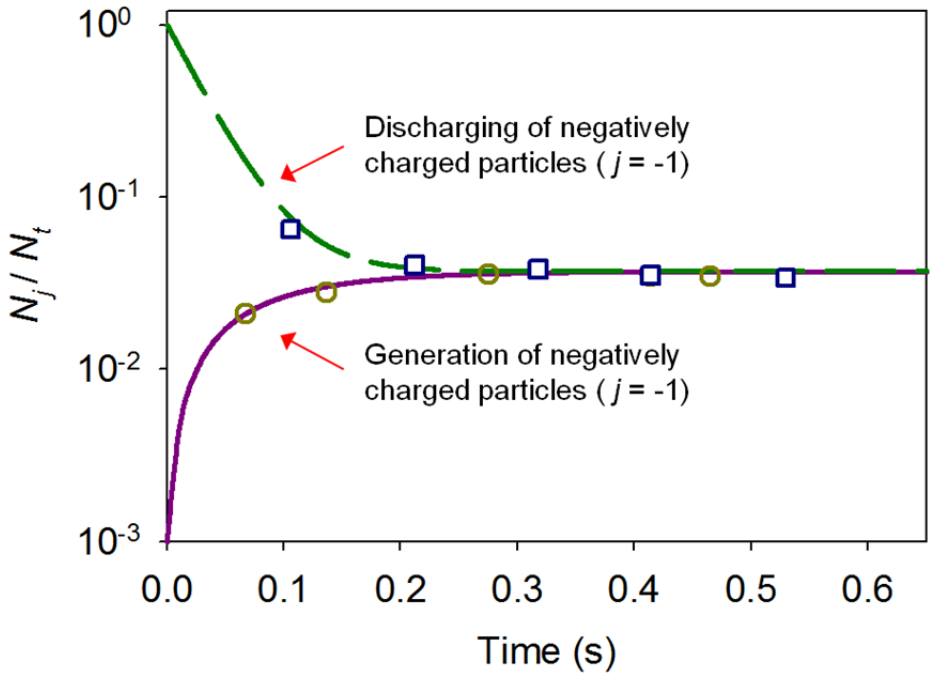

Figure 5.5. Timescale to reach steady-state charge accumulation rates of 7.1 nm nanoparticles. The lines are the simulation results of Approach 1. The symbols are the measurements of Alonso et al.(1997). Charging timescales were estimated using equation 5.8 ($\tau_{charging}$ = 0.042 s and $\tau_{discharging}$ = 0.017 s), as well as Approach 1 and the measurements.

Approach 1 and the observations provided exact timescales, while τ in equation 5.8 is a scaling parameter. Similar results were also obtained for different initial conditions, as well as for the ^{137}Cs particles (see Table 5.2).

Equation 5.8 is based on the assumptions that (i) $X \approx 1$, (ii) all particles are initially uncharged, and (iii) the ion concentrations are constant (Clement and Harrison, 1992). As seen in Figure 5.6, when all the assumptions were applied, the diffusion charging rate of the radioactive particles became -8.1×10^{-3} at the timescale provided by equation 5.8, which corresponds to approximately 63% of the steady-state self-charging rate. If the timescale is increased by a factor of five, the diffusion charging rate reaches about 99 % of the steady-state self-charging rate. Similar results were obtained for other cases with radioactive particles. Thus, equation 5.8 is valid if the assumptions can be used, and a reliable timescale to reach a steady state (e.g., 99%) can be obtained by multiplying the equation by a factor of 5. However, because the assumptions cannot be used in typical atmospheric conditions, such as $X \neq 1$ (Harrison and Carslaw, 2003), the steady-state assumption of Approach 3 should be evaluated using Approaches 1 or 2.

So far, we have evaluated the validity of the methods used in the three approaches to predict charge accumulation on atmospheric particles. The evaluation results suggest that the method employed in Approach 1 can accurately simulate charging of particles in the free molecule ($d_k < 10$ nm), transition ($d_k = 10 – 200$ nm), and continuum ($d_k > 200$ nm) regimes. The methods used in Approaches 2 and 3 can reliably forecast charging rate of atmospheric particles larger than 40 nm.

Table 5.2. Timescales required for particles to reach steady-state charge.

Charging mechanism	Particle diameter (nm)	Steady-state mean ion concentration (m^{-3})	τ (s) (equation 5.8)	Numerical timescale (s) (Approach 1 or 2)	Timescale from measurments (s)	Reference
Diffusion charging	7.1	8.0×10^{12}	0.04	0.2 ~ 0.4	0.3	Alonso et al. (1997)
	7.0	2.0×10^{13}	0.02	0.2 ~ 0.4	0.3	
	2.7	8.0×10^{12}	0.04	0.2 ~ 0.4	0.3	
	2.6	2.0×10^{13}	0.02	0.2 ~ 0.4	0.3	
Diffusion charging and self-charging	0.82	2.1×10^{9}	171.1	> 1,000	-	Gensdarmes et al.(2001)
	0.82	1.5×10^{10}	23.6	> 200	-	
	1.05	7.6×10^{8}	471.6	> 3,000	-	
	1.05	7.0×10^{9}	51	> 500	-	

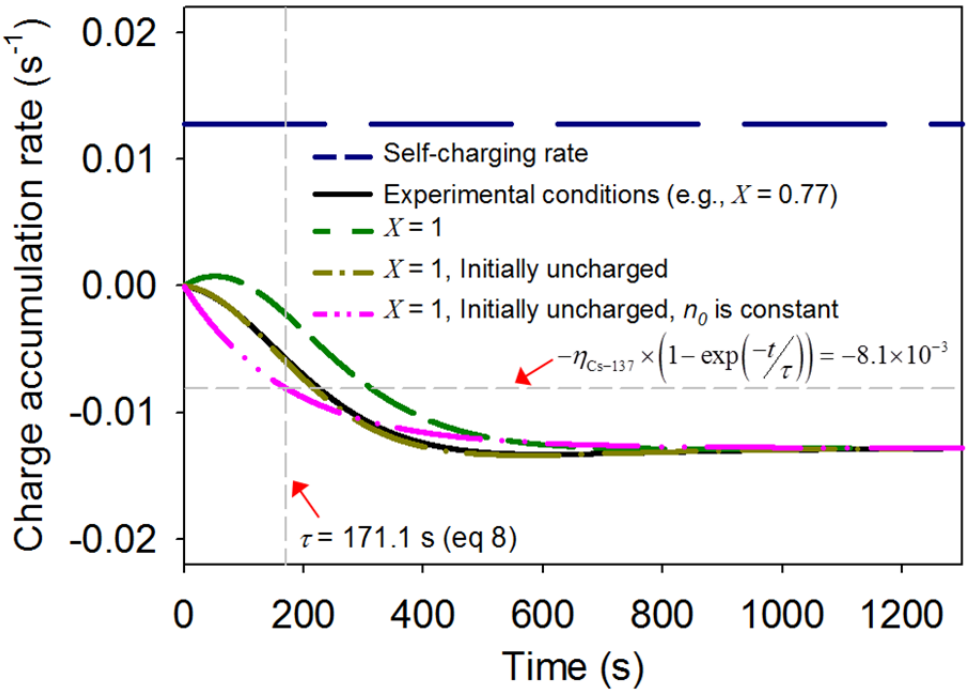

Figure 5.6. Charge accumulation rate of ^{137}Cs particles for each charging mechanism (d_k = 0.82 μm; $A_{Cs\text{-}137}$ = 12.8 mBq; $q_I = 7.1\times10^6$ m^{-3} s^{-1}). The assumptions used in equation 5.8 were applied to evaluate the validity of the equation. $\eta_{Cs\text{-}137}$ corresponds to the self-charging rate of the radioactive particles.

5.3.2. Validity of the Three Approaches to Couple Particle Charging with Coagulation

5.3.2.1. Bivariate population balance model for Approach 1

Alonso (1999) suggested an approximate analytical solution to simultaneously investigate charging and coagulation kinetics of nonradioactive particles, smaller than 20 nm in diameter. In this study, the same analytical solution was used to evaluate Approach 1 because Approaches 2 and 3 are inapplicable to particles smaller than 20 nm, as shown in Figure 5.2a. In integrating equation 5.11, an equidistant diameter grid was used for discretization. Particles were assumed to be initially uncharged, monodispersed (d_p = 3 nm, $N_t = 10^9$ cm^{-3}), with a constant ion concentration. The mobility of negative ions was slightly greater than that of positive ions, according to the properties taken from Alonso et al. (1997) (See Table 5.1). Figure 5.7 shows the time dependent concentration of particle charge classes. The concentration of uncharged 3-nm particles decreased with time because of loss due to coagulation and charging by captured ions. However, the loss of particle concentration caused by diffusion charging was negligible because the ion-particle attachment coefficient was small, suggesting that the time-evolution of the charged-particle concentration depends on the uncharged-particle concentration. More negative than positive ions were captured by the uncharged 3-nm particles and, thus, the concentration of the negatively charged 3-nm particles is slightly higher than that of the positively charged 3-nm particles. The concentrations of larger particles (e.g., charged and uncharged 6-nm particles) increased over time because of the size growth of small particles due to coagulation, as well as the diffusion-charging mechanism. These evolution patterns predicted by Approach 1 were in good agreement with the prediction results given by the analytical solution. As can be seen in Figures 5.2 and 5.5, the ion balance and charge balance models of Approach 1 accurately predicted the diffusion charging of nanoparticles, suggesting that the numerical solution of the bivariate population balance model (equation 5.11) reliably predicts coagulation of particles

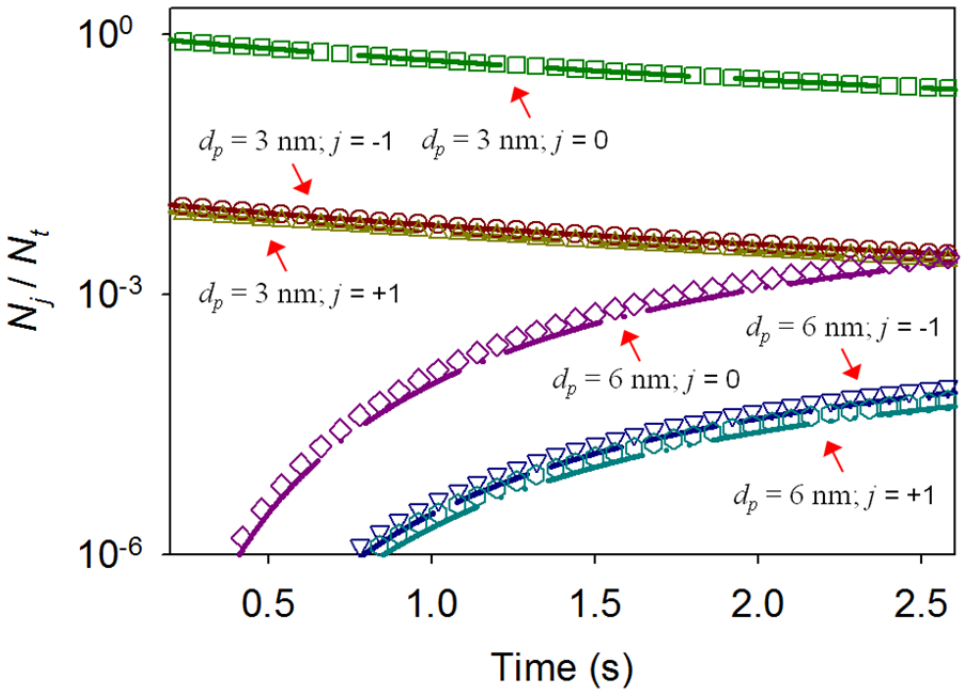

Figure 5.7. Validation of the numerical solution for the bivariate population balance model under a monodispersed initial condition (d_k = 3 nm, $N_t = 10^9$ cm^{-3}, and $n_0 = 10^{12}$ cm^{-3}). The lines and symbols represent the results of the analytical solution of Alonso (1999) and equation 5.11, respectively.

acquiring charge.

5.3.2.2. Average collision efficiency of Approaches 2 and 3

Approaches 2 and 3 employ an average collision efficiency and are coupled to the monovariate, instead of the bivariate, population balance model. These approaches provided accurate particle charge distributions for various cases (e.g., Figures 5.2 and 5.4; Kim et al., 2014), suggesting that their validity may be highly influenced by the accuracy of the average collision efficiency. Thus, we compared simulation results of Approach 2 with those of Approach 1 to check if the average collision efficiency (equation 5.15) can appropriately account for the influence of the charge distributions of particles on their size growth via coagulation. For comparison, simulation results of Approach 2 using the mean charge (equation 5.13), as well as those for uncharged particles, were included. Similarly to Oron and Seinfeld (1989 a&b), we assumed monodispersed initial size distributions (d_k = 0.1 μm, 0.5 μm, 1 μm, $N_t = 10^7$ cm^{-3}, and $n_0 = 10^{10}$ cm^{-3}). The geometrical grids ($x_{k+1} = 2x_k$) were used to cover a wide particle-size range. Other basic assumptions were similar to those considered for the validation test of Approach 1.

Figure 5.8 shows the time-evolution of the particle size distributions induced by particle charging and coagulation. The simulation conditions led to the accumulation of more negative than positive charges on the particles. At t = 1 min, the number fraction of the negatively charged particles was 0.7, while that of the positively charged and uncharged particles was 0.16 and 0.14, respectively. Thus, the size growth of the particles by coagulation was suppressed due to the generation of strong repulsive electrostatic forces (Approaches 1 and 2 vs Uncharged).

While most particles were negatively charged, some particles captured positive ions. Owing to electrostatic attractive forces, the positively charged particles can more frequently coagulate with the negatively charged particles and grow. Therefore, the

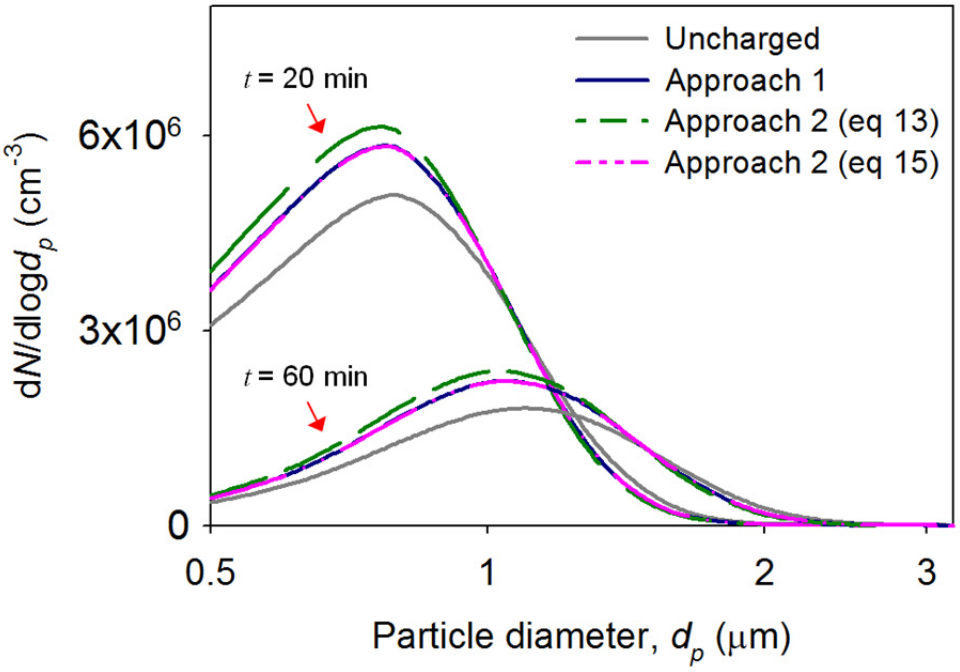

Figure 5.8. Time-evolution of the particle size distributions predicted by the monovariate population balance model with the average collision efficiency (equation 5.15) under a monodispersed initial condition (d_k = 0.5 μm, $N_t = 10^7$ cm^{-3}; $n_0 = 10^{10}$ cm^{-3}). Approach 1 was used as a reference that includes the mutual effect of surface charging and coagulation on the particle size and charge distributions.

coagulation rates predicted by Approach 2 with the average collision efficiency were slightly higher than those for the case assuming that all particles were negatively charged [Approach 2 (equation 5.13) vs Approach 2 (equation 5.15)]. These coagulation patterns predicted by Approach 2 using the average collision efficiency were in good agreement with those given by Approach 1 [Approach 1 vs Approach 2 (equation 5.15)], as well as the particle charge distributions in various size ranges (Figure 5.9).

Similar results were obtained for different initial particle size distributions (d_k = 0.1 μm; d_k = 1 μm). Thus, the monovariate population balance model using the average collision efficiency can be used to simultaneously investigate charging and coagulation kinetics of atmospheric particles. These validation tests suggest that all the approaches developed can be used to reliably couple particle charging with coagulation kinetics of atmospheric particles.

5.3.3. Applications

5.3.3.1. Radioactive Neutralizer

Radioactive neutralizers are typically used to control the charge of atmospheric particles in many laboratory-scale experiments. The applicability of the three approaches to studies using radioactive neutralizers was evaluated using the experiments of Alonso et al. (1998) who measured the size distribution of nanometer-size particles passing by a ^{241}Am radioactive neutralizer under various residence times.

Figure 5.10 shows the size distribution of negatively charged particles when the residence time, t = 0.318 s. All particles were initially uncharged, but some particles became charged by capturing positive and negative ions in the neutralizer. Approach 1 accurately predicted the size distribution of the negatively charged particles, while the predictions by Approaches 2 and 3 were different from the measurements. The particle

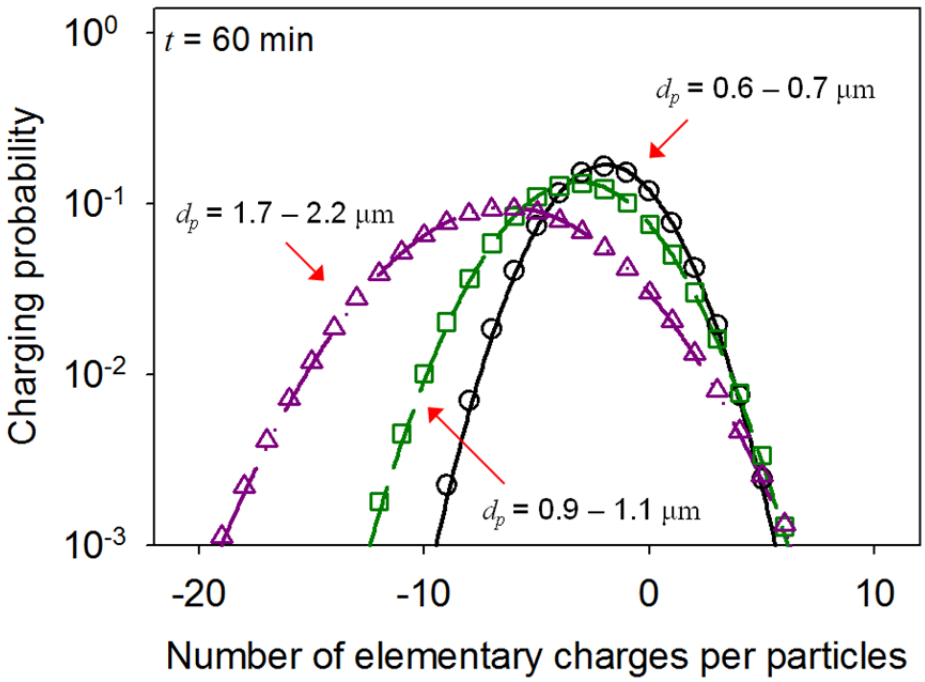

Figure 5.9. Charge distributions of particles undergoing coagulation under a monodispersed initial condition (d_k = 0.5 μm, $N_t = 10^7$ cm^{-3}; $n_0 = 10^{10}$ cm^{-3}). The charging probability was obtained according to Renard et al.(2013). The lines and symbols represent the simulation results of Approaches 1 and 2, respectively. Three size bins are chosen to compare the simulation results of the approaches.

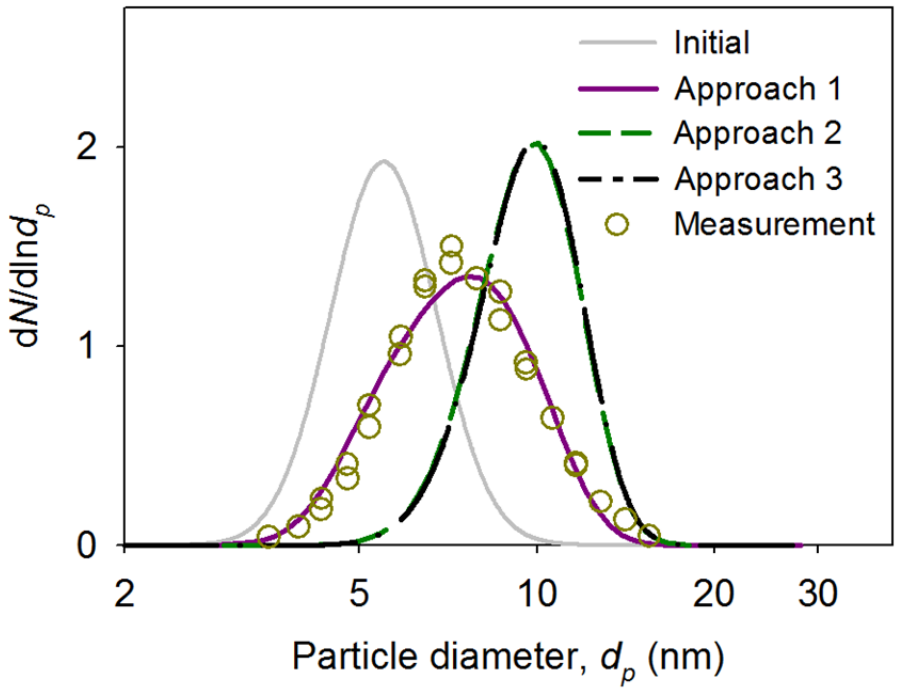

Figure 5.10. Evolution of the size distribution of negatively charged particles in a ^{241}Am radioactive neutralizer. For the initial condition, d_g = 5.5 nm, σ_g = 1.23, and $N_t = 5\times10^9$ cm^{-3}. The simulation time is 0.318s. The measurements were taken from Alonso et al.(1998).

size distributions predicted by all the approaches were similar (not shown). It can be concluded that the Gaussian distribution used in Approaches 2 and 3 cannot accurately predict the charge distributions of very small particles (See Figure 5.2). Thus, Approaches 2 and 3 should not be used for particles smaller than 40 nm.

As shown in Figures 5.2-5.5, Approach 1 can accurately predict the charge accumulation rate of radioactive and nonradioactive particles in the free-molecule, transition, and continuum regimes. Approach 1 employs the interpolation formula of Fuchs that can be used to compute the collision frequency of the particles in these regimes, revealing that this approach can also precisely predict the charge distribution of larger particles undergoing coagulation. These results suggest that Approach 1 can be a reasonable option to simultaneously simulate charging and coagulation of particles of any size in laboratory-scale experiments.

5.3.3.2. Charging and Coagulation of Nonradioactive Particles in Urban Atmosphere

Hoppel (1985) simulated charging of 0.06-μm urban aerosols by diffusion charging; however, effects of coagulation on their steady-state charge distribution were excluded from the simulation. Changes in the particle charge and size distributions by charging and coagulation were investigated in this work on the basis of the simulation of Hoppel (1985) for comparison. The simulation time was approximately 100 min, but for completeness, we repeated and extended the Hoppel (1985) simulation to 1 day. The extended results were compared with prediction results of Approach 1, which involves the effects of coagulation on the particle charge distribution. It was assumed that cosmic rays and natural radioactivity generate ion pairs in the atmosphere, giving $q_b \approx 10^7$ m^{-3} s^{-1} (Hoppel, 1985).

Figure 5.11 presents changes in the particle charge and size distributions vs time. The simulation results performed by Hoppel (1985) showed that the particle charge

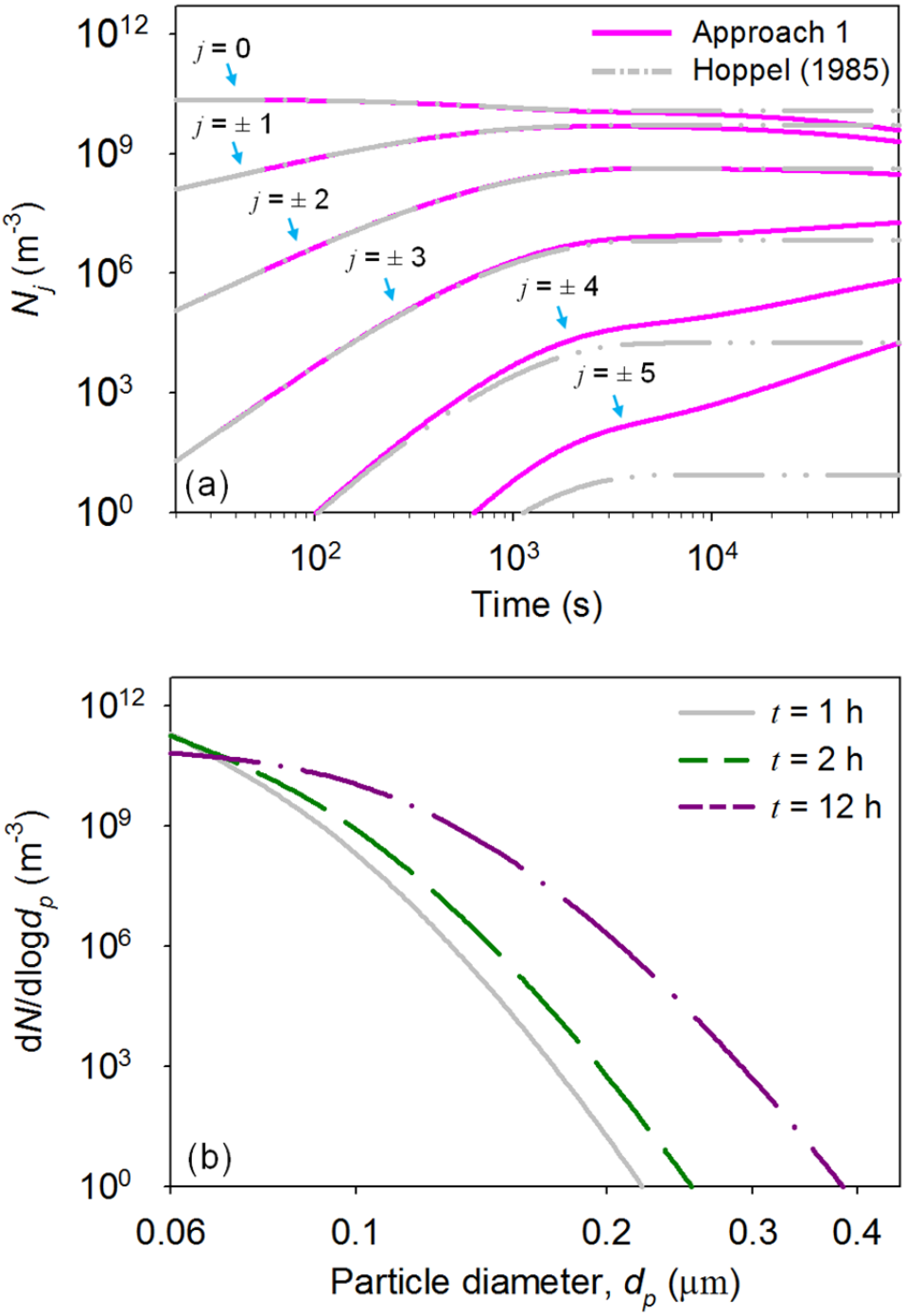

Figure 5.11. Time-evolution of the charge (a) and size (b) distributions of atmospheric particles in the postulated atmosphere of Hoppel (1985) (d_k = 0.06 μm, N_t = 2.3×10^{10} m^{-3}; q = 10^7 m^{-3} s^{-1}). Approach 1 was used to involve the effects of coagulation on the Hoppel (1985) simulation.

distribution approached its steady-state value after approximately 90 min. However, as time elapsed, the particles grew in size due to coagulation. The size growth led to the generation of large particles capturing many ions, thereby modifying the particle charge distribution.

The simulation results of Hoppel (1985) also indicated that the ion concentrations became unchanged after reaching a steady state. However, coagulation reduced the particle number concentrations which can affect the loss rate of ions by diffusion charging (see equations 5.1 and 5.2). The reduction in the particle concentrations creased the ion concentrations, thereby enhancing the electrical conductivity of the postulated atmosphere (Figure 5.12). The ion concentrations and electrical conductivity are expected to increase until ion-ion recombination becomes the major ion removal mechanism. These results suggest that coagulation can affect the electrical properties in the atmosphere, as well as the particle charge distribution.

5.3.3.3. Charging and Coagulation of Radioactive Particles in the Atmosphere

5.3.3.3.1. Comparison with results by Greenfield (1956)

Nuclear events can release particles carrying radionuclides. Greenfield (1956) simulated time-evolution of the charge distribution of 0.1 μm radioactive particles emitting energetic electrons at 6-km altitude. Because Greenfield (1956) assumed that the particle size distribution is constant for 4 hours, the influence of coagulation on the particle charge distribution was evaluated using the simulation conditions postulated by Greenfield (1956).

Figure 5.13 shows changes in the particle charge distributions vs time. Both self-charging and diffusion charging influenced the charge accumulation on radioactive particles. Due to many ion pairs produced by beta radiation (Figure 5.14), positive charge accumulated on the particles by self-charging was rapidly neutralized by capturing negative ions. Thus, the particle charge distribution given by Approach 1 was slightly

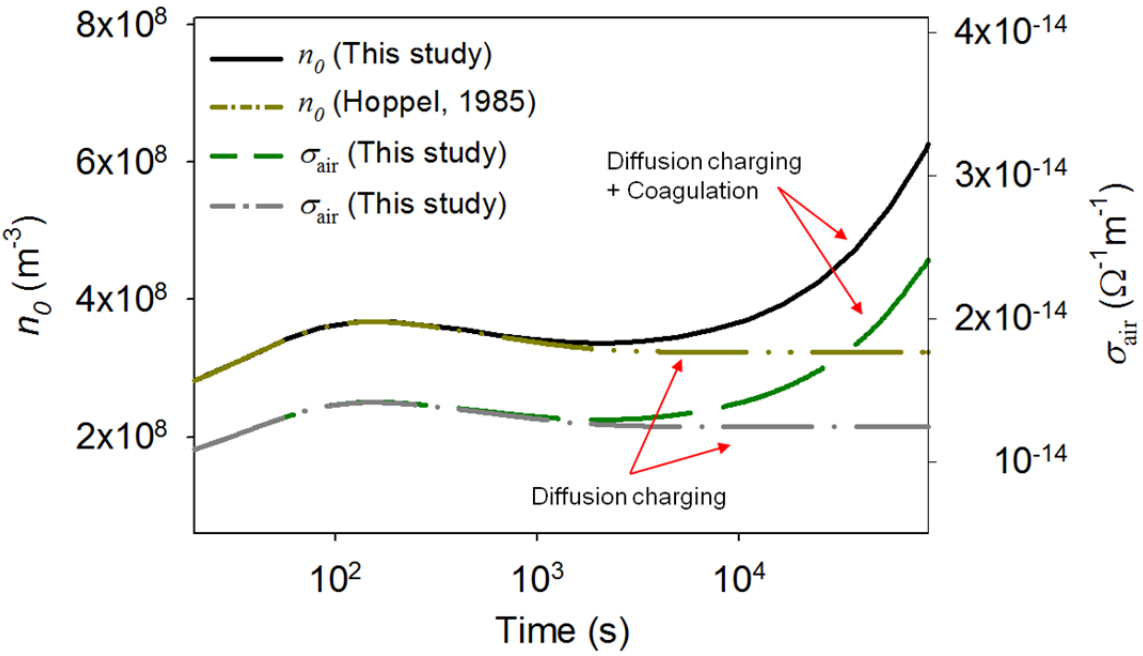

Figure 5.12. Time-evolution of the mean ion concentration, n_0 and air conductivity, σ_{air} in the postulated atmosphere of Hoppel (1985) (d_k = 0.06 μm, $N_t = 2.3\times10^{10}$ m^{-3}; $q = 10^7$ m^{-3} s^{-1}).

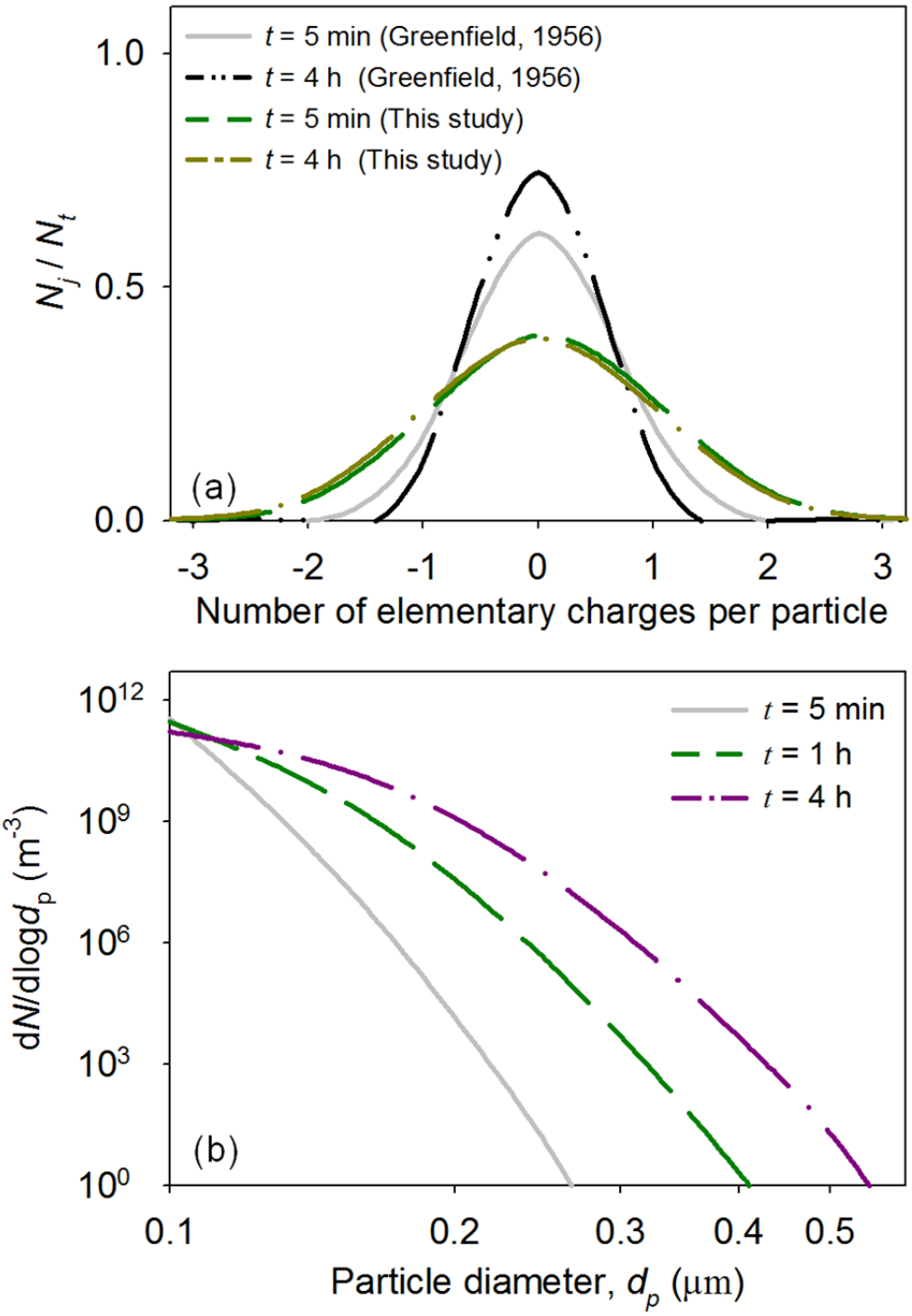

Figure 5.13. Time-evolution of the charge (a) and size (b) distributions of monodispersed radioactive particles at 6 km altitude (d_k = 0.1 μm, $N_t = 3.55\times10^{10}$ m^{-3}; $I = 1.5\times10^{4}$ s^{-1}). Approach 1 was used to simultaneously simulate surface charging and coagulation of radioactive particles.

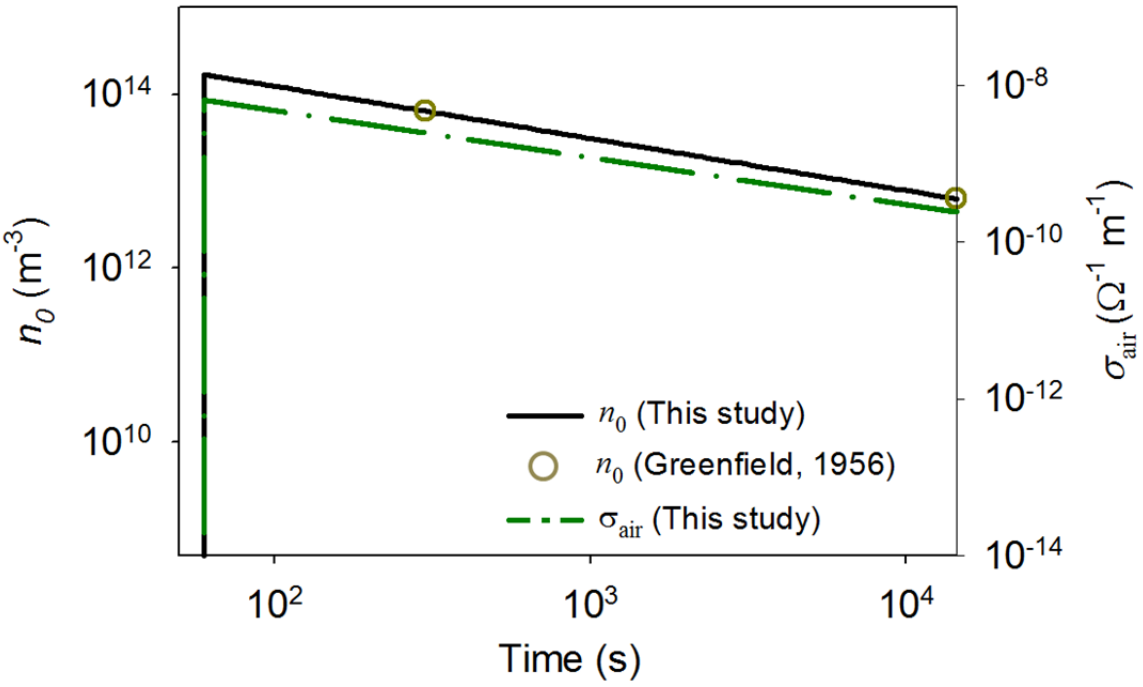

Figure 5.14. Time-evolution of the mean ion concentration, n_0 and air conductivity σ_{air} induced by monodispersed radioactive particles at 6 km altitude (d_k = 0.1 μm, N_t = 3.55×10^{10} m^{-3}; I = 1.5×10^4 s^{-1}). The lines represent the simulation results of Approach 1. The symbols represent the estimation of Greenfield (1956).

shifted to the right of the zero elementary charge in Figure 5.13(a), although large particles with a high level of radioactivity were generated by coagulation. As time elapsed, the particle charge distribution was slightly moved to the left. Because the decay rates of the highly radioactive particles were reduced over time, their self-charging rates also decreased, and this led to the slight movement of the charge distribution to the left in Figure 5.13(a).

The discrepancies between the predictions of Approach 1 and Greenfield (1956) result mainly from the ion-particle attachment coefficient used in the simulation. The values assumed by Greenfield (1956) were beyond the ion-particle attachment coefficient found by other researchers (e.g., Hoppel and Frick, 1986), leading to the discrepancies observed (Kim et al., 2015).

Beta radiation caused by radioactive decay rapidly increased the ion concentrations, thereby enhancing the electrical conductivity in the atmosphere (Figure 5.14). In contrast to the case shown in Figure 5.12, the ion concentrations and air conductivity significantly decreased with time because the ionization rate of air molecules decreased considerably, and ion-ion recombination was responsible for the change in the concentrations. Nevertheless, the air conductivity enhancement by beta radiation was much higher than that by cosmic rays and natural radioactivity.

After the Chernobyl and Fukushima accidents, short- and long-range transport of particles carrying radionuclides, such as ^{137}Cs and ^{134}Cs, affected the electrical properties of the local atmosphere in many places (Israelsson and Knudsen, 1986; Yamauchi et al., 2012). In particular, beta radiation led to significant changes in the electrical conductivity and potential gradient in the local atmosphere (Kim et al., 2015). Israelsson et al. (1987) suggested that an increase in the electrical conductivity led to enhancement of lightning activities at radioactively contaminated sites in Sweden. These observations reveal that the approaches developed in this study can be employed to investigate the influence of radionuclides on electrification phenomena in the atmosphere.

5.3.3.3.2. Steady-state assumption of radioactive particle charging

The steady-state assumption of particle charging can be useful to simulate coagulation of radioactive particles in model studies of radioactivity transport. Charging and coagulation kinetics of radioactive particles were investigated using Approaches 2 and 3 to evaluate the validity of the steady-state assumption of radioactive particle charging. For comparison, the size growth of particles by coagulation was simulated by assuming the Boltzmann charge distribution.

We used the simulation condition employed to validate the average collision efficiency, but additionally presumed that radioactive decay of ^{134}Cs is responsible for the ionization of air molecules. The specific radioactivity of ^{134}Cs was obtained from Clement and Harrison (1992). The ionization rate of ^{134}Cs was estimated according to Kim et al. (2015). Under these conditions, eq 4.8 revealed that $5\tau \approx 4.3$ ms. Thus, we assumed that charge accumulation rates of ^{134}Cs particles instantaneously reach steady state, and evaluated this assumption for the simulation conditions of $X \approx 0.7$ and ion concentration given by $q_I = I_{\text{Cs-134}} \times A_{\text{Cs-134}} \times N_t$ (a function of ion-particle attachment, ion-ion recombination, and beta radiation).

Figure 5.15 shows the charge and size distributions of the ^{134}Cs particles after 2 hours of evolution. The prediction results of Approach 3 were different from those of the case assuming the Boltzmann charge distribution, but agreed well with those of Approach 2, suggesting that the steady-state assumption of radioactive particle charging can be valid if τ is small. We also tested the assumption of Approach 3 using different initial conditions (e.g., $d_k = 0.3$ μm), and the agreement was still maintained (not shown).

5.3.4. Computational costs

The computational costs to predict transport of particles containing contaminants depends on the number of ordinary differential equations (ODEs) solved during simulation. Thus, the number of ODEs involved in the three approaches was evaluated by

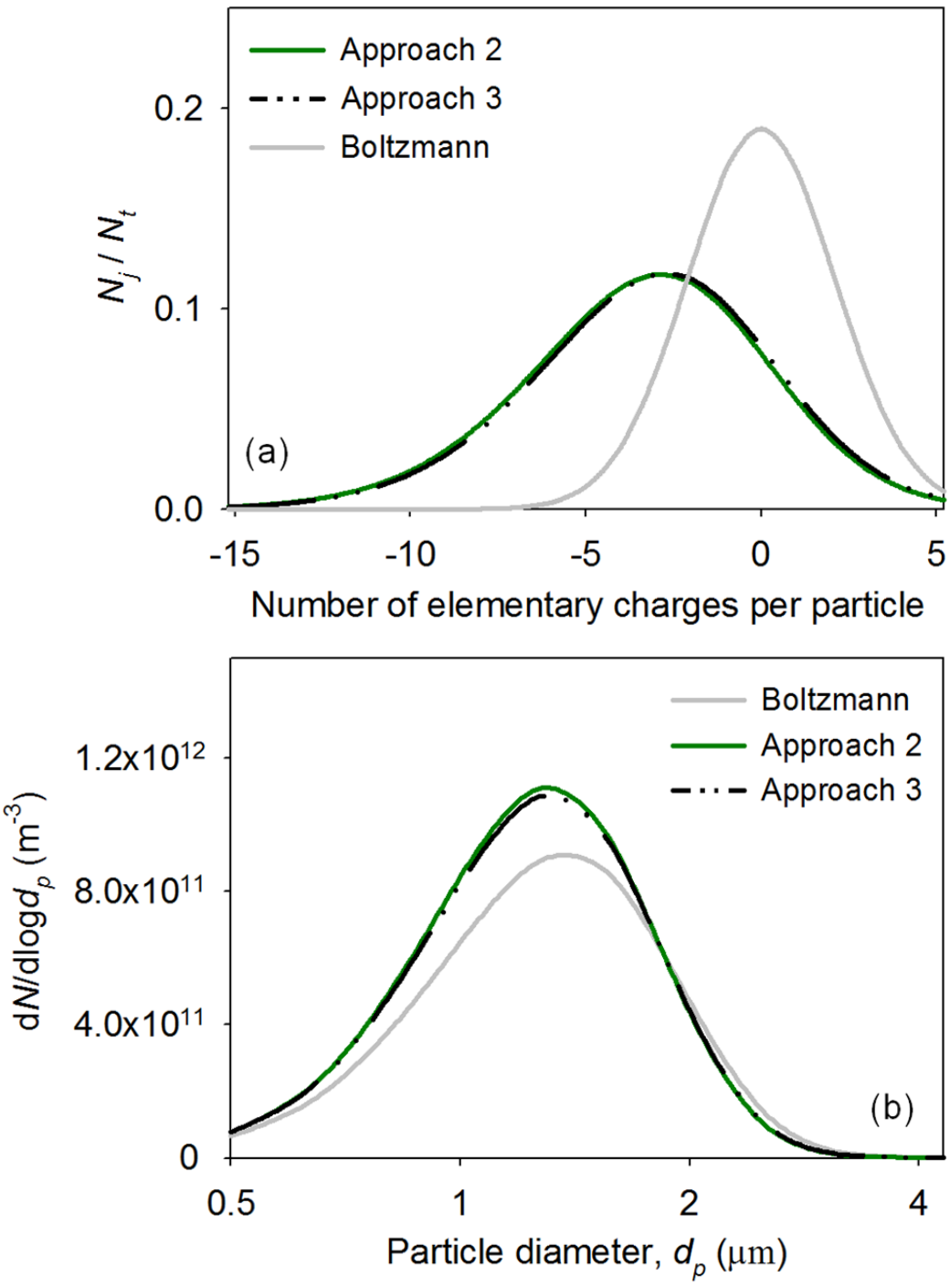

Figure 5.15. The charge (a) and size (b) distributions of initially monodispersed ^{134}Cs particles (d_k = 0.5 μm, $A_{Cs\text{-}134}$ = 14.5 Bq; $N_t = 10^{13}$ m^{-3}). The simulation time is 2 hours.

assuming 30 size bins, which corresponds to those used in the two-moment aerosol sectional microphysics model, covering particle diameters from 0.01 μm to 10 μm. Table 5.3 shows an example of the computational costs of the three approaches. For Approach 1, we assumed that atmospheric particles can acquire up to fifteen elementary charges regardless of their sign, thereby resulting in 932 ODEs. Because Approaches 2 and 3 employed the monovariate population balance model, a fewer number of ODEs were involved in these Approaches than in Approach 1, suggesting that they are computationally more efficient. For instance, compared to Approach 1, Approaches 2 and 3 more quickly computed the charge accumulation and coagulation rates of urban aerosols.

A simple way to reduce the number of ODEs included in Approach 1 is to assume that atmospheric particles acquire only a few electrical charges. For example, Laakso et al. (2002) assumed that submicron particles can acquire elementary charges from -5 to +5. This assumption can be valid if the particle size is small [see Figure 5.2 (a)]. However, when the simulation conditions were used, we observed loss of submicron particles because they can acquire more elementary charges (Figure 5.16). To preserve mass and charge, one may optimize the minimum number of elementary charges using the charge balance model of Approach 1, and then begin the simulation of charging of particles undergoing coagulation.

Approach 3 includes all the physics of charging and coagulation to predict the particle size/charge distribution, but, compared to Approaches 1 and 2, it is computationally more suitable for use in a 3-D global transport model to predict the transport of radioactivity in the environment after a radiological event such as a nuclear plant accident.

Table 5.3. Computational costs of the approaches used.

Example: 30 size bins		Approach 1	Approach 2	Approach 3
The number of ODEs	Ion balance model	2	2	-
	Charge balance model	30 × 31 = 930	30	-
	Population balance model		30	30
	Total	932	62	30
Computational time for urban aerosol[a,b] (s)		12724.2	302.6	8.5

[a] Simulation conditions: $d_g = 0.116$ μm, $\sigma_g = 1.46$, $N_t = 6.718\times10^9$ m^{-3} and $q = 10^7$ m^{-3} s^{-1} (Kim et al., 2015). The simulation time is 6 hours.

[b] Computational resources: Intel(R) Core(TM)2 Duo CPU E6850 @ 3.00 GHz with 4GB RAM and Matlab ODE solver.

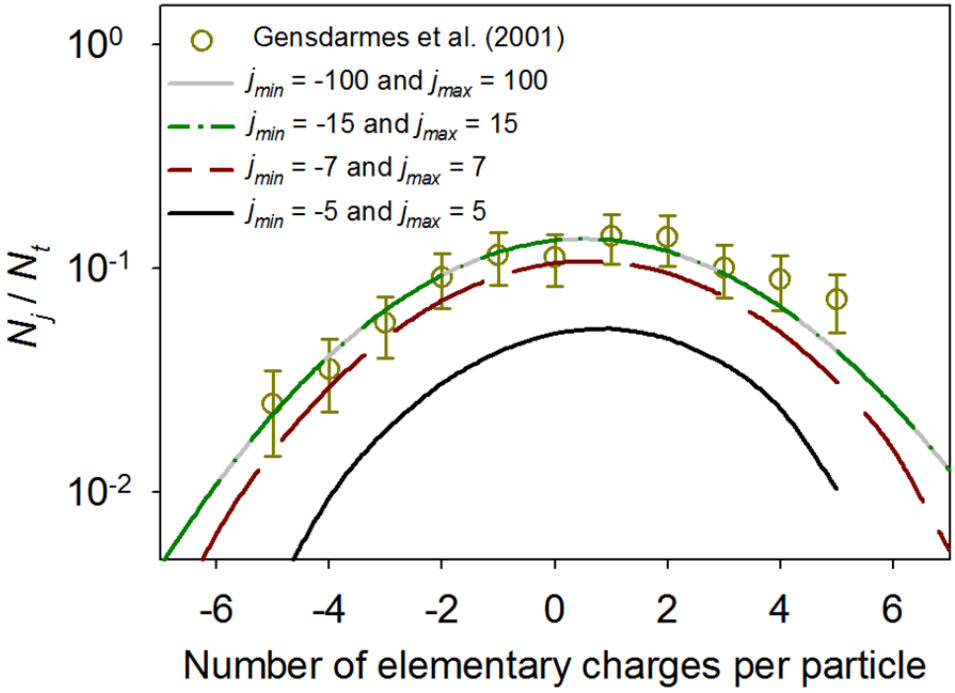

Figure 5.16. The charge distributions of monodispersed ^{137}Cs particles predicted under various boundary conditions (d_k = 0.82 µm, $A_{Cs\text{-}137}$ = 12.8 mBq, and $q_I = 7.1\times10^6$ m^{-3} s^{-1}). j_{min} and j_{max} represent the minimum and maximum values for particle charge classes.

5.4. Summary

Understanding the behavior of atmospheric particles is important to accurately predict short- and long-range transport of contaminants. Particle charging and coagulation processes can strongly affect the behavior of atmospheric particles because these processes can change their important physical and electrical properties, such as size and charge. This study has shown three approaches with a wide range of complexity and applications to involve the mutual effects of charging and coagulation processes in the simulation of particle charge and size distributions vs time. Depending on the initial conditions, these approaches can be employed to accurately predict the behavior of atmospheric particles carrying radioactive contaminants. We have shown the approaches to be applicable to a wide variety of atmospheric (laboratory and field) applications. The accuracy of the approaches depends on the assumptions made to reduce computational cost. The developed approaches can be readily incorporated into microphysical and transport models of any scale to account for charging phenomena of atmospheric particles.

5.5. Acknowledgements

This chapter involves contributions from coauthors and was published in: Kim, Y-H., Yiacoumi, S., Nenes, A., Tsouris, C. 2015b. Charging and coagulation of radioactive and nonradioactive particles in the atmosphere. *Atmos. Chem. Phys. Discuss.*, 15, 23795-23840.

CHAPTER 6

INFLUENCE OF RADIOACTIVITY ON TIME-EVOLUTION OF CHARGE AND SIZE OF RADIOACTIVE AND NONRADIOACTIVE PARTICLES IN THE ATMOSPHERE

Radioactivity can influence the dynamic evolution of the particle charge and size distributions in air. However, the radioactivity effects have been typically neglected in modeling studies of radioactivity transport largely because of lack of information and simulation tools. This study investigates the influence of radioactivity on time-evolution of the charge and size distributions of radioactive and nonradioactive particles in air and develops simple approaches for further investigations. Involving charging, aggregation, and electrostatic dispersion, a comprehensive population balance model (PBM) has been developed to examine particle charge/size distribution dynamics. It is shown that, compared to nonradioactive particles, the charge and size distributions of radioactive particles may evolve differently with time because radioactivity and electrostatic dispersion can significantly affect the charging and aggregation kinetics of the particles. It is found that, after the Fukushima accident, background aerosols in the pathway of radioactive plumes might be highly charged due to ionizing radiation, suggesting that radiation fields may strongly influence in-situ measurements of charged atmospheric particles. The comprehensive PBM is simplified, and the validity and application of the simplified PBMs are discussed. This study provides useful insight into how radioactivity can affect the dynamic behavior of particles in atmospheric systems including radiation sources.

6.1. Introduction

Charge and size, dynamically evolving properties of particles, can govern the particle behavior in various atmospheric systems such as ambient air (Tripathi and Harrison, 2001), containment systems of nuclear reactors (Clement et al., 1995), dusty plasma (Fortov et al., 2001), human respiratory systems (Cohen et al., 1998), particle measurement systems (Rosinski et al., 1962; Yeh et al., 1978; Gensdarmes et al., 2001), radioactive neutralizers (Cooper and Reist, 1973), and thermal spas (Nikolopoulos and Vogiannis, 2007). In these systems, charge and size of particles can affect their charging, aggregation, and dry and wet depositions, which are also vital processes in radioactivity transport modeling (Hu et al., 2014; Katata et al., 2012; Kim et al., 2014, 2015a&b) and in-situ measurements of charged particles (Renard et al., 2013). These systems included various radiation sources such as natural radioactivity (Nikolopoulos and Vogiannis, 2007) and fission products (Clement et al., 1995; Cooper and Reist, 1973; Fortov et al., 2001; Gensdarmes et al., 2001; Rosinski et al., 1962; Tripathi and Harrison, 2001; Yeh et al., 1978). Because such radiation sources can affect evolution patterns of the particle charge and size distributions, understanding the influence of radioactivity is necessary to investigate many microphysical processes occurring in atmospheric systems including radiation sources.

Radioactivity is a property of atoms emitting energetic particles such as alpha and beta particles (Sawyer et al., 1994). The release of energetic particles can lead to charge accumulation on radioactive and nonradioactive particles due to self-charging and diffusion charging mechanisms (Clement and Harrison, 1992; Kim et al., 2014; Kweon et al., 2013; Walker et al., 2010; Yeh et al., 1978). The charging of particles may subsequently affect their size growth by aggregation (Clement et al., 1995; Kim et al., 2015b), the removal of the particles by rain scavenging (Tripathi and Harrison, 2001), and adsorption/condensation of gas molecules (Kweon et al., 2015) by generating

electrostatic interactions. However, radioactivity-induced charging and the subsequent charging effects have been typically neglected in modeling studies of radioactivity transport, mainly due to insufficient information on particle charge/size distribution dynamics (Hu et al., 2014) and lack of simulation tools to couple particle transport with charging effects (Kim et al., 2015b).

Previous attempts to incorporate electrostatic interactions into charge/size distribution dynamics include those of Clement and Harrison (1992) and Clement et al. (1995) who investigated radioactivity-induced charging and its subsequent influence on particle collision. However, the investigations assumed no size evolution of radioactive particles. Adachi et al. (1981), Oron and Seinfeld (1989a), and Vemury et al. (1997) developed sectional models to predict time-dependent changes in the charge and size distributions of particles undergoing aggregation and electrostatic dispersion, but the models excluded particle-ion dynamics. Oron and Seinfeld (1989b) improved the sectional model to include particle-ion dynamics, but the model is still not applicable to radioactive particles because self-charging was omitted. Thus, a more comprehensive predictive model is required to examine charge/size distribution dynamics of radioactive and nonradioactive particles in the atmosphere.

This study investigates the time-evolution of charge and size distributions of radioactive and nonradioactive particles using a bivariate population balance model (PBM) which establishes charge and size as independent variables. In our previous work (Kim et al., 2015a&b), the bivariate PBM included particle-ion dynamics and radioactivity-induced charging. In the present study, we have incorporated electrostatic dispersion of particles and ions into the bivariate PBM to comprehensively consider electrostatic interactions. The bivariate PBM has been simplified by reducing the number of the independent variables. The validity and application of the simplified PBM have been investigated.

6.2. Background: Electrostatic Interactions of Charged Objects

Electrical charge generates electrostatic forces between charged objects such as colloidal particles and ions (Chin et al., 1998; Fuchs, 1989; Hiemenz and Rajagopalan, 1997; Taboada-Serrano et al., 2005; Tsouris et al., 1995). In a spatially homogeneous atmospheric system containing charged particles and ions, positively charged particles can easily collide with particles and ions with negative charge because of electrostatic attractive forces generated between positive and negative charges. Concurrently, the positively charged particles mutually repel each other and positive ions because of electrostatic repulsive forces. In particular, as shown in Figure 6.1, mutual repulsion may lead to the transport of positively charged particles and positive ions outside the system boundaries until the system reaches charge equilibrium:

$$\rho = e\left[n_+ - n_- + \sum_{j=-\infty}^{\infty} j \sum_{k=1}^{M} N_{kj} \right] = 0 \tag{6.1}$$

where ρ is the space charge density, e is the electrical charge, $n_{\pm}$ represents the concentrations of positive and negative ions, j is the number of elementary charge carried by single particles, and M is the total number of the size bins.

The transport of the charged particles and ions can decrease their concentrations (Oron and Seinfeld, 1989a&b):

$$\frac{dN_{kj}}{dt} = -\frac{B_k j e N_{kj} \rho}{\varepsilon}, \tag{6.2}$$

$$\frac{dn_{\pm}}{dt} = \mp \frac{\mu_{\pm} n_{\pm} \rho}{\varepsilon}, \tag{6.3}$$

where N_{kj} is the concentration of size k particles carrying elementary charge j, B is the particle mobility, $\mu_{\pm}$ are the mobilities of positive and negative ions, and ε is the

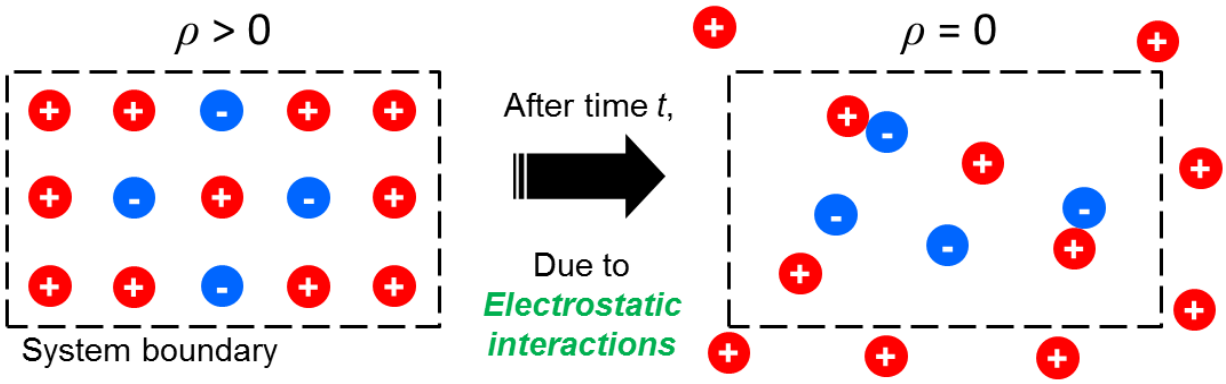

Figure 6.1. Electrostatic interactions of charged objects in a spatially homogeneous colloidal system.

permittivity of vacuum. This phenomenon has been observed in many laboratory-scale experiments and has been called electrostatic dispersion (Whitby et al., 1965; Adachi et al., 1981; Kasper, 1981).

6.3. Model Development

6.3.1. Bivariate Population Balance Model (PBM)

In a spatially homogeneous system, the size and charge distributions of radioactive and nonradioactive particles can be influenced by charging, aggregation, and electrostatic dispersion. Time-evolution of the distributions by the first two processes can be predicted using a bivariate PBM with two independent variables, size and charge (Kim et al., 2015b). The effects of electrostatic dispersion on the distributions can be taken into account by incorporating equation 6.2 into the bivariate PBM:

$$\begin{aligned}\frac{dN_{kj}}{dt} = {} & sA\left(N_{k,j-m} - N_{k,j}\right) + \beta^{+}_{k,j-1} n_{+} N_{k,j-1} - \beta^{+}_{k,j} n_{+} N_{k,j} + \beta^{-}_{k,j+1} n_{-} N_{k,j+1} \\ & - \beta^{-}_{k,j} n_{-} N_{k,j} + \sum_{j'=-\infty}^{\infty} \sum_{\substack{l,m \\ x_{k-1} \le x_l + x_m \le x_{k+1}}}^{l \ge m} \left(1 - \frac{1}{2}\delta^{Kr}_{l,m}\right) \eta_{l,m} F_{l,m,j-j',j'} N_{l,j-j'} N_{m,j'} \\ & - \sum_{j'=-\infty}^{\infty} \sum_{l=1}^{M} F_{k,l,j,j'} N_{k,j} N_{l,j'} - \frac{B_k j e N_{kj} \rho}{\varepsilon}\end{aligned} \tag{6.4}$$

where s is the self-charging coefficient (i.e., the number of charges accumulated on single particles per decay), A is the radioactivity of single particles, $\beta^{\pm}_{k,j}$ represents the ion-particle attachment coefficients, l and m are the size bin numbers, δ^{Kr} is the Kronecker delta, η is a property distribution factor between two size bins, and F is the aggregation frequency.

The first term on the right-hand-side (RHS) of equation 6.4 accounts for self-charging of radioactive particles. The second to fifth terms represent diffusion charging resulting from diffusion of positive and negative ions onto particles. The sixth and

seventh terms account for the production and loss of particles via aggregation. The last term represents the loss of particles by electrostatic dispersion.

In equation 6.4, particle charging is parameterized by s, A, $\beta_{k,j}^{\pm}$, and $n_{\pm}$. The self-charging coefficient, s, is characteristic of the decay modes of radionuclides [e.g., s = 9 for $^{238}PuO_2$ (Yeh et al., 1978); s = 1 for beta-emitting particles (Clement and Harrison, 1992)]. For nonradioactive particles, the self-charging term disappears from eq 6.4 because the particle radioactivity, A, is zero. The ion-particle attachment coefficient, $\beta_{k,j}^{\pm}$, is highly influenced by the properties of particles and ions (e.g., particle size and ion mobility). Various sources and sinks affect the ion concentrations in the atmosphere; thus, $n_{\pm}$ is given by ion balance involving equation 6.3 (Oron and Seinfeld, 1989b; Kim et al., 2015a&b):

$$\frac{dn_+}{dt} = -n_+ \sum_k \sum_j \beta_{k,j}^{+} N_{k,j} - \alpha_{rc} n_+ n_- - \frac{\mu_+ n_+ \rho}{\varepsilon} + q, \tag{6.5}$$

$$\frac{dn_-}{dt} = -n_- \sum_k \sum_j \beta_{k,j}^{-} N_{k,j} - \alpha_{rc} n_+ n_- + \frac{\mu_- n_- \rho}{\varepsilon} + q + q_e, \tag{6.6}$$

where α_{rc} is the recombination rate coefficient of positive and negative ions, q is the production rate of ion pairs, and q_e is the generation rate of electrons. The first three terms on the RHS of equations 6.5 and 6.6 represent the loss of ions by ion-particle attachment, ion-ion recombination, and electrostatic dispersion, respectively. Note that in equation 6.6, the sign of the third term is positive because negative ions can be removed by electrostatic dispersion when $\rho < 0$. The fourth term on the RHS of equations 6.5 and 6.6 stands for ionization of air molecules by ionizing radiation. The last term on the RHS of equation 6.6 accounts for electrons emitted by radioactive decay.

For Brownian aggregation, the aggregation frequency in equation 6.4 can be estimated from the collision frequency, β^{Br} (Fuchs, 1989):

$$\beta_{kl}^{Br} = 2\pi\left(d_k + d_l\right)\left(D_k + D_l\right)\left(\frac{d_k + d_l}{d_k + d_l + \sqrt{\delta_k^{\,2} + \delta_l^{\,2}}} + \frac{8\left(D_k + D_l\right)}{(d_k + d_l)\sqrt{\bar{v}_k^{\,2} + \bar{v}_l^{\,2}}}\right)^{-1}, \qquad (6.7)$$

with

$$\delta_k = \frac{1}{3d_k L_k}\left(\left(d_k + L_k\right)^3 - \left(d_k^2 + L_k^2\right)^{\frac{3}{2}}\right) - d_k,\ L_k = \frac{8D_k}{3d_k \bar{v}_k},\ \bar{v}_k = \sqrt{\frac{8k_B T}{\pi x_k}},$$

where d_k is the particle diameter, D_k is the diffusion coefficient of single particles, k_B is the Boltzmann coefficient, T is the temperature, and x_k is the mass of individual particles. Equation 6.7 does not include the effects of electrostatic particle-particle interactions on the aggregation frequency. The influence of electrostatic interactions can be included by multiplying the collision frequency, β^{Br}, by the collision efficiency, α^{Br} (Fuchs, 1989):

$$\alpha_{kl}^{Br} = \frac{z}{e^z - 1} \qquad (6.8)$$

with $z = \frac{j_k j_l e^2}{2\pi\varepsilon(d_k + d_l)k_B T}$.

6.3.2. Simplification of Bivariate PBM

For computational efficiency, the bivariate PBM can be simplified via two approaches (Adachi et al.1981; Kim et al., 2015b). The first approach focuses on tracking time-evolution of the size distribution and mean charge of particles (Kim et al., 2015b), while the second concentrates on predicting time-dependent changes in the charge distribution and mean size of particles (Adachi et al., 1981). Hereafter, we refer to the approaches by the monovariate and monodisperse PBMs, respectively.

6.3.2.1. Monovariate PBM

Changes in the particle charge and size distributions vs time can be predicted using simple charge balance and the monovariate PBM (Kim et al., 2015b). Similarly to the charging terms of equation 6.4, particle charging can be described using the four charging parameters: the self-charging coefficient, radioactivity per particle, ion-particle attachment coefficients, and ion concentrations (Clement and Harrison, 1992; Kim et al., 2014; 2015b).

$$\frac{dJ_k}{dt} = sA_k + \beta_{k,J}^{+} n_{+} - \beta_{k,J}^{-} n_{-}, \tag{6.9}$$

where J_k is the mean charge of size k particles. The ion concentrations on the RHS of equation 6.9 can be obtained by simplifying the first terms on the RHS of equations 6.5 and 6.6 as:

$$\frac{dn_{+}}{dt} = -n_{+}\beta_{k,J}^{+} N_k - \alpha_{rc} n_{+} n_{-} - \frac{\mu_{+} n_{+} \rho}{\varepsilon} + q, \tag{6.10}$$

$$\frac{dn_{-}}{dt} = -n_{-}\beta_{k,J}^{-} N_k - \alpha_{rc} n_{+} n_{-} + \frac{\mu_{-} n_{-} \rho}{\varepsilon} + q + q_e. \tag{6.11}$$

The mean charge of particles predicted by solving equations 6.9-6.11 can be approximately converted to the particle charge distribution using a Gaussian distribution:

$$N_{kj} = \frac{N_k}{\sqrt{2\pi}\sigma_k} \exp\left(-\frac{(j - J_k)^2}{2\sigma_k^2} \right), \tag{6.12}$$

where σ_k is the standard deviation given by Clement et al. (1995). Then, the approximate charge distribution is used to compute ρ and the rates of aggregation and electrostatic dispersion in the monovariate PBM with only the particle size as the independent variable:

$$\frac{dN_k}{dt} = \sum_{\substack{l,m \\ x_{k-1} \le x_l + x_m \le x_{k+1}}}^{l \ge m} \left(1 - \frac{1}{2}\delta_{l,m}^{Kr}\right)\eta_{l,m} F_{l,m} N_l N_m - \sum_{l=1}^{M} F_{k,l} N_k N_l - \sum_{j=-\infty}^{\infty} \frac{B_k j e N_{kj} \rho}{\varepsilon}. \quad (6.13)$$

In equation 6.13, the first two terms on the RHS account for particle aggregation. The third term describes electrostatic dispersion. The influence of distributed charges on particle aggregation can be involved by replacing equation 6.8 with the average collision efficiency (Kim et al., 2015b):

$$\bar{\alpha}_{kl}^{Br} = 1 + \frac{\sum_{j_k j_l \neq 0} N_{k,j_k} N_{l,j_l} \left(\alpha_{kl}^{Br} - 1\right)}{\sum_{j_k} N_{k,j_k} \sum_{j_l} N_{l,j_l}}. \quad (6.14)$$

6.3.2.2. Monodisperse PBM

Adachi et al. (1981) developed the monodisperse PBM to simulate aggregation and electrostatic dispersion of particles:

$$\frac{dN_j}{dt} = \frac{1}{2}\sum_{j'=-\infty}^{\infty} F(V, j, j') N_{j-j'} N_{j'} - \sum_{j'=-\infty}^{\infty} F(V, j, j') N_j N_{j'} - \frac{B(V) j e N_j \rho}{\varepsilon} \quad (6.15)$$

where V is the average volume of particles. By assuming the monodisperse size distribution, the mean size of single particles can be given as (Vemury et al., 1997):

$$V = \frac{V_t}{N_t}, \quad (6.16)$$

where V_t and N_t are the total volume and number concentration of particles, respectively. The charging terms of equation 6.4 can be easily modified and incorporated into equation 6.15 to include particle charging.

6.3.3. Algorithm to Simulate Electrostatic Dispersion

The aforementioned PBMs include the electrostatic dispersion terms. Figure 6.2 shows an algorithm to involve the effects of electrostatic dispersion on the time-evolution of the particle charge and size distributions and ion concentrations. The algorithm allows the concentrations of particles and ions to decrease due to electrostatic dispersion when the space charge of the system is nonzero. The electrostatic dispersion terms of the models disappear under a condition of zero space-charge (e.g., the Boltzmann equilibrium).

6.3.4. Simulation

The PBM was used to investigate the dynamics of charge and size distributions of radioactive and nonradioactive particles. ^{238}Pu, ^{137}Cs, and ^{131}I were chosen as alpha- and beta-emitting radionuclides, respectively, because particles containing these radionuclides are typically studied in particle measurement systems, as well as model studies (Yeh et al., 1978; Clement and Harrison, 1992; Gensdarmes et al., 2001; Hu et al., 2014; Kim et al., 2015a). The decay of ^{238}Pu emits single alpha particles with kinetic energy of 5.593 MeV, while those of ^{137}Cs and ^{131}I release single beta particles of mean kinetic energy 0.1921 MeV and 0.1812 MeV, respectively. To involve alpha- and beta-radiations leading to ionization of air molecules in simulation, we assumed that ^{238}Pu can produce 15,000 ion pairs per alpha decay (Clement and Harrison, 1992), while ^{137}Cs and ^{131}I can generate 2,067 and 1,945 ion pairs per beta decay, respectively (Kim et al., 2015a).

For diffusion charging, $\beta_{k,j}^{\pm}$ was computed from Fuchs (1963) and Hoppel and Frick (1986). For the computations, because negative ions have typically higher mobility than positive ions, we assumed that $\mu_{-} = 1.65$ m^2 V^{-1} s^{-1}, $\mu_{+} = 1.15$ m^2 V^{-1} s^{-1}, $m_{-} = 80$ atomic mass unit (amu), and $m_{+} = 150$ amu (Alonso et al., 1997; Kim et al., 2015b). Typical values for the properties of background air were quoted from Harrison and

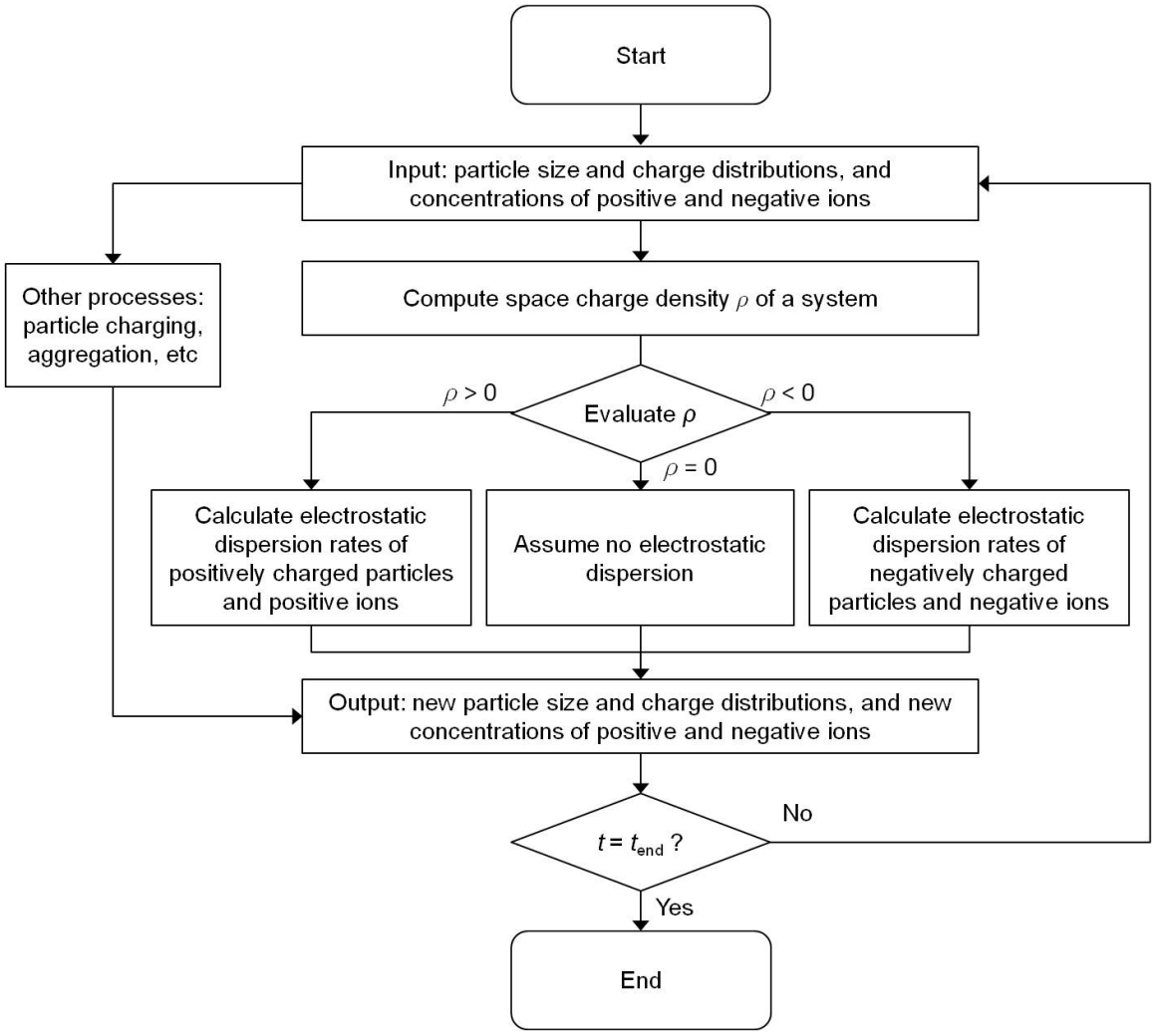

Figure 6.2. Algorithm to simulate electrostatic dispersion of particles and ions.

Carslaw (2003): (i) the air contains 5×10^8 ion pairs m^{-3}, (ii) the background ionization rate is 10^7 ion pairs m^{-3} s^{-1}, and (iii) α_{rc} is 1.6×10^{-12} m^{-3}. For discretization, similarly to Oron and Seinfeld (1989a), we assumed geometric grid ($x_{k+1} = 2x_k$).

6.4. Results and Discussion

6.4.1. Validation Tests of Bivariate PBM

The bivariate PBM includes four processes causing electrostatic interactions: self-charging, diffusion charging, aggregation, and electrostatic dispersion. The first three processes of the bivariate PBM were validated in our previous work (Kim et al., 2015a&b). In brief, the bivariate PBM, excluding electrostatic dispersion, accurately predicted the charging and aggregation of radioactive and nonradioactive particles under various initial conditions. In the present study, the computational codes to solve the electrostatic dispersion equations (equations 6.2 and 6.3) were first evaluated with analytical solutions. Then, the validity of the bivariate PBM involving the electrostatic dispersion equations was assessed using Adachi et al. (1981) and Oron and Seinfeld (1989).

6.4.1.1. Electrostatic dispersion of particles and ions

Results of the numerical analysis of equations 6.2 and 6.3 were compared with those of the analytical solutions given by Whitby et al. (1965) and Kasper (1981), respectively. Figure 6.3 shows time-dependent changes in particle and ion concentrations by electrostatic dispersion under three initial conditions: (i) monodisperse 1-μm particles with single positive charge, (ii) positive ions, and (iii) negative ions. Because the initial concentrations were similar, electrostatic dispersion rates of the particles and ions depended on their mobilities. Compared to the change in the particle concentration vs time, the ion concentrations became more rapidly reduced by electrostatic dispersion

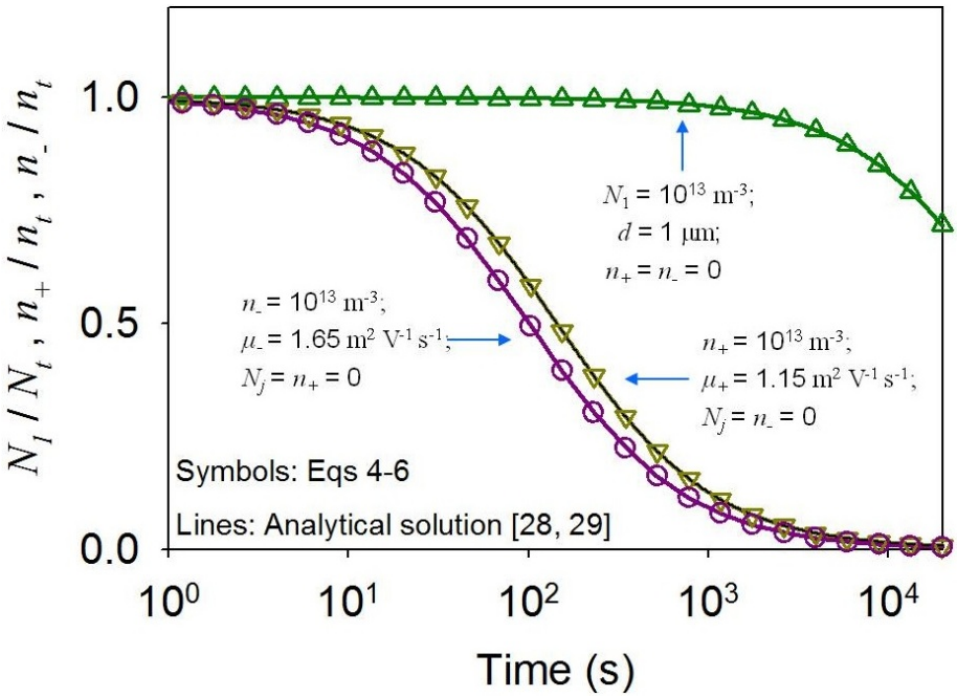

Figure 6.3. Time-dependent changes in the concentrations of particles with j = +1 and positive and negative ions. The lines and symbols represent the results of analytical solutions (Whitby et al., 1965; Kasper, 1981) and numerical analysis of equations 6.2-6.3 (this study), respectively.

because the ions were more mobile than the charged particles. These results obtained from the analysis of equations 6.2 and 6.3 were in good agreement with the electrical dispersion rates predicted by the analytical solutions.

6.4.1.2. Electrostatic dispersion of particles undergoing aggregation

6.4.1.2.1. Algorithm effects

Theoretical investigations have been extensively performed to predict electrostatic dispersion of particles undergoing aggregation (Adachi et al., 1981; Oron and Seinfeld, 1989a; Vemury et al., 1997). In these investigations, electrostatic dispersion rates of particles are typically obtained by estimating the last term in equation 6.4. However, the sign of the electrostatic dispersion term depends on space charge. To calculate electrostatic dispersion rates of particles as a function of space charge of a system, the bivariate PBM used in this study employs the algorithm shown in Figure 6.2. The effectiveness of the algorithm was assessed using simulation results of Adachi et al. (1981) and Oron and Seinfeld (1989a). The charging terms in equation 6.4 and ion balance (equations 6.5 and 6.6) were neglected during the evaluation of the algorithm included in the bivariate PBM.

Figure 6.4 shows time-evolution of the particle charge distributions under initially asymmetric uni- and bi-modal charge distributions. When equation 6.4 was solved without the algorithm shown in Figure 6.2, the simulation results were comparable to those of Adachi et al. (1981) and Oron and Seinfeld (1989a), respectively. However, discrepancies were found between the simulation results of the bivariate PBM including the algorithm and those of Adachi et al. (1981) and Oron and Seinfeld (1989a), respectively. The discrepancies might arise from the treatment of the electrostatic dispersion term in equation 6.4 by the algorithm. Because the initial conditions of the test cases produced negative space charge, electrostatic dispersion did not affect the concentrations of positively charged particles. Thus, the electrostatic dispersion term for

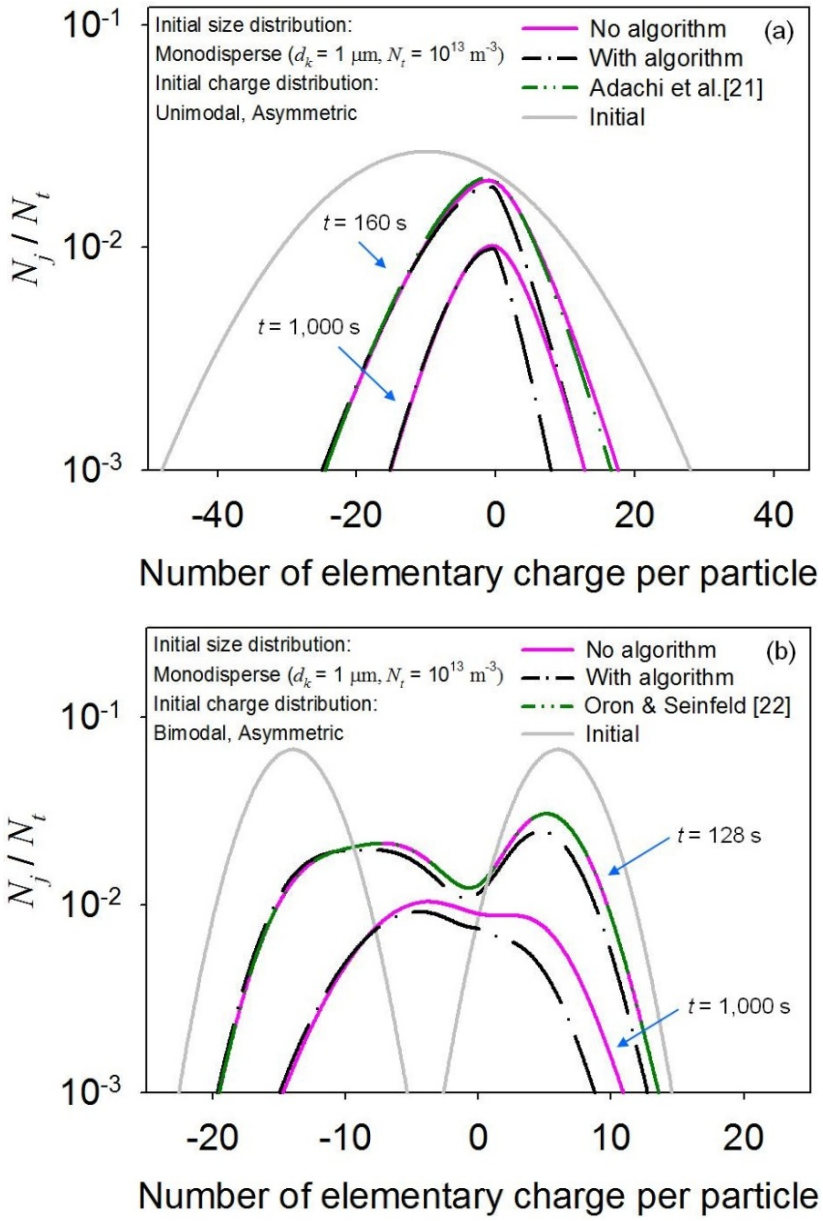

Figure 6.4. Time-dependent changes in the particle charge distributions predicted using the bivariate PBM including and excluding the algorithm of Figure 6.2, respectively. The simulation results obtained from solving equation 6.4 without the algorithm were in good agreement with those of Adachi et al. (1981) and Oron and Seinfeld (1989a), but were different from those obtained from solving equation 6.4 with the algorithm.

the positively charged particles was neglected in the simulation of the bivariate PBM using the algorithm, while it was involved in the other cases. Because of the negative space charge, the electrostatic term for the positively charged particles was positive. Therefore, the simulation results obtained from the bivariate PBM excluding the algorithm [e.g., Adachi et al. (1981)] could slightly overestimate the concentration of positively charged particles, thereby affecting the concentration of negatively charged particles with time.

For other initially symmetric uni- and bi-modal particle charge distributions, the prediction results obtained from equation 6.4 including the algorithm were comparable to those of Adachi et al. (1981) and Oron and Seinfeld (1989a) because space charge rarely formed during the simulations (not shown).

6.4.1.2.2. Comparison with measurements

The validity of the bivariate PBM including electrostatic dispersion was tested using the measurements of Adachi et al. (1981) who investigated the time-evolution of the electrical mobility distribution of particles with an asymmetric bimodal charge distribution. Two peaks of the initial charge distribution were observed at j = -104 and 49. For comparison, simulations were performed with only the aggregation and electrostatic dispersion terms, respectively.

Figure 6.5 shows the electrical mobility distribution of negatively charged particles at t = 5 min. The results of the simulation involving both aggregation and electrostatic dispersion were closer to the measurements than those including each process, respectively. The discrepancies in the simulation results indicate that the bipolarly charged particles might simultaneously undergo aggregation and electrostatic dispersion because of their electrostatic interactions.

It has been shown that the developed bivariate PBM can accurately calculate electrostatic dispersion rates of charged particles undergoing aggregation, as well as

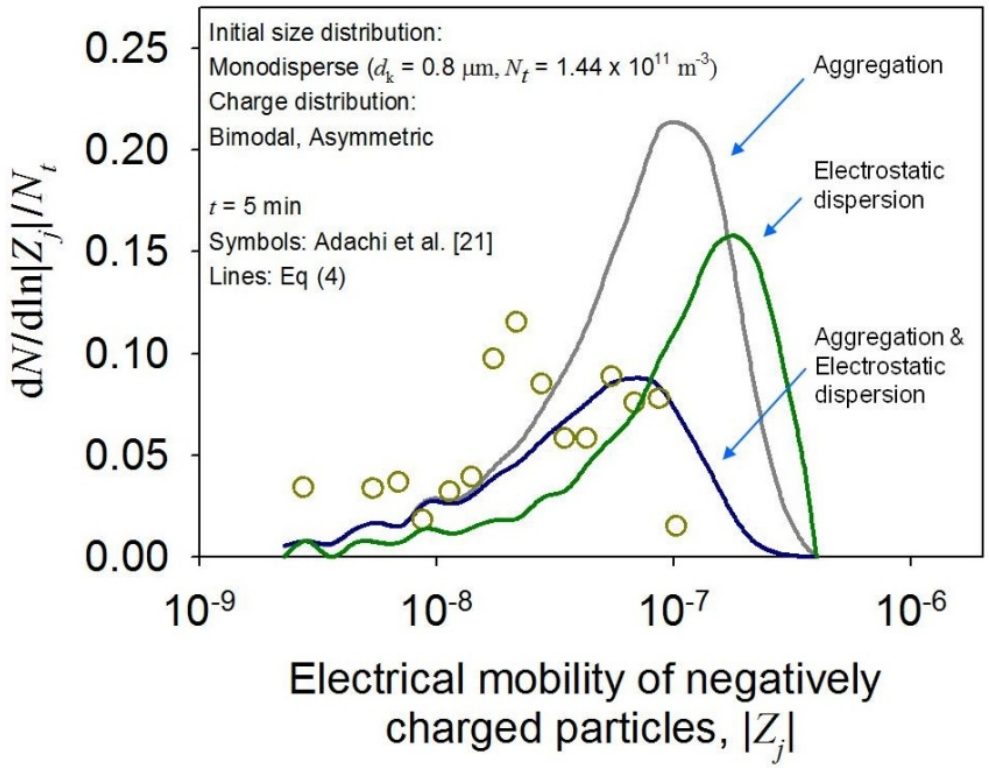

Figure 6.5. Electrical mobility distribution of negatively charged particles at t = 5 min. The symbols and lines represent the measurements of Adachi et al. (1981) and the simulation results of the bivariate PBM of this work, respectively.

precisely computing the aggregation rates of particles accumulating charges (Kim et al., 2015b). These validation tests suggest that the developed bivariate PBM can accurately predict charge and size distribution dynamics of particles undergoing charging, aggregation, and electrostatic dispersion.

6.4.2. Influence of radioactivity on time-evolution of charge and size of radioactive particles

Charge and size distribution dynamics of radioactive particles was investigated with the bivariate PBM employing the developed algorithm shown in Figure 2. Similarly to the previous tests, we assumed monodisperse particles with $N_t = 10^{13}$ m^{-3}. The initial charge distribution was estimated using equation 6.12. Simulation results for nonradioactive particles were provided as a reference.

6.4.2.1. Alpha decay vs beta decay: Effects of kinetic energy

Time-dependent changes in the charge and size distributions of ^{238}Pu and ^{131}I particles were investigated. The properties of charged monodisperse $^{238}PuO_2$ particles [J_k = 2.84; d_k = 0.96 μm; $A_{Pu\text{-}238}$ = 1.92 Bq (Yeh et al., 1978)] were used to postulate the initial charge distribution of ^{238}Pu particles. For comparison, we assumed that the values of ^{131}I particles for J_k, d_k, and A are comparable to those of the ^{238}Pu particles.

Figure 6.6 shows changes in the charge and size distributions of the ^{238}Pu and ^{131}I particles vs time. The initial charge distributions of the radioactive particles instantaneously shifted to the left and then became widely dispersed over time, while no such response was observed in the reference simulation [Figure 6.6(a)]. Radioactivity-induced charging and electrostatic dispersion of positive ions caused the horizontal movement of the particle charge distributions. The initial changes indicated that the ^{238}Pu particles accumulated more negative charge than that acquired by the ^{131}I particles. The different charging states affected the size growth of the radioactive particles due to

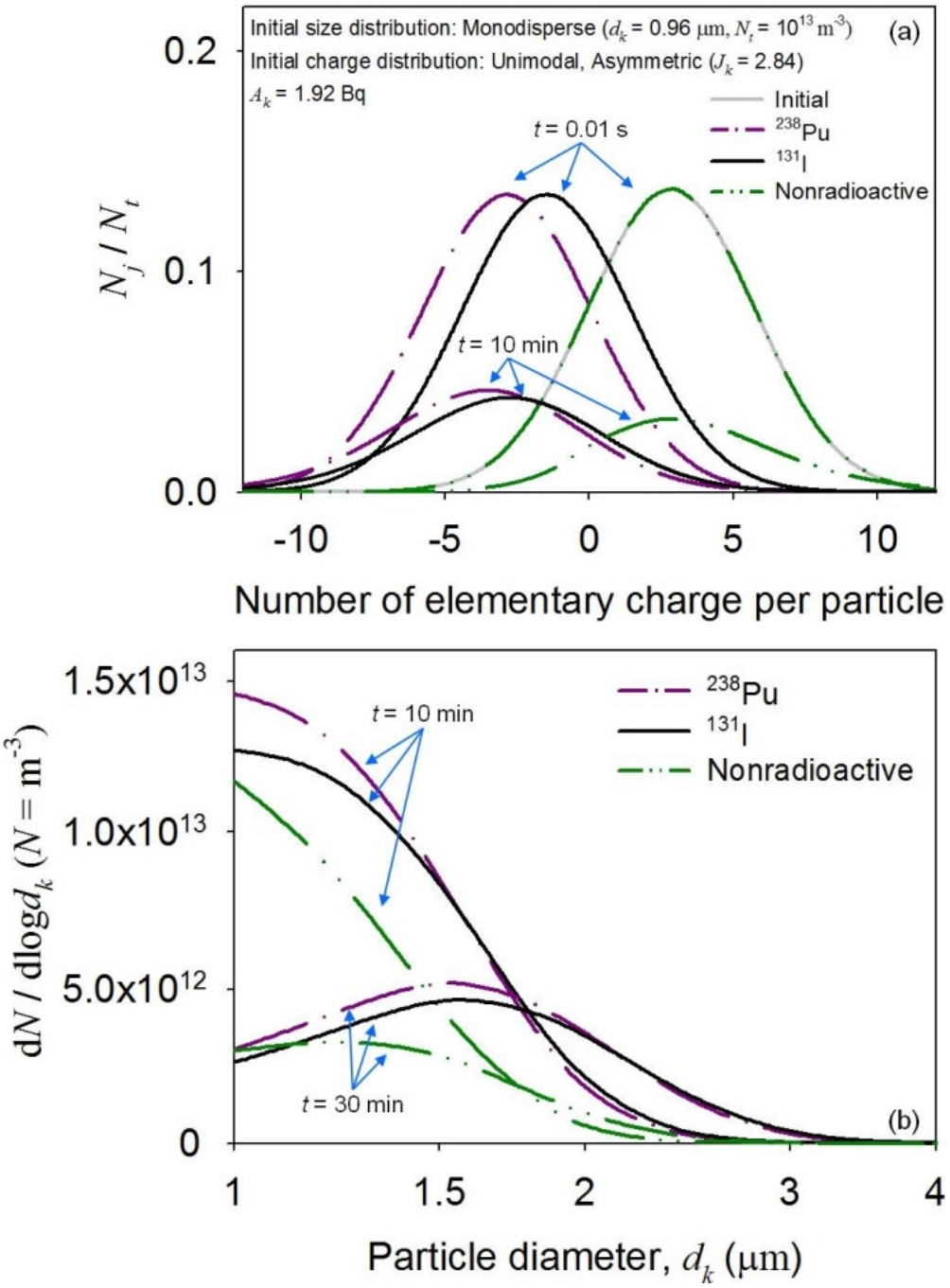

Figure 6.6. Time-dependent changes in the charge (a) and size (b) distributions of monodispersed ^{238}Pu and ^{131}I particles (d_k = 0.96 μm; N_t = 10^{13} m^{-3}; $A_{Pu\text{-}238}$ = $A_{I\text{-}131}$ = 1.92 Bq). The simulation time is 30 min. The charge (a) and size (b) distributions of nonradioactive particles (A = 0) were given as a reference.

aggregation [Figure 6.6(b)].

The different charge accumulation and aggregation rates of the radioactive particles were mainly attributed to their decay modes, which emitted alpha and beta particles of different energy levels. Because the kinetic energy of the alpha particles of ^{238}Pu was much higher than that of the beta particles of ^{131}I, the alpha-emitting particles produced more ion pairs than those generated by the beta-emitting particles. Due to the high mobility of negative ions, production of more ion pairs led to the acquisition of many negative charges by more ^{238}Pu than ^{131}I particles [Figure 6.6(a)]. Positive charge accumulated via particle self-charging was immediately neutralized (the first term vs the fourth and fifth terms in equation 6.4). Thus, the ^{238}Pu particles aggregated less frequently due to stronger electrostatic repulsive forces generated between them [Figure 6.6(b)].

Electrostatic dispersion indirectly influenced the particle charge and size distributions by affecting the time-evolution of the ion concentrations. Although radioactivity-induced ionization produced ion pairs, the concentration of negative ions quickly increased at the early phase because many positive ions were rapidly removed by electrostatic dispersion caused by the initial positive space-charge. The electrostatic dispersion of positive ions suppressed the increase in the positive ion concentration, which hindered the ion-ion recombination (see equations 6.5-6.6). Due to the suppression of the ion-ion recombination, more negative ions were captured by the radioactive particles, thereby generating more negatively charged particles. Increase in the concentration of negatively charged particles modified the aggregation rates of the particles since more particles were affected by strong electrostatic repulsive forces. This indirect effect was more significant for the initial distribution movement of the ^{131}I particles than ^{238}Pu particles because it took longer time to counterbalance the initial positive space-charge (not shown).

6.4.2.2. Beta decay of ^{137}Cs vs beta decay of ^{131}I: Effects of composition

Time-evolution of the charge and size distributions of ^{137}Cs and ^{131}I particles was investigated. Because fission products can be carried by sulfate aerosols (Baltensperger et al., 1987), it was assumed that (i) the beta-emitting radionuclides are embedded in $(NH_4)_2SO_4$ aerosols and (ii) the radioactive fractions of the ^{137}Cs particles and ^{131}I particles are similar. The initial charge distribution of ^{137}Cs-$(NH_4)_2SO_4$ particles was obtained from the properties of charged monodisperse particles containing radioactive cesium [$J_k = 0.75$; $d_k = 0.82$ μm; $A_{Cs\text{-}137} = 12.8$ mBq (Gensdarmes et al., 2001)]. Using the radioactivity level of radioactive cesium, the fractions of ^{137}Cs and $(NH4)_2SO_4$ per particles can be obtained (Clement et al., 1995). For comparison, it was assumed that the fractions of ^{131}I and $(NH_4)_2SO_4$ per particle are similar to those of the ^{137}Cs particles.

Figure 6.7 shows time-dependent changes in the charge and size distributions of the ^{137}Cs and ^{131}I particles. Similarly to the initial distribution movements shown in Figure 6.6, the initial charge distributions of the radioactive particles were rapidly shifted to the left in contrast to the reference simulation [Figure 6.7(a)]. However, the charge distribution of the ^{137}Cs particles became symmetric while that of the ^{131}I particles remained asymmetric, which affected the time-evolution of the particle size distributions [Figure 6.7(b)].

The dissimilar charging and aggregation rates of the radioactive particles were largely attributed to the different levels of radioactivity. Despite the similar radioactive fraction per particle, $A_{\text{I-131}} \approx 17.9$ Bq, while $A_{\text{Cs-137}} \approx 12.8$ mBq because the radioactivity level of short-lived radionuclides is higher than that of long-lived radionuclides when their radioactive fractions are similar ($t_{1/2,\ \text{I-131}} \approx 8$ days while $t_{1/2,\ \text{Cs-137}} \approx 30.1$ years) (Clement et al., 1995; Hu et al., 2014). Due to the different radioactivity levels, the ^{137}Cs particles produced much fewer ion pairs compared to those produced by ^{131}I particles. Thus, the indirect effects of electrostatic dispersion mainly forced the initial distribution changes of the ^{137}Cs particles, while both charging and electrostatic dispersion affected

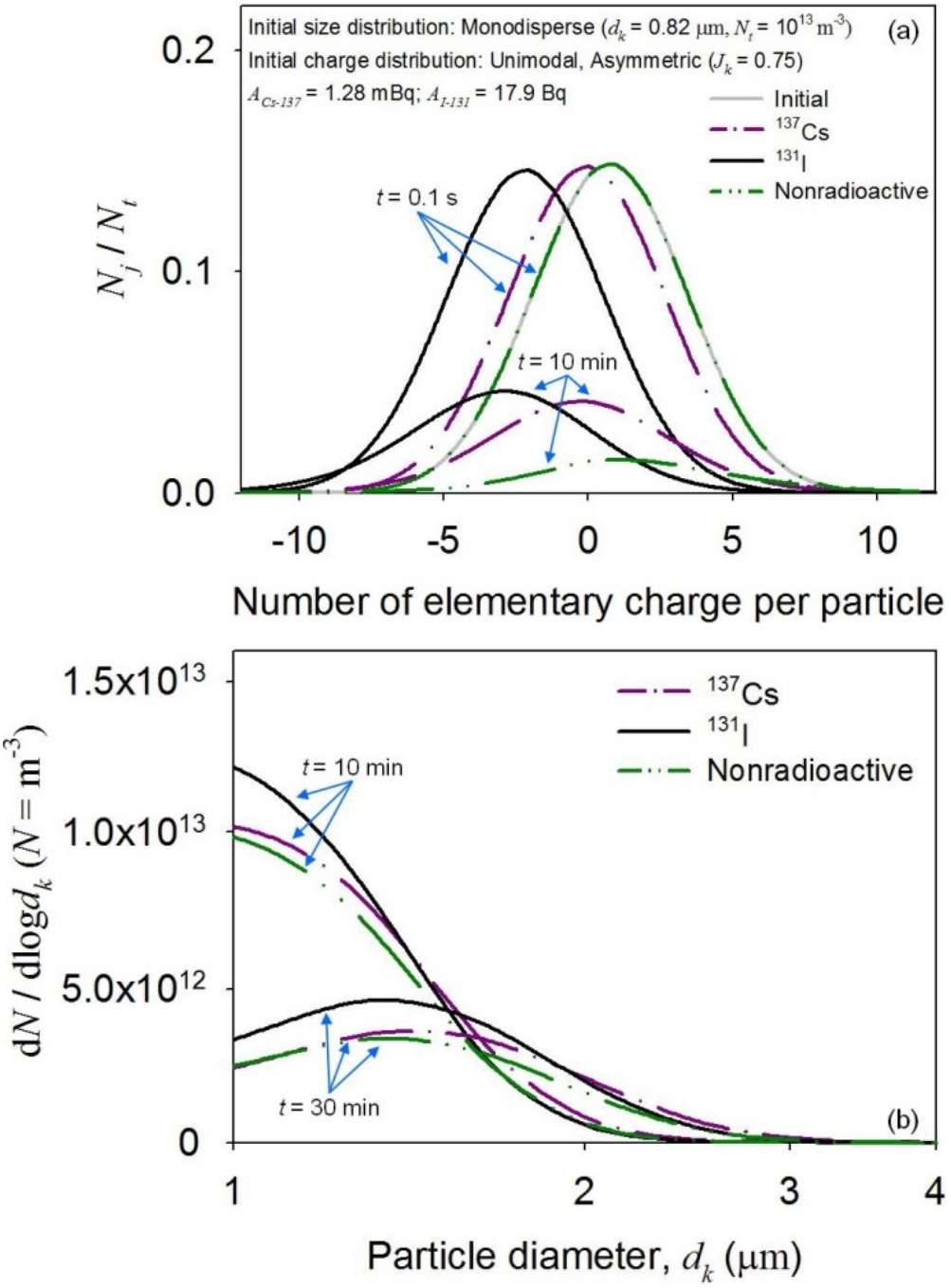

Figure 6.7. Time-dependent changes in the charge (a) and size (b) distributions of monodispersed ^{137}Cs and ^{131}I particles (d_k = 0.82 μm; N_t = 10^{13} m^{-3}; $A_{Cs\text{-}137}$ = 1.28 mBq; $A_{I\text{-}131}$ = 17.9 Bq). The simulation time is 30 min. The charge (a) and size (b) distributions of nonradioactive particles (A = 0) are shown for comparison.

the dispersion of the ^{131}I particles [Figure 6.7(a)]. Negative charge on the ^{131}I particles produced strong electrostatic repulsive forces, thereby hindering their size growth by aggregation [Figure 6.7(b)].

Although the mean charge of the ^{137}Cs and nonradioactive particles was similar at the very early phase (t = 0.1 s), their charge and size evolved differently with time [Figures 6.7(a) and (b)]. The discrepancies in the distributions largely arose from the effects of electrostatic dispersion. In contrast to the ^{137}Cs particles, positive space charge of the system containing nonradioactive particles continuously decreased due to electrostatic dispersion of the particles. Thus, the concentration of the nonradioactive particles decreased more rapidly with time.

It has been shown that radioactive decay can induce dispersion of the charge and size distributions of radioactive particles. The distributions evolved differently as a function of decay modes, radioactivity levels, and initial charge. These results suggest that time-evolution of the charge and size distributions of radioactive particles can significantly differ from that of nonradioactive particles in the atmosphere.

6.4.3. Potential effects of radioactivity on background aerosols

The Fukushima nuclear plant accident resulted in atmospheric dispersion of many radionuclides, such as ^{137}Cs, thereby increasing air dose rates in many areas of Japan. Changes in the concentrations of charged background aerosols were investigated as a function of air dose rates observed in Iwaki, tens of kilometers away from the accident site (Katata et al., 2012). The observed values were converted into ionization rates by assuming that ionizing radiation produces 2.2×10^{11} ion pairs m^{-3} μGy^{-1} (Subramanian et al., 2012). We assumed log-normal distributions of uncharged background aerosols to obtain the initial particle charge and size distributions (Kim et al., 2015a).

Figure 6.8 illustrates changes in the concentrations of charged and uncharged background aerosols vs air dose rates. The total particle concentration gradually

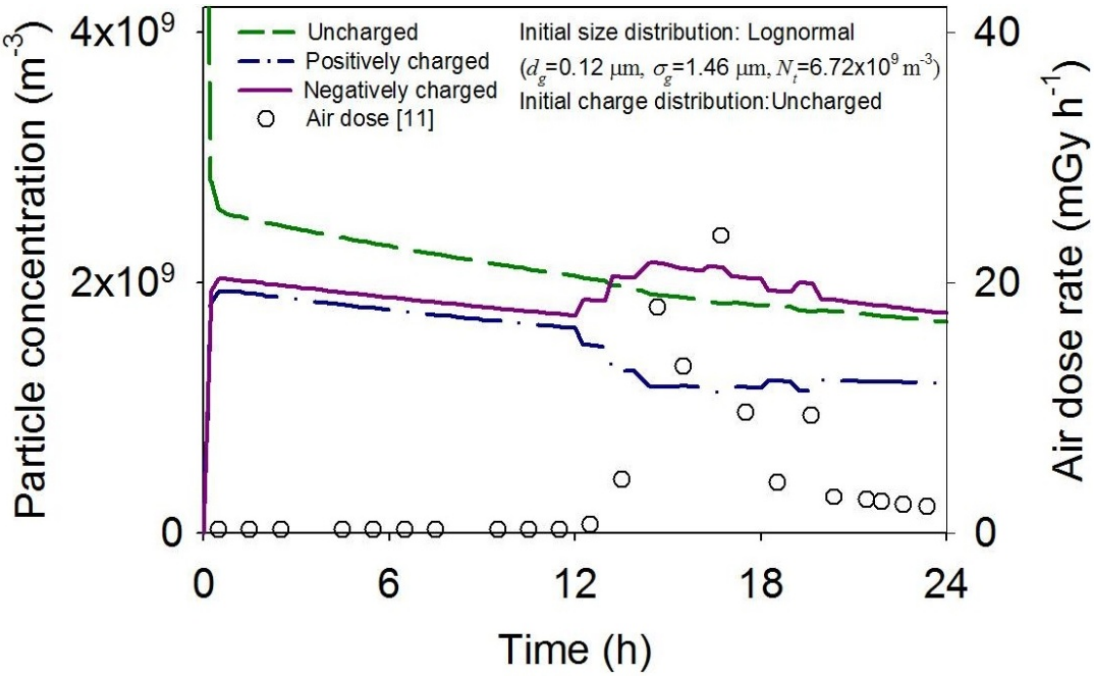

Figure 6.8. Changes in the concentrations of charged and uncharged particles vs air dose rates. Lines represent the simulation results. Symbols represent air dose rates measured at Iwaki, Japan after the Fukushima nuclear plant accident (Katata et al., 2012).

decreased with time due to particle aggregation. At an early stage, background ionization led to diffusion charging, which created a discrepancy in the concentrations of charged particles because of their dissimilar properties. However, as ionizing radiation occurred, the concentration of negatively charged particles became much higher than that of positively charged particles due to changes in ion concentrations. Similar results were obtained for simulations using different ion properties given by Kim et al. (2015b) and air dose rates measured at other places (Katata et al., 2012). These results suggest that if radiation fields are created in the atmosphere, negatively charged particles may be more easily detected during field measurements of charged particles.

The generation of more negatively than positively charged particles indicates that the background aerosols may interact more frequently with beta-emitting radionuclides in gas and particulate phases, which could acquire positive charge by beta emission. Recent experiments performed at the microscopic level showed that electrostatic interactions can enhance uptake of water molecules by charged particles (Kweon et al., 2015), suggesting that more radioactive gas molecules might be accumulated on the background aerosols with negative charge. Also, using the average radioactivity of single ^{137}Cs particles contained in the first plume of the Fukushima accident (Adachi et al., 2013) and the maximum air dose rates observed in Iwaki, calculations suggest that particles containing ^{137}Cs might be positively charged because of their self-charging during long- and short-range transport (not shown). Thus, the negatively charged background aerosols might more easily aggregate with the positively charged radioactive particles due to electrostatic attractive forces among them. These results suggest that radioactivity, which creates many ion pairs, may facilitate acquisition of radioactivity by background aerosols and affect their charging behavior and size growth.

6.4.4. Monovariate and monodisperse PBMs

6.4.4.1. Validation tests

The bivariate PBM can be replaced by the monovariate and monodisperse PBMs in model studies of transport of contaminants carried by charged particles, as well as investigations using particle measurement systems. The validity of the simpler PBMs was assessed using the bivariate PBM; we focused on testing the validity of the third term of equation 6.13 and the incorporation of the charging terms of equation 6.4 into equation 6.15, respectively. It is assumed that (i) particles are nonradioactive and uncharged, (ii) the initial particle size distribution is monodispersed, and (iii) $n_{\pm} = 10^3 N_0$ during simulation. For reference, simulation results were obtained using equation 6.4 in the absence of the electrostatic dispersion term.

Simulation results of the bivariate PBMs are depicted in Figure 6.9. Particles were charged by capturing ions. Because the ion concentrations were constant in the simulation, the particle charge caused electrostatic dispersion of the charged particles, leading to discrepancies in the results of the bivariate PBM and the reference simulation (Bivariate PBM vs Reference). Compared with the monodisperse PBM, the simulation results of the monovariate PBM were in better agreement with those of the bivariate PBM (Bivariate PBM vs Monovariate PBM; Bivariate PBM vs Monodisperse PBM). Compared to the bivariate PBM, the monodisperse PBM slightly overestimated the mean particle size and space charge in absolute value. The monovariate PBM accurately predicted both particle size and charge distributions, while the monodisperse PBM forecasted only the particle charge distribution.

6.4.4.2. Application of monovariate PBM

In case of a severe nuclear reactor accident, highly radioactive particles in a pressurized water-reactor-containment system may be released into the atmosphere. The monovariate PBM, which can predict both particle charge and size distributions, was

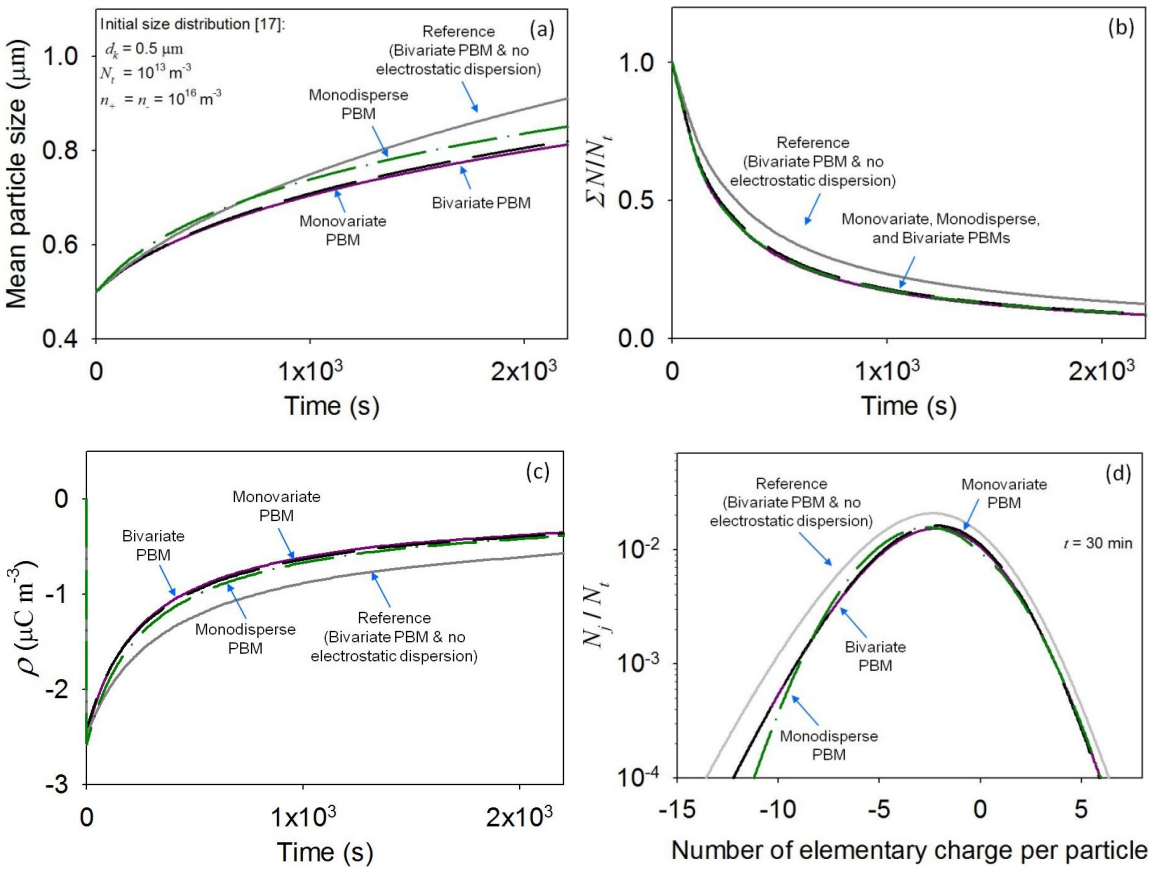

Figure 6.9. Time-dependent changes in the mean size (a) and total concentration (b) of particles, the space charge density (c), and particle charge distribution (d) in a spatially homogeneous atmospheric system.

applied to investigate the charging of highly radioactive particles and subsequent effects on particle collision after the release. The initial conditions were quoted from the containment system postulated by Clement et al. (1995), where radioactivity induced the charging of ^{131}I particles (d_g = 0.4 μm; σ_g = 2; $N_t = 10^9$ m^{-3}).

Figure 6.10 shows changes in the mean charge and average collision efficiency of the ^{131}I particles after the release into the atmosphere. The charging state of the ^{131}I particles was immediately modified in the atmosphere because the radioactive particles acquired many positive charges, while diffusion charging counterbalanced self-charging [Figure 6.10(a)]. The modification of the charging states affected the particle collision efficiency because strong electrostatic attractive and repulsive forces were generated between the ^{131}I particles [Figure 6.10(b)], indicating that the charging and aggregation patterns of highly radioactive particles in the atmosphere can be different from those in the containment system. The effects of electrostatic dispersion were insignificant due to the low space charge of the containment system and high radioactivity levels of the particles.

6.6. Summary

Charge and size evolutions of atmospheric particles involving radioactive particles are vital to transport modeling of radioactivity, as well as in-situ particle measurements in the atmosphere. This study presents the bivariate PBM taking into account radioactivity-induced charging, aggregation, and electrostatic dispersion as well as ion balance. Using the PBM, it has been shown that size and charge distribution dynamics of radioactive particles can be substantially different from those of nonradioactive particles because of radioactivity-induced charging and electrostatic dispersion, which subsequently can affect particle growth due to aggregation.

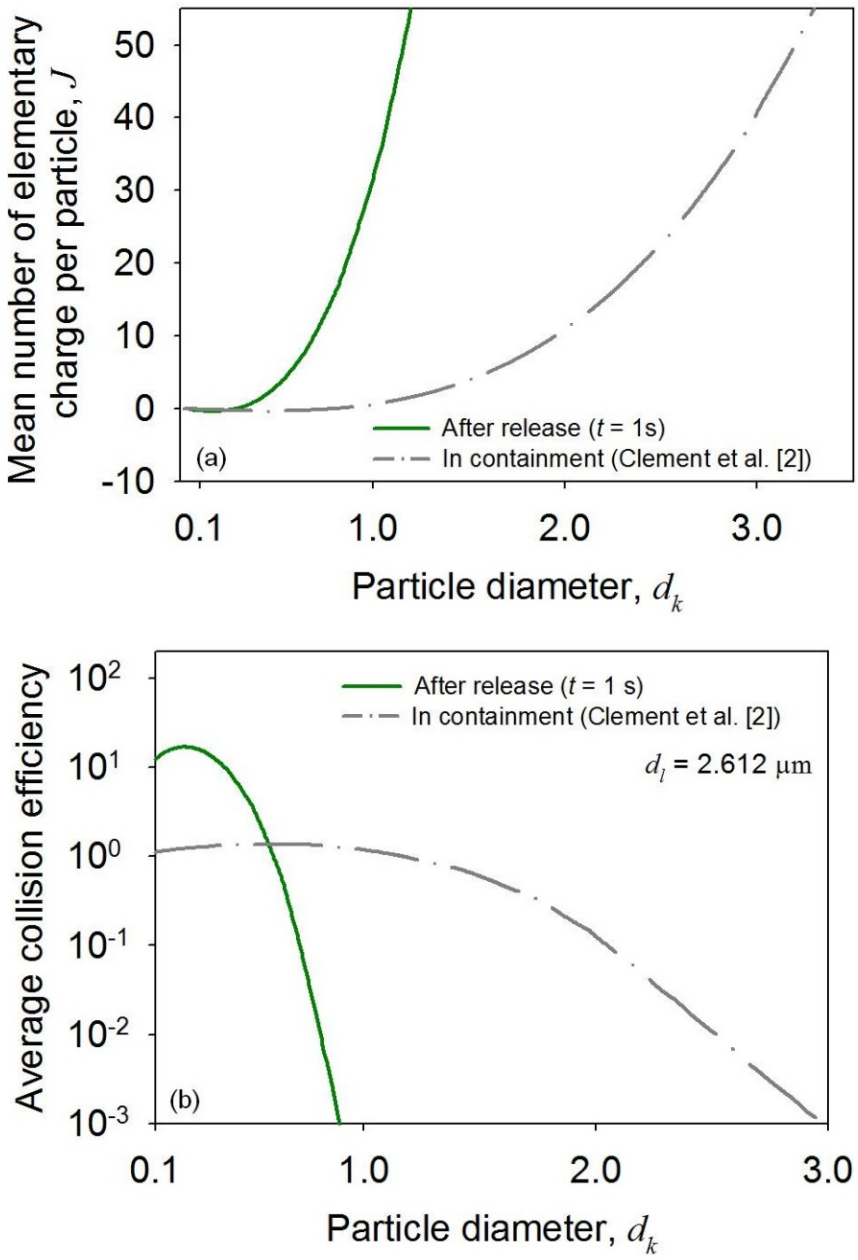

Figure 6.10. Time-evolution of mean charge (a) and average collision efficiency (b) of ^{131}I particles released from postulated pressurized water reactor containment.

These results suggest that the monovariate PBM can be used to include radioactivity-induced charging and electrostatic dispersion, and the subsequent effects on particle aggregation in predictive studies of radioactivity transport. Furthermore, ionizing radiation may affect the acquisition of charge and radioactivity by background aerosols, possibly influencing in-situ detection of charged particles in radiation fields. The bivariate PBM has been simplified to two different PBMs, which can be applied to model studies of radioactivity transport. This study offers useful insight into the dynamic behavior of particles in atmospheric systems with radiation sources.

CHAPTER 7

INFLUENCE OF RADIOACTIVITY ON HOMOGENEOUS AND HETEROGENEOUS AGGREGATION OF MULTICOMPONENT RADIOACTIVE PARTICLES IN THE ATMOSPHERE

Radioactivity can influence the charge and size of radioactive particles, which can affect the microphysical processes of the particles during short- and long-range transport in the atmosphere. Radioactivity effects have been assessed for single-component radioactive particles; however, real radioactive particles are typically composed of mixtures of radionuclides and, thus, understanding of radioactivity effects on multicomponent radioactive particles is necessary for predictive studies of radioactivity transport. This chapter focused on the influence of radioactivity on particle charge accumulation and aggregation rates in homogeneous and heterogeneous populations containing radioactive mixtures. Several models including radioactive transformation, charge balance, and population balance have been combined to predict the time-evolution of the activity, charge, and size distributions of radioactive particles, as well as compositional changes of particles. It is found that, because of radioactive transformation, the composition of radioactive particles can change with time. The aggregation of multicomponent radioactive particles in homogeneous/heterogeneous populations can be hindered/facilitated because the particles can be strongly charged with multiple elementary charges and, thus, strong electrostatic repulsive/attractive forces can be generated between the particles. This study provides useful insight into the transport characteristics of mixtures of various airborne radionuclides, as well as internal/external mixing of radioactive plumes in the atmosphere.

7.1. INTRODUCTION

Because of public health implications, as well as environmental issues, understanding the behavior of radionuclides in the environment is essential, as they spread radioactivity and emit decay products. Nuclear plant accidents, such as the Chernobyl and Fukushima accident, released many radionuclides into the atmosphere (Adachi et al., 2013; Baltensperger et al., 1987; Hu et al., 2014). During long-range transport, dry deposition of mixtures of radionuclides cause radioactive contamination both locally and globally. Particularly, long-lived radionuclides (e.g., ^{137}Cs) cause radioactive contamination for longer periods of time than short-lived radionuclides. Thus, accurately predicting the distribution of released radionuclides is necessary in making short-term and long-term plans for public health protection and environmental remediation.

Most radionuclides are carried by atmospheric particles via various physicochemical processes including adsorption, condensation, and precipitation. Surface interactions of atmospheric radioactive particles may differ from those of nonradioactive particles because the decay of radionuclides and the resulting ionization accumulate charge on the surface of radioactive particles (Clement et al., 1995; Kim et al., 2014; Walker et al., 2010). The charge accumulation rate of particles containing a single radionuclide element has been studied and found to depend on the radioactivity level, the particle size, as well as the ionization rate (Clement and Harrison, 1992; Gensdarmes et al., 2001; Kim et al., 2014). Atmospheric radioactive particles can be mixtures of short- and long-lived radionuclides having different decay and ionization rates (Kim et al., 2015a), but there has been little information about effects of these parameters on the charge accumulation of particles containing mixtures of radionuclides. Involving effects of each type of radionuclides on charge accumulation induced by radioactivity can reduce uncertainty in determining the steady-state charging of atmospheric radioactive particles.

Radioactivity-induced charge influences aggregation rates of atmospheric radioactive particles by generating electrostatic forces, which either facilitate or suppress the aggregation of the particles (Clement et al., 1995). Differences in aggregation rates can cause radioactive particles to behave differently from nonradioactive particles with respect to dry deposition rates and dispersion distances (Clement et al., 1995; Walker et al., 2010). Existing predictive transport models for radioactivity, such as the Weather Research and Forecasting-Chemistry model, involve dry and wet deposition of radioactive particles, but the charging effects have not been considered yet because of lack of information (Hu et al., 2014).

Numerical and experimental investigations have been conducted to study charging effects on the aggregation of homogeneous populations containing radionuclides (Rosinski et al., 1962; Kim et al., 2015b); however, populations of atmospheric radioactive particles are heterogeneous. Although important parameters of their charging and aggregation characteristics are still unknown, safety issues and technical difficulties arise in experimental investigations. Modeling studies of charge accumulation and aggregation of particles containing mixtures of radionuclides may be useful not only to provide information about possible critical parameters for experimental studies, but also to establish a basis for quantifying particle aggregation, deposition, and dispersion rates, which are important processes in predictive transport models of radioactivity.

The aim of this chapter is to investigate the influence of radioactivity on the charge accumulation and aggregation rates of multicomponent radioactive particles in homogeneous and heterogeneous populations. Various models of radioactive transformation, charge release, ion, and population balances have been coupled to predict time-dependent changes in the particle activity, charge, and size distributions in homogeneous and heterogeneous radioactive populations. The charging of particles ^{106}Ru,

^{131}I, ^{132}Te, and ^{137}Cs and the subsequent charging effects on particle aggregation have been investigated for homogeneous and heterogeneous populations.

7.2. Methodology

7.2.1. Radioactive Transformation

Radionuclides, unstable isotopes of elements, are continuously transformed into different nuclides until they become stable. For a serial radioactive decay chain, $i \xrightarrow{\lambda_i} ii \xrightarrow{\lambda_{ii}} iii$, transformation rates of radionuclide *i* carried by a particle of the size class *k* can be given by:

$$\frac{dZ_i}{dt} = -\lambda_i Z_i , \tag{7.1}$$

$$\frac{dZ_{ii}}{dt} = \lambda_i Z_i - \lambda_{ii} Z_{ii} , \tag{7.2}$$

$$\frac{dZ_{iii}}{dt} = \lambda_{ii} Z_{ii} - \lambda_{iii} Z_{iii} , \tag{7.3}$$

where Z_i is the number of nuclides contained in single particles, λ is the decay constant, and t is the time. For the initial condition: $Z_i = Z_{i,0}$ and $Z_{ii} = Z_{iii} = 0$ at $t = 0$ s, equations 7.1-7.3 can be easily solved using the integrating factor method. The following analytical solutions can be found:

$$Z_i = Z_{i,0} \exp\left(-\lambda_i t\right), \tag{7.4}$$

$$Z_{ii} = \lambda_i Z_{i,0} \left(\frac{\exp\left(-\lambda_i t\right) - \exp\left(-\lambda_{ii} t\right)}{\lambda_{ii} - \lambda_i} \right), \tag{7.5}$$

$$Z_{iii} = \lambda_i \lambda_{ii} Z_{i,0} \left(\frac{\exp(-\lambda_i t)}{(\lambda_{ii} - \lambda_i)(\lambda_{iii} - \lambda_i)} + \frac{\exp(-\lambda_{ii} t)}{(\lambda_i - \lambda_{ii})(\lambda_{iii} - \lambda_{ii})} + \frac{\exp(-\lambda_{iii} t)}{(\lambda_i - \lambda_{iii})(\lambda_{ii} - \lambda_{iii})} \right). \quad (7.6)$$

Equations 7.4-7.6 are comparable to the analytical solutions of equations 7.1-7.3 given using an algebraic approach (Moral and Pacheco, 2003). When the transformed nuclides are stable, the decay constant becomes zero and the chain ends. The radioactivity per particle, A_k, given by the serial decay chain, is obtained by

$$A_k = \sum_i \lambda_i Z_i \,. \quad (7.7)$$

7.2.2. Ionization

Because beta decay emits energetic electrons into the atmosphere, gas molecules near radioactive particles can be ionized. The ionization rate of gas molecules by background ionization and by the presence of multicomponent radioactive particles, q, is given by (Kim et al., 2015a):

$$q = q_b + \sum_k N_k \sum_i \lambda_i Z_i I_i \quad (7.8)$$

where q_b is the background ionization rate, I is the ionization rate coefficient representing the number of ion pairs generated per beta decay, and N_k is the number concentration of radioactive particles. In open air, I is highly influenced by the kinetic energy of the energetic electrons and the density of air.

7.2.3. Particle charging

Beta-emitting radioactive particles can be charged via emission of electrons and diffusion of ions corresponding to self-charging and diffusion charging, respectively (Clement and Harrison, 1992; Kim et al., 2014). Charge accumulation on radioactive

particles by these charging mechanisms can be described using charge balance (Clement and Harrison, 1992; Kim et al., 2015b):

$$\frac{dJ_k}{dt} = A_k + \beta_{k,J}^{+} n_{+} - \beta_{k,J}^{-} n_{-} \tag{7.9}$$

where J_k is the mean charge of radioactive particles, $\beta_{k,J}^{\pm}$ represent the particle-ion attachment coefficients, and $n_{\pm}$ represent the concentrations of negative and positive ions. In equation 7.9, the first term on the right-hand-side (RHS) accounts for self-charging, while the other terms describe diffusion charging. $n_{\pm}$ can be obtained via ion balance (Clement et al., 1995; Kim et al., 2014):

$$\frac{dn_{+}}{dt} = -n_{+}\beta_{k,J}^{+} N_k - \alpha_{rc} n_{+} n_{-} + q\,, \tag{7.10}$$

$$\frac{dn_{-}}{dt} = -n_{-}\beta_{k,J}^{-} N_k - \alpha_{rc} n_{+} n_{-} + q + \sum_k N_k \sum_i A_{k,i}\,, \tag{7.11}$$

where α_{rc} is the recombination coefficient. In equations 7.10 and 7.11, the first two terms on the RHS account for the loss rates of positive and negative ions by diffusion charging and recombination, respectively. The third term represents the production rates of ion pairs by ionization (equation 7.8). The last term on the RHS of equation 7.11 accounts for the electron emission rates of beta-emitting radioactive particles. At steady state, where self-charging is counterbalanced by diffusion charging, the mean particle charge is given by (Clement et al., 1995; Kim et al., 2015b):

$$J_k = \begin{cases} y - \left(\dfrac{y(X-1)}{\exp(2\omega y) - 1} \right) & \omega y > 0.22 \quad (7.12a) \\ y + \dfrac{X-1}{2\omega} & \omega y \le 0.22 \quad (7.12b) \end{cases} \tag{7.12}$$

with $\omega = \frac{e^2}{4\pi\varepsilon_0 d_k k_B T}$, $y = \frac{\varepsilon_0 A_k}{e\mu_- n_0}$, $n_0 = \sqrt{\frac{q + \sum_k A_k N_k}{\alpha_{rc}}}$, $X \approx \frac{\mu_+}{\mu_-}$,

where e is the electrical charge, ε_0 is the vacuum permittivity, d_k is the diameter of the size class k particles, k_B is the Boltzmann constant, T is the temperature, and $\mu_\pm$ represent the mobilities of positive and negative ions. In calculating the steady-state mean charge, the effects of diffusion charging are included in the dimensionless parameters ω and X, while those of self-charging are considered in y. For particles larger than 40 nm, J_k can be used to approximate the particle charge distribution assuming a Gaussian distribution (Clement et al., 1995; Kim et al., 2015b):

$$N_{kj} = \frac{N_k}{\sqrt{2\pi}\sigma} \exp\left(-\frac{(j - J_k)^2}{2\sigma^2}\right) \tag{7.13}$$

with $\sigma^2 = y + \frac{1}{2\omega}$,

where j is the number of elementary charges per particle. At Boltzmann charge equilibrium, the particle charge distribution is obtained assuming that the mean particle charge is zero (i.e., $J_k = 0$) (Clement and Harrison, 1992).

7.2.4. Particle aggregation

7.2.4.1. Homogeneous population

Aggregation of homogeneous particles does not affect the compositional fraction of the particles. For example, aggregation of two pure ^{137}Cs particles with each having volume x produces a pure ^{137}Cs particle whose volume is $2x$. Aggregation rates of homogeneous particles undergoing Brownian motion can be calculated using a monovariate population balance model (PBM) (Kumar and Ramkrishna, 1996):

$$\frac{dN_k}{dt} = \sum_{\substack{l,m \\ x_{k-1} \le x_l + x_m \le x_{k+1}}}^{l \ge m} \left(1 - \frac{1}{2}\delta_{l,m}^{Kr}\right) \eta_{l,m} \alpha_{l,m}^{Br} \beta_{l,m}^{Br} N_l N_m - \sum_{l=1}^{M} \alpha_{k,l}^{Br} \beta_{k,l}^{Br} N_k N_l \tag{7.14}$$

where the indices *k, l*, and *m* represent the particle size classes, δ^{Kr} denotes the Kronecker delta, η is the distribution factor of the particle volume, α^{Br} is the Brownian collision efficiency, and β^{Br} is the Brownian collision frequency. In equation 7.14, the two terms on the RHS represent the production and loss rates of homogeneous particles by aggregation, respectively. The collision efficiency, α^{Br} depends on particle-particle interactions. Assuming that the effects of electrostatic particle interactions surpass those of other particle interactions, the average Brownian collision efficiency, $\bar{\alpha}^{Br}$, of particles with distributed charges is given by (Clement et al., 1995; Kim et al., 2015b):

$$\bar{\alpha}_{kl}^{Br} = 1 + \frac{\sum_{j_k j_l \neq 0} N_{k,j_k} N_{l,j_l} \left(\alpha_{kl}^{Br} - 1\right)}{\sum_{j_k} N_{k,j_k} \sum_{j_l} N_{l,j_l}} \tag{7.15}$$

with $\alpha_{kl}^{Br} = \frac{u}{e^u - 1}$, $u = \frac{j_k j_l e^2}{2\pi\varepsilon_0 (d_k + d_l) k_B T}$.

The validity of equation 7.15 was assessed in our previous work (Kim et al., 2015b). The collision frequency, β^{Br}, can be calculates using the interpolation formula of Fuchs (1964):

$$\beta_{kl}^{Br} = 2\pi \left(d_k + d_l\right)\left(D_k + D_l\right) \left(\frac{d_k + d_l}{d_k + d_l + \sqrt{\delta_k^{\,2} + \delta_l^{\,2}}} + \frac{8\left(D_k + D_l\right)}{(d_k + d_l)\sqrt{\bar{v}_k^{\,2} + \bar{v}_l^{\,2}}} \right)^{-1} \tag{7.16}$$

with $\delta_k = \frac{1}{3 d_k L_k} \left(\left(d_k + L_k\right)^3 - \left(d_k^2 + L_k^2\right)^{\frac{3}{2}} \right) - d_k$, $L_k = \frac{8 D_k}{3 d_k \bar{v}_k}$, $\bar{v}_k = \sqrt{\frac{8 k_B T}{\pi x_k}}$,

where D_k is the diffusion coefficient of particles.

7.2.4.2. Heterogeneous population

Aggregation of primary particles with different compositions can affect the compositional fraction of the aggregated particles. When a particle of volume x containing $Z_{\text{Te-132}}$ aggregates with a particle of volume $2x$ embedding $Z_{\text{Te-132}}$, the compositional fraction of the aggregate is dissimilar to that of the primary particles. For particles having different compositions, time-dependent changes in size/composition distributions by aggregation can be predicted using a bivariate PBM (Vale and McKenna, 2005):

$$\frac{dN_{kp}}{dt} = \sum_{\{l,m,q,r\}\in\Omega_{kp}} \left(1-\frac{1}{2}\delta_{l,q}^{Kr}\delta_{m,r}^{Kr}\right)\eta_{k,p}\,\overline{\alpha}_{l,q,m,r}^{Br}\beta_{l,q,m,r}^{Br}N_{l,q}N_{m,r} - \sum_{l,q}\overline{\alpha}_{k,p,l,q}^{Br}\beta_{k,p,l,q}^{Br}N_{k,p}N_{l,q} \quad (7.17)$$

with $\Omega_{kp} = \left\{\{l,m,q,r\} : 1\le l\le k, 1\le m\le p, m\le r\le p, 1+\delta_{m,r}^{Kr}(l-1)\le q\le k\right\}$,

where the indices p, q, and r represent the size classes. In equation 7.17, the two terms on the RHS account for the formation and loss of particles having different compositional fraction by aggregation, respectively. Similarly to equation 7.14, the effects of the particle charge distribution on aggregation were taken into account.

7.2.5. Simulation

The models of radioactive transformation, particle charging, and aggregation were coupled to investigate time-dependent changes in the activity, charge, and size distributions of radioactive particles. The coupled model was simulated on the basis of the calculation procedure developed in our previous work (Kim et al., 2015b). The simulation scheme is depicted in Figure 7.1. The radioactivity of single particles was estimated using the analytical solutions of the radioactive transformation equations. The activity distributions were obtained by multiplying the radioactivity of single particles by the particle number concentrations. The mean charge of single radioactive particles was

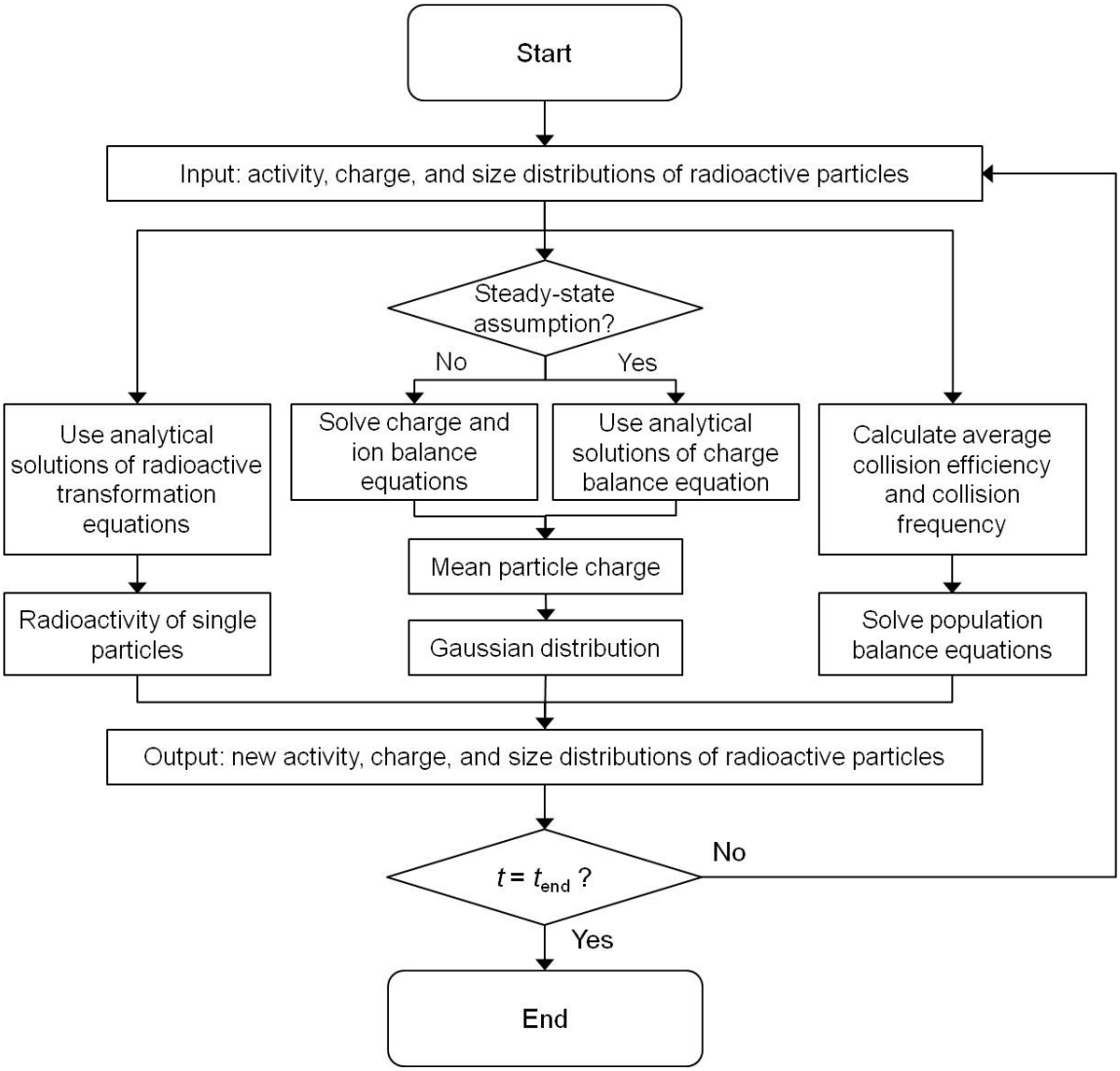

Figure 7.1. Simulation scheme to solve the coupled equations of radioactive transformation, particle charging, and aggregation.

estimated by solving numerically equations 7.9-7.11. For the steady-state assumption of particle charging, the mean particle charge was calculated from equation 7.12. The mean charge of single particles was employed to approximate the particle charge distributions using equation 7.13. The size distribution of radioactive particles was obtained using the mono- and bivariate PBMs. Because time-dependent changes in the activity, charge, and size distributions are mutually related, the coupled model can involve the charging effects caused by radioactivity on the time-evolution of the three distributions.

In case of nuclear plant accidents, NH_4^+ and SO_4^{2-} can be the major nonradioactive components of aerosols carrying radionuclides (Baltensperger et al., 1987). In this study, it was assumed that radionuclides are contained in $(NH_4)_2SO_4$ aerosols. ^{106}Ru, ^{131}I, ^{132}Te, and ^{137}Cs were chosen because they were found in radioactive particles released during the Chernobyl and Fukushima nuclear plant accidents. The decay chains and radiological properties of the radionuclides are given in Table 7.1.

The initial values for Z can be given by (Clement et al., 1995; Kim et al., 2015a):

$$Z_i = \frac{\rho_p N_A f_i}{\mu_{mean}} \left(\frac{\pi d_k^3}{6} \right) \tag{7.18}$$

where N_A is Avogadro's number, f_i is the mole fraction of radionuclides contained in single particles, ρ_p is the particle density (2,000 kg m^{-3}), and μ_{mean} is the mean atomic weight. The Fukushima nuclear plant accident released 2.6 μm ^{137}Cs particles with $A_{\text{Cs-137}}$ = 3.27 Bq (Adachi et al., 2013). For ^{137}Cs-$(NH_4)_2SO_4$ particles of 2.6 μm with $f_{\text{Cs-137}}$ = 0.05, the radioactivity per particle is ~3 Bq. For ^{137}Cs-^{131}I-$(NH_4)_2SO_4$ particles of 2 μm with $f_{\text{Cs-137}} = f_{\text{I-131}} = 0.05$, the radioactivity per particle is ~1,908 Bq, which exists between 300 and 3000 Bq, a typical radioactivity range of 2 μm ^{137}Cs^{131}I particles (Barrett et al., 2009). Thus, in this study, 0.05 was set as the standard value of f_i.

In the numerical solution of equations 7.9-7.11, $\beta_{k,j}^{\pm}$ was calculated using a limiting-

Table 7.1. Radionuclides found in radioactive particles released during the Chernobyl and Fukushima nuclear plant accidents (Martin, 2000; Kim et al., 2015a).

Z_i	Decay chains ($Z_i \xrightarrow{\lambda_{Z_i}} Z'_{i'}$ or $Z_i \xrightarrow{\lambda_{Z_i}} Z'_{i'} \xrightarrow{\lambda_{Z'_{i'}}} Z''_{i''}$)	Decay constant, λ (s^{-1})		Ionization rate coefficient, I	
		Z_i	$Z'_{i'}$	Z_i	$Z'_{i'}$
$^{106}_{44}Ru$	$^{106}_{44}Ru \rightarrow {}^{106}_{45}Rh \rightarrow {}^{106}_{46}Pd$	2.82×10^{-8}	2.33×10^{-2}	110	16286
$^{131}_{53}I$	$^{131}_{53}I \rightarrow {}^{131}_{54}Xe$	1.00×10^{-6}	-	1945	-
$^{132}_{52}Te$	$^{132}_{52}Te \rightarrow {}^{132}_{53}I \rightarrow {}^{132}_{54}Xe$	2.50×10^{-6}	8.39×10^{-5}	748	5863
$^{137}_{55}Cs$	$^{137}_{55}Cs \rightarrow {}^{137m}_{56}Ba \rightarrow {}^{137}_{56}Ba$	7.31×10^{-10}	4.5×10^{-3}	2067	-

sphere theory (Fuchs, 1963; Hoppel and Frick, 1986). The ion mass and mobilities of ions are required for the calculation of $\beta_{k,j}^{\pm}$. The mass and mobilities of positive and negative ions were quoted from Alonso et al. (1997) (e.g., μ_- = 1.65 m^2 V^{-1} s^{-1} and μ_+ = 1.15 m^2 V^{-1} s^{-1}). We assumed typical atmospheric conditions given by Harrison and Carslaw (2003): $q_b = 10^7$ m^{-3} s^{-1} and $\alpha_{rc} = 1.6 \times 10^{-12}$ m^{-3}. In addition, we assumed that all particles are initially neutralized; thus, electrostatic dispersion of charged radioactive particles can be neglected (see Chapter 6).

Decay modes of the radionuclides shown in Table 7.1 involve beta and gamma decay. Clement and Harrison (1992) and Gensdarmes et al. (2001) showed that the charging of ^{137}Cs and ^{198}Au particles can be accurately predicted by including only the effects of beta decay. In this study, the effects of gamma radiation on particle charging were excluded.

7.3. Results and Discussion

7.3.1. Model Validation

In this study, several models were coupled to simulate homogeneous and heterogeneous aggregation of multicomponent radioactive particles, which involved radioactive transformation (equations 7.4-7.6), charge balance (equations 7.9 and 7.12), ion balance (equations 7.10 and 7.11), and mono- and bivariate PBMs (equations 7.14 and 7.17). The charge and ion balance equations were validated in our previous studies (Kim et al., 2014; 2015b). Briefly, the numerical solution of equations 7.9-7.11 and the analysis using equation 7.12 accurately forecasted the charging of ^{137}Cs particles of 0.82 and 1.05 μm, respectively. The charge distribution of the ^{137}Cs particles obtained from the Gaussian approximation (equation 7.13) agreed well with the measurements performed by Gensdarmes et al. (2001). Both analytical and numerical approaches to forecast radioactivity-induced charging can be coupled with population balance models

(Kim et al., 2015a). Thus, in this study, we focused on evaluating the validity of coupling the analytical solutions of the radioactive transformation equations with the PBMs.

7.3.1.1. Radioactive Transformation

The validity of equations 7.4-7.6 was evaluated using numerical results obtained from the solution of the radioactive transformation equations (equations 7.1-7.3). We assumed a pure ^{132}Te particle of 1 μm. Figure 7.2 shows time-dependent changes in the composition and radioactivity of the ^{132}Te particle. As time elapsed, ^{132}Te was transformed into ^{132}I, which was subsequently transformed to ^{132}Xe. The radioactivity of the particle reached a maximum level at $t \approx 10$ h and then, it was reduced over time. Because the decay constant of ^{132}I is moderately higher than that of ^{132}Te, the serial decay chain reached transient equilibrium after $t \approx 12$ h, in which the radioactivity of ^{132}I remained slightly greater than that of ^{132}Te. These transformations predicted using analytical solutions were in good agreement with the prediction results obtained by employing numerical analysis. These results suggest that changes in the radioactive composition of single particles can be correctly estimated using equations 7.4-7.6.

7.3.1.2. Discretization of mono- and bivariate PBMs

The validity of the mono- and bivariate PBMs depends on discretization (Kumar and Ramkrishna, 1996; Vale and McKenna, 2005). In this study, the size classes of particles were discretized using the following relationships: $x_{k+1} = 2x_k$ (moderate size classes) and $x_{k+1} = 1.2x_k$ (fine size classes.) The accuracy of the two PBMs using the discretized size classes was tested with the analytical solutions provided by Jacobson et al. (1994) and Vale and McKenna (2005), respectively. The initial size distribution was obtained assuming exponentially distributed particles with $N_t = 10^{11}$ m^{-3}.

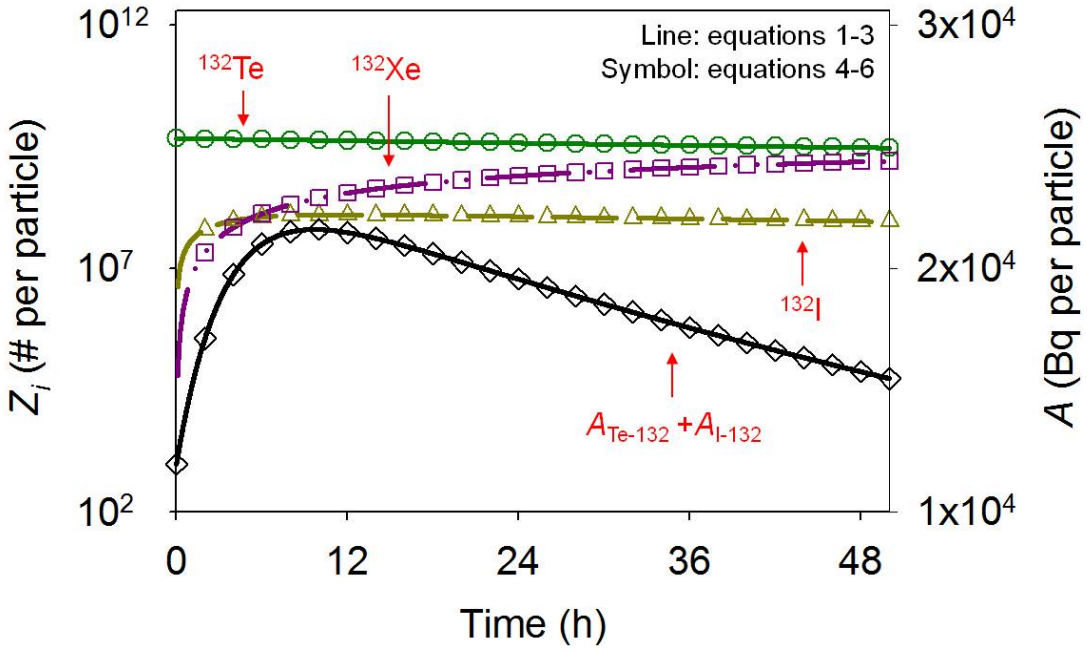

Figure 7.2. Time-evolution of the composition and radioactivity of a pure ^{132}Te particle of 1-μm diameter. Lines and symbols represent the results of the numerical solutions of equations 7.1-7.3 and the analytical solutions (equations 7.4-7.6), respectively.

The simulation results of the two PBMs for the stated initial condition are depicted in Figure 7.3. For the bivariate PBM, good agreement was found between the results of the numerical analysis and the analytical solution. For the monovariate PBM, the results obtained with the fine size classes agreed well with those produced by the analytical solution. The use of the moderate size classes led to slight overestimation of the concentration of large particles. Thus, the validity of the monovariate PBM employing the moderate size classes was additionally assessed using the numerical analysis suggested by Jacobson et al. (1994). For log-normal distributions of particles (d_g = 0.02μm; σ_g = 1.4; $N_t = 10^{12}$ m^{-3}), the aggregation rates of the particles calculated from the moderate size classes were in good agreement with those given by Jacobson et al. (1994) (not shown). Therefore, in this study, the moderate size classes were used for discretization of the PBMs in order to cover a wide size range with less computational cost.

7.3.1.3. Compositional changes in radioactive particles undergoing radioactive transformation and aggregation

For the derivation of the coupled model used in this study, it was assumed that the compositional changes of radioactive particles undergoing simultaneously radioactive transformation and aggregation can be predicted by incorporating equations 7.4-7.6 into the PBMs. The validity of the assumption was evaluated using an aggregation-tracer model developed by Burd et al. (2000). The aggregation-tracer model can tract the time-evolution of both size and activity distributions of radioactive particles. The monovariate PBM (equation 7.14) was used for comparison. The initial particle size and activity distributions were obtained by assuming log-normal distributions of ^{132}Te-^{137}Cs-$(NH_4)_2SO_4$ particles (d_g = 0.5 μm, σ_g = 1.5, $N_t = 10^{11}$ m^{-3}, $f_{(NH4)2SO4}$ = 0.9, $f_{Te\text{-}132}$ = 0.05, $f_{Cs\text{-}137}$ = 0.05.) The charge of radioactive particles was neglected in the assessment.

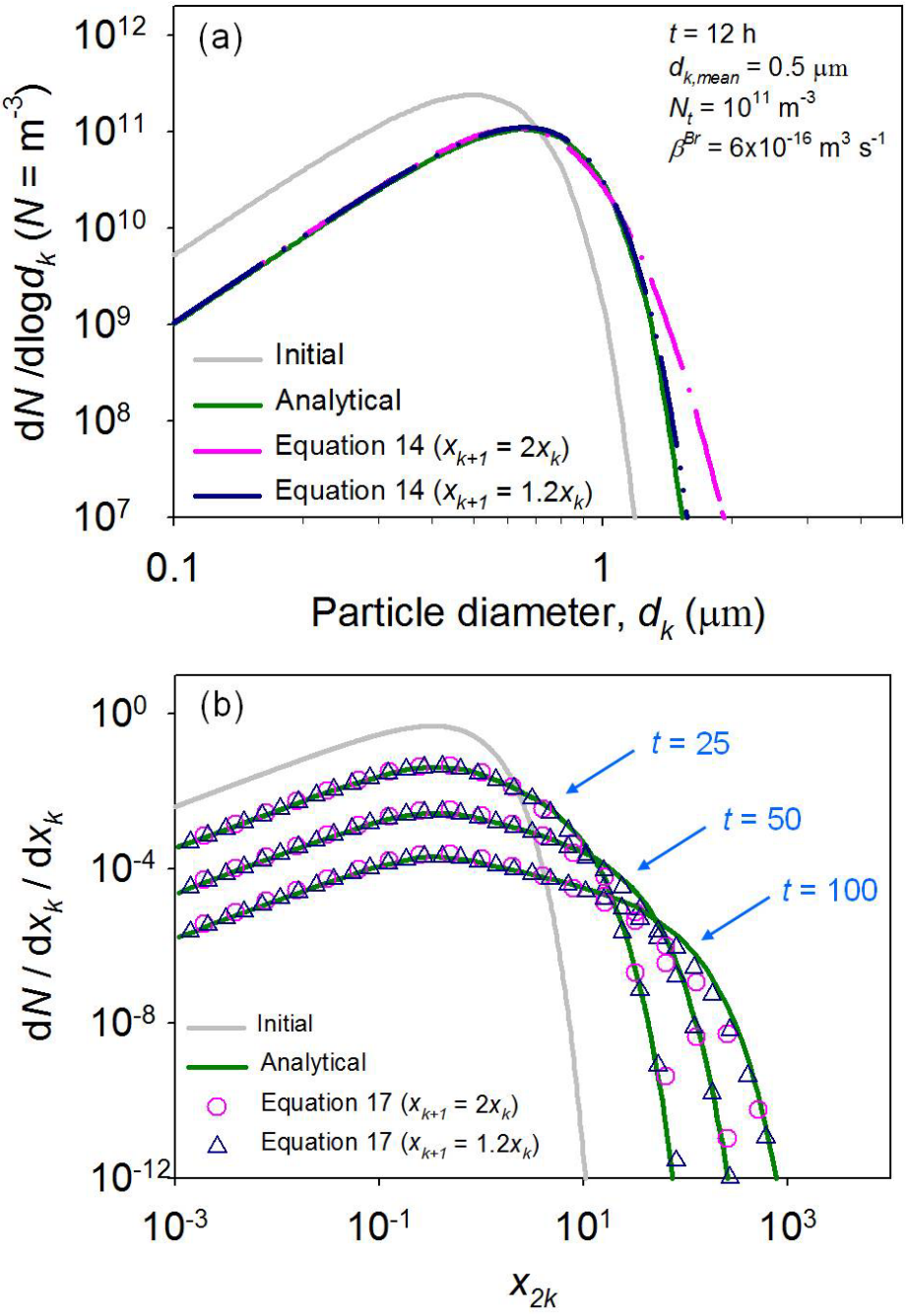

Figure 7.3. Particle size distributions predicted using different size classes: (a) monovariate PBM, (b) bivariate PBM. Results obtained from solving equations 7.14 and 7.17 were compared with those of the analytical solutions, respectively. The analytical solution of the monovariate PBM is given by Jacobson et al. (1994), while that of the bivariate PBM is provided by Vale and McKenna (2005).

Figure 7.4 shows simulation results of the coupled model for the initial condition discussed above. Because of radioactive transformations, the radioactive composition of the particles changed to ^{132}Te, ^{132}I, ^{132}Xe, ^{137}Cs, ^{137m}Ba, and ^{137}Ba over time. The time-evolution of the particle size distribution depended on particle aggregation [(Figure 7.4(a)], while that of the activity distributions was the result of both aggregation and radioactive transformations [Figure 7.4(b)]. For example, despite the decrease in radioactivity of ^{132}Te per particle due to radioactive decay, the activity distribution of the radioactive tellurium shifted to the upper right direction mainly because of aggregation. Then, the ^{132}Te activity distribution moved to the bottom right due to radioactive decay and aggregation. Because the decay chain reached transient equilibrium (Figure 7.2), the activity distribution of ^{132}Te became slightly lower than that of ^{132}I after t = 12 h. These simulation results obtained from the coupled model were in good agreement with those given by the aggregation-tracer model. Similar accuracy was obtained for the time-evolution of the activity distributions of ^{137}Cs and ^{137m}Ba, respectively (not shown).

It has been shown that the monovariate PBM involving the analytical solutions of radioactive transformation can accurately predict the time-evolution of the particle activity and size distributions. Thus, in this study, time-dependent changes in the activity, charge, and size distributions of radioactive particles were forecasted using the coupled model involving radioactive transformation, particle charging, and aggregation.

7.3.2. Particle Charging and Aggregation in Homogeneous Radioactive Population

Homogeneous aggregation of multicomponent radioactive particles was investigated using the coupled model involving radioactive transformation, charge balance, ion balance, and aggregation of homogeneous population. The initial particle size distribution was assumed to be lognormal (d_g = 0.5 μm, σ_g = 1.5, $N_t = 10^{11}$ m^{-3}). Simulation results obtained by assuming the Boltzmann particle charge distribution were provided as reference.

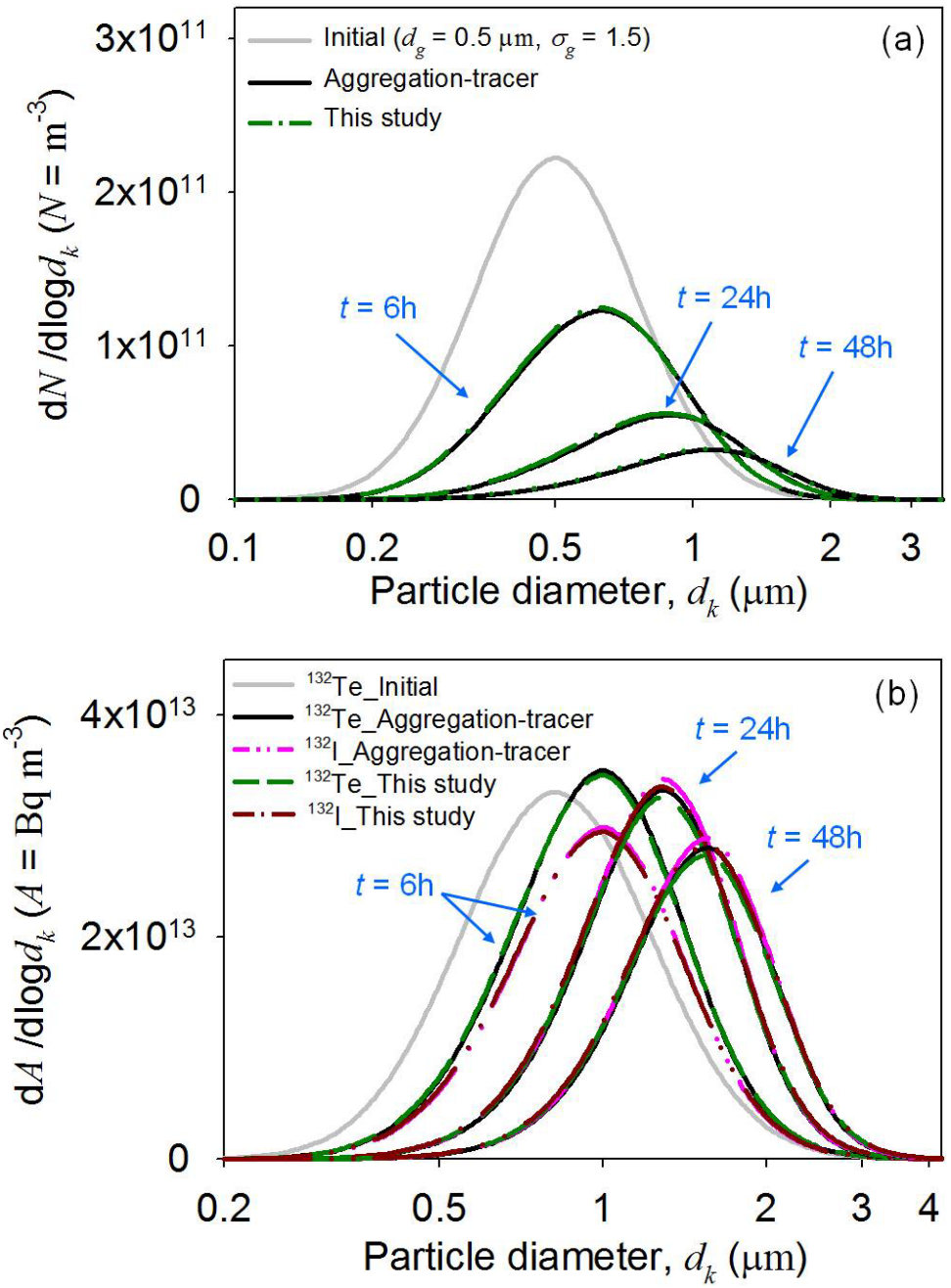

Figure 7.4. Time-dependent changes in the size (a) and activity (b) distributions of radioactive particles. The results of equations 7.4-7.6 and 7.13 were compared to those of the aggregation-tracer model of Burd et al. (2000). The initial activity and size distributions were given by d_g = 0.5 μm, σ_g = 1.5, $N_t = 10^{11}$ m^{-3}, $f_{(NH4)2SO4}$ = 0.9, $f_{Te\text{-}132}$ = 0.05, and $f_{Cs\text{-}137}$ = 0.05.

7.3.2.1. Effects of radioactivity level

The charging and aggregation rates of particles initially carrying different amounts of ^{132}Te were predicted to evaluate the effects of radioactivity levels of the particles (Figure 7.5). The ^{132}Te with $f_{\text{Te-132}} = 0.001$ acquired more negative than positive charges because more negative than positive ions were attached to their surface (the second vs third terms in equation 7.9) [Figure 7.5(a)]. The ^{132}Te particles accumulated positive charges by self-charging until establishing steady state. As $f_{\text{Te-132}}$ increased, many radioactive particles became positively charged due to the enhancement of self-charging at increased radioactivity levels. The dissimilar charge accumulation rates of the radioactive particles affected their size growth by aggregation [Figure 7.5(b).] Compared to the ammonium sulfate aerosols with Boltzmann charge distribution, the ^{132}Te particles with $f_{\text{Te-132}} = 0.001$ aggregated less frequently due to the electrostatic repulsive forces produced between the particles. In contrast, the radioactive particles under $f_{\text{Te-132}} = 0.5$ aggregated more quickly due to electrostatic attractive forces generated between the negatively and positively charged particles. After reaching certain size, however, the highly radioactive particles grew very slowly in their size via aggregation since the net charge of most particles was positive and thus, strong electrostatic repulsive forces were created between them. Also, the particle size distribution became narrow over time because small particles aggregated while large particles did not. The charge distribution of radioactive particles with $f_{\text{Te-132}} = 0.05$ was different from the Boltzmann charge distribution [Figure 7.5(a)]. However, the overall aggregation rates of the radioactive particles were similar to those of the reference simulation because the charging effects counterbalanced each other.

7.3.2.2. Effects of radioactive progeny

The influence of radioactive progeny, which refers to the decay products of parent radionuclides (e.g., ^{132}I produced by the decay of ^{132}Te shown in Figure 7.2), on particle

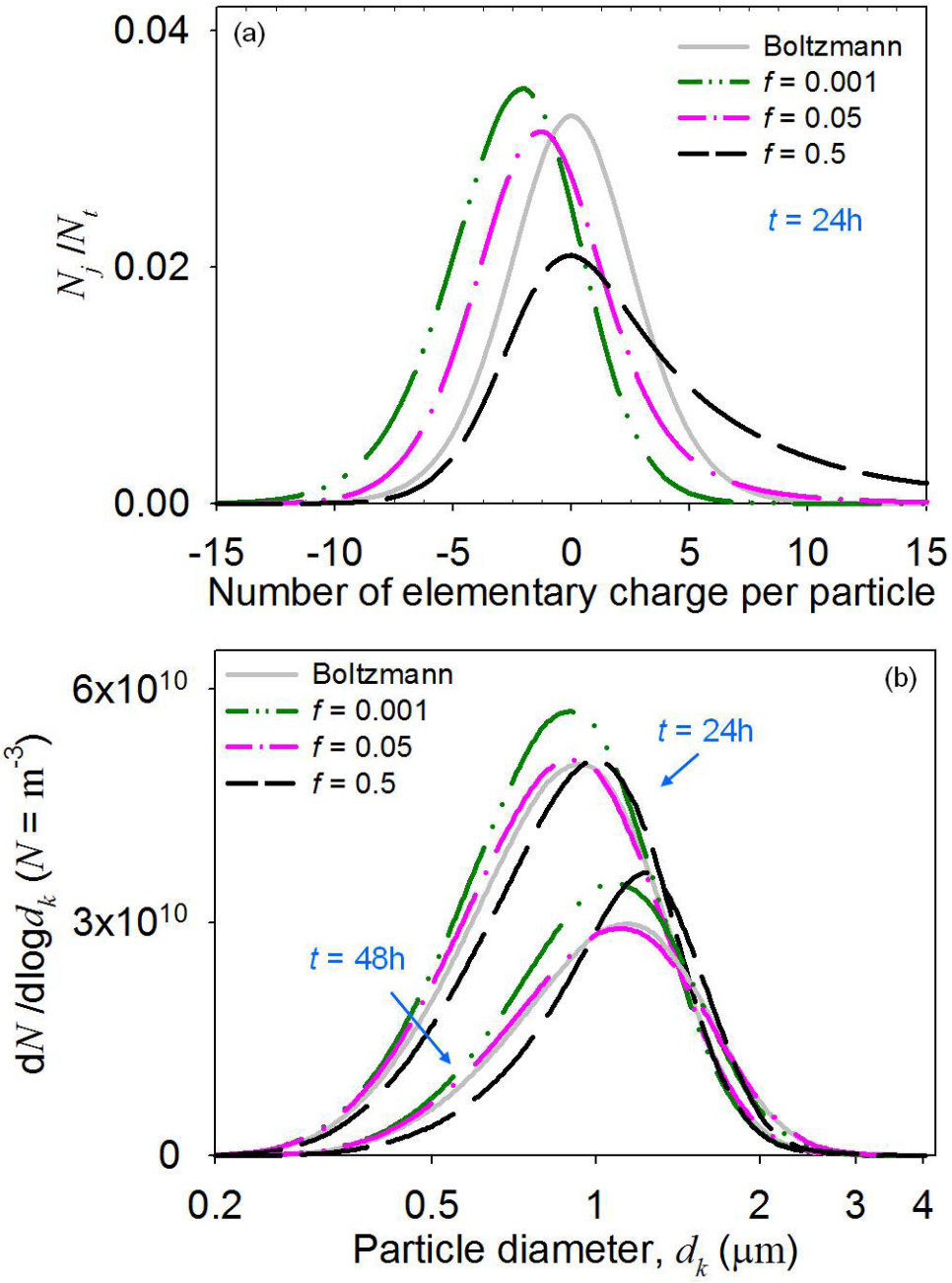

Figure 7.5. The charge (a) and size (b) distributions of particles carrying initially different amounts of ^{132}Te. d_g = 0.5 μm, σ_g = 1.5, and $N_t = 10^{11}$ m^{-3}.

charging and aggregation was investigated using particles containing ^{106}Ru and ^{132}Te, respectively. The initial activity distributions of ^{106}Ru and ^{132}Te were attained with f_i = 0.05. Simulation results obtained by neglecting the production of ^{106}Rh and ^{132}I were provided as reference.

Figure 7.6 shows the charge and size distributions of particles initially containing ^{106}Ru and ^{132}Te, respectively. Compared to the reference simulation, more ^{106}Ru-^{106}Rh particles were negatively charged because of the effects of the radioactive progeny [Figure 7.6(a)]. Due to the high decay constant of ^{106}Rh, the decay chain of ^{106}Ru rapidly reached secular equilibrium, which refers to an equilibrium type of serial decay chains (Martin, 2005), indicating that the radioactivity of the particles become twice more than those given solely by ^{106}Ru over time. Despite increase in the particle radioactivity by ^{106}Rh, more negative charges were accumulated on the radioactive particles because the ionization rate coefficient of ^{106}Rh is much greater than that of ^{106}Ru (Table 7.1), leading to higher diffusion charging than self-charging. Accumulation of more negative charge resulted in the suppression of the particle aggregation [Figure 7.6(b)]. ^{132}I affected the charging and aggregation rates of the ^{132}Te-^{132}I particles in a similar way. These effects became significant as f_i increased.

7.3.2.3. Effects of radioactive composition

The charging and aggregation of particles containing a mixture of ^{106}Ru, ^{131}I, ^{132}Te, and ^{137}Cs were simulated to investigate the influence of radioactive composition on the time-evolution of charge and size distributions. The charge and size distributions of particles solely containing ^{137}Cs and ^{132}Te were calculated as a reference. As shown in Figure 7.7, the charge and size evolution of particles containing the mixture was different from that of the ^{137}Cs and ^{132}Te particles, respectively. The different evolution patterns arose from the differences in the radiological characteristics of the radionuclides (Table 7.1). Because of the dissimilarities of the radiological properties of the radionuclides,

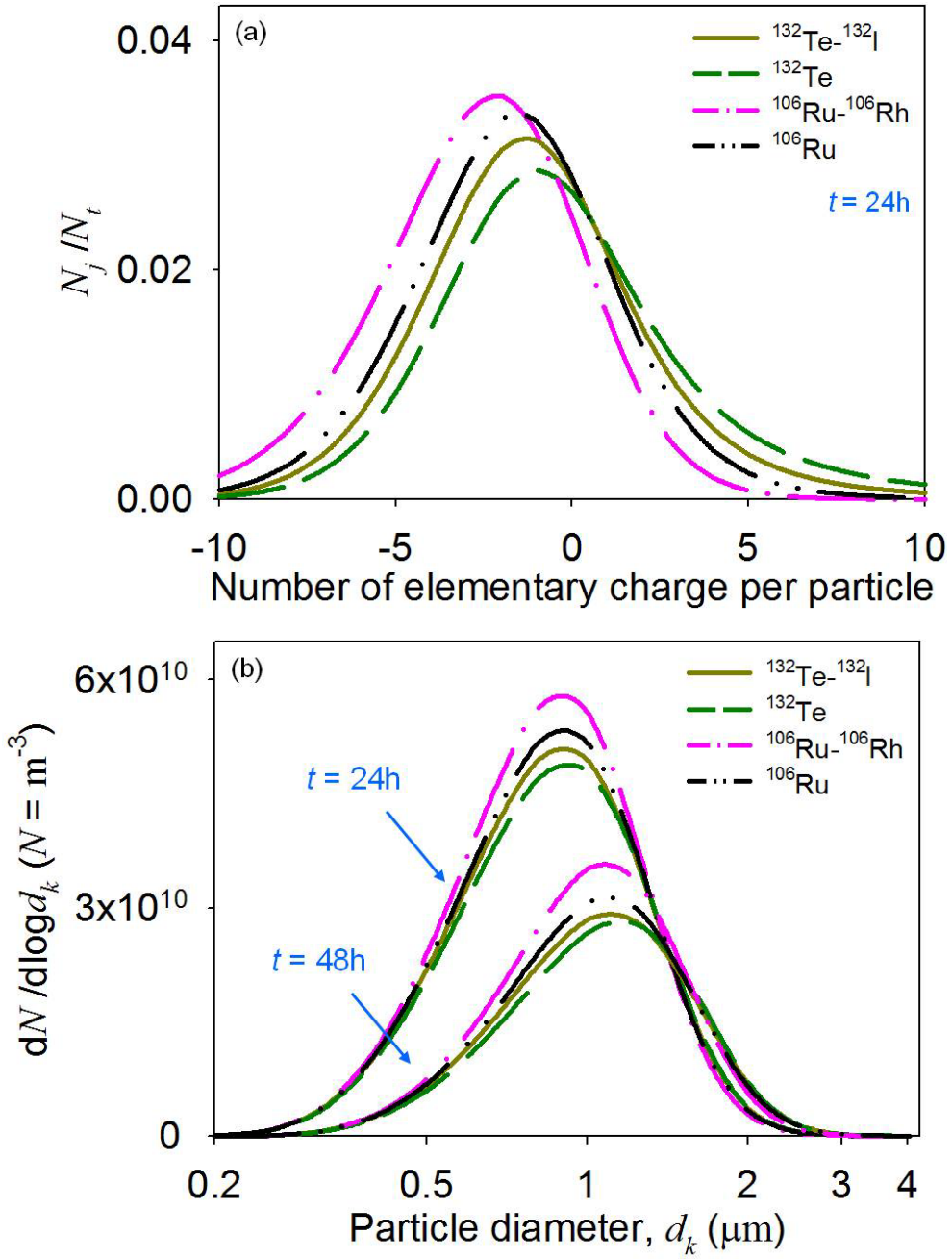

Figure 7.6. Time evolution of the charge (a) and size (b) distributions of particles initially containing ^{132}Te and ^{106}Ru. $f_{\text{Ru-106}} = f_{\text{Te-132}} = 0.05$, $d_g = 0.5$ μm, $\sigma_g = 1.5$, and $N_t = 10^{11}$ m^{-3}.

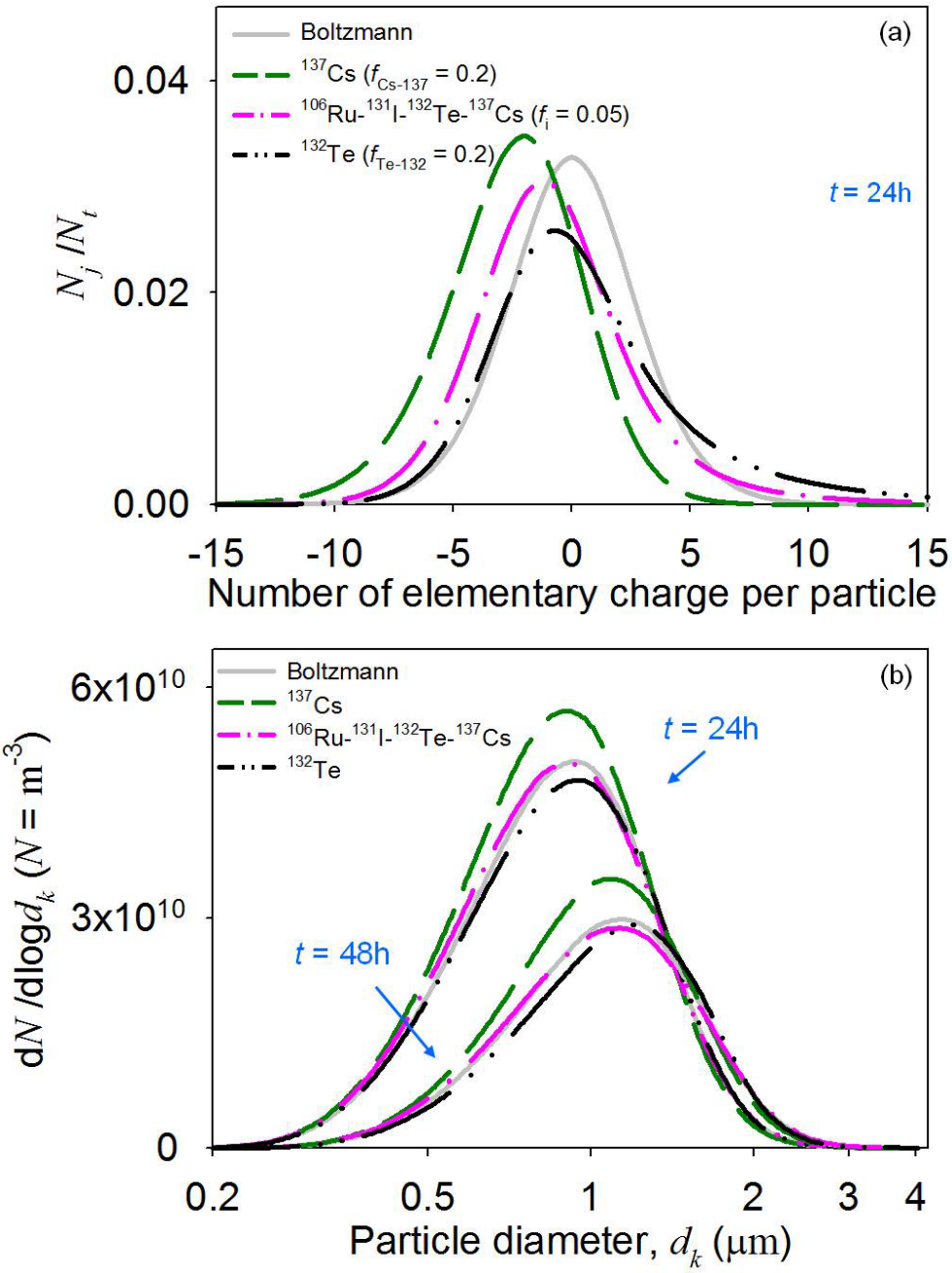

Figure 7.7. Time-dependent changes in the size (a) and charge (b) distributions of radioactive particles having different radioactive compositions.

as well as the radioactive progeny, the radioactive particles had different radioactive levels and were charged at different ion concentrations although the radioactive fraction of the particles was similar (i.e., $\Sigma_i f_i = 0.2$.) Thus, radioactive particles containing a mixture of radionuclides led to a different charge distribution, which affected the size growth of the radioactive particles by aggregation.

It has been shown that the composition of radioactive particles can be modified with time because of radioactive transformations. For particles containing radionuclides involved in serial decay chains, the radioactivity levels of radioactive particles can exceed their initial levels over a certain period of time (e.g., Figure 7.2.) Furthermore, homogeneous aggregation of multicomponent radioactive particles can be hindered/ facilitated as a function of the particle radioactivity levels, the progeny of radionuclides, and the radioactive composition. These results suggest that understanding the radiological characteristics of radionuclides carried by atmospheric particles is necessary to accurately forecast the microphysical processes of radioactive particles during atmospheric dispersion.

7.3.3. Particle Charging and Aggregation in Heterogeneous Radioactive Population

Aggregation rates of two heterogeneous radioactive populations were calculated using the coupled model involving the bivariate PBM. It was assumed that (i) radioactive particles in each population are monodispersed ($d_{k,1} = d_{k,2} = 0.5$ μm, $N_{t,1} = N_{t,2} = 5\times10^{10}$ m^{-3}) and (ii) the particles instantaneously obtain a steady-state charge. Thus, equation 7.12 was used to take into account the radioactivity effects. Time-evolution of the size and charge distributions of two homogeneous ^{137}Cs populations were predicted for comparison.

Figure 7.8 shows the time-evolution of the size/composition distributions of homogeneous and heterogeneous populations containing various radionuclides. Compared to the homogeneous radioactive population, the ^{137}Cs particles more

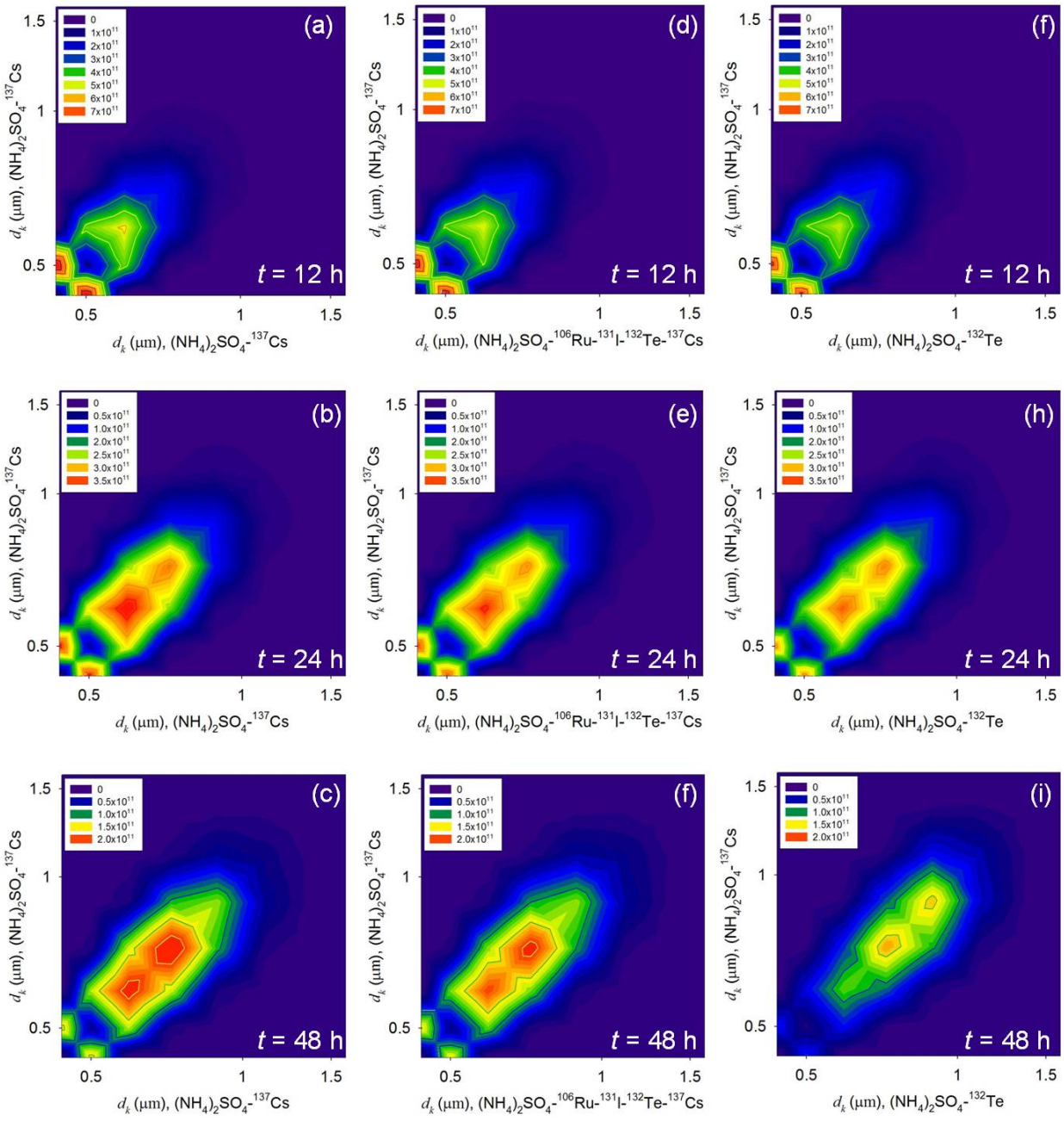

Figure 7.8. Time-evolution of the particle size distributions in two populations: ^{137}Cs vs ^{137}Cs with $f_{Cs\text{-}137} = 0.05$ (a-c), ^{137}Cs vs ^{106}Ru-^{131}I-^{132}Te-^{137}Cs with $f_i = 0.05$ (d-f), and ^{137}Cs vs ^{132}Te with $f_{Cs\text{-}137} = 0.05$ and $f_{Te\text{-}132} = 0.5$ (g-i). The simulation time was 48 h. We assumed initially monodisperse 0.5-μm particles. The initial concentration of each population was 5×10^{10} m^{-3}, respectively. The contour plots represent $dN/d\log_{10}d_k$ $d\log_{10}d_k$ ($N = \text{m}^{-3}$).

frequently aggregated with the particles containing the mixture of ^{106}Ru, ^{131}I, ^{132}Te, and ^{137}Cs (f_i = 0.05), and the aggregated particles were more widely distributed [Figures 7.8(a)-(c) vs (d)-(f)]. The aggregation rates of radioactive particles in the heterogeneous population containing a large amount of ^{132}Te ($f_{\text{Te-132}}$ = 0.5) were different from those of the heterogeneous population containing the radioactive mixture [Figures 7.8(d)-(f) vs (g)-(i)]. Similarly to Figure 7.6, the radioactive particles containing numerous ^{132}Te atoms rarely grew in size by aggregation, leading to the generation of distorted size/composition distributions [Figure 7.8(h) vs (i)]. The different aggregation behavior of radioactive particles in those populations was attributed to the dissimilar charge evolution patterns of the particles (Figure 7.9).

In the homogeneous population, most radioactive particles were negatively charged because of their low self-charging rates and the presence of numerous negative ions with high mobility. In contrast, the number of the positively charged particles increased in the heterogeneous populations because of the presence of highly radioactive particles that accumulated many positive charges via self-charging. Thus, the radioactive particles in the heterogeneous populations more frequently aggregated than those in the homogeneous population because strong electrostatic attractive forces were generated between positively and negatively charged particles. These results suggest that the aggregation rates of two particle populations having different levels of radioactivity can be significantly different from those of the homogeneous population because of strong electrostatic interactions created between charged particles.

7.4. Summary

Possible physical phenomena adding uncertainty to predictive transport modeling of radioactivity may involve charge accumulation of a mixture of radionuclides, which has not been considered yet. It has been shown in this work that short-lived radionuclides,

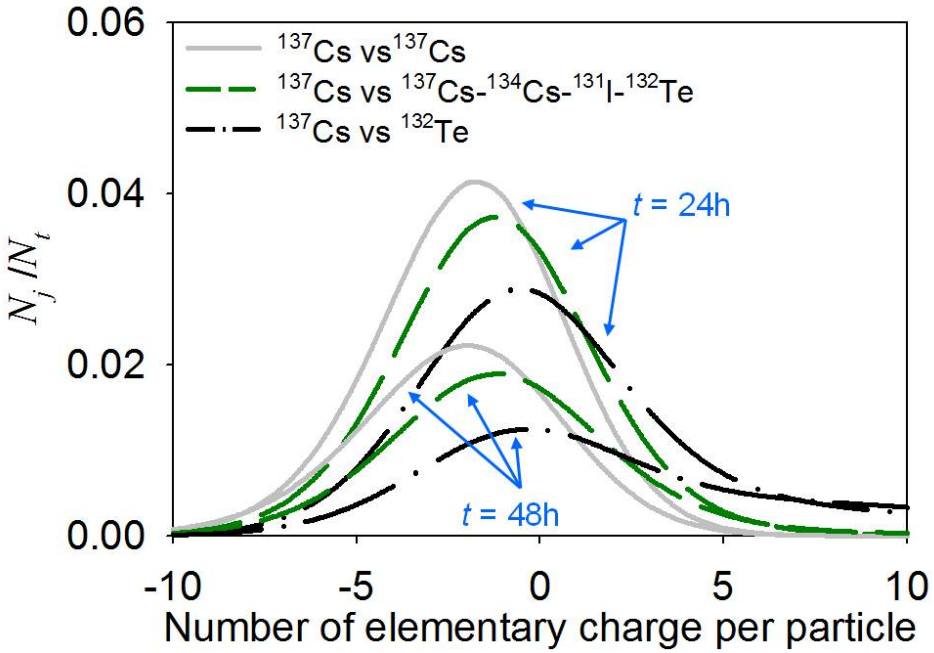

Figure 7.9. Time-evolution of particle charge distributions of two radioactive populations.

such as ^{132}Te, can highly influence the charge accumulation and aggregation kinetics of particles containing long-lived radionuclides (e.g., ^{137}Cs) by influencing their self-charging rates, as well as ionization rates of the air, indicating that it is necessary to consider the effects of major radionuclides in transport modeling of radioactivity. This study suggests a systematic approach to more accurately include the charging effects caused by each radionuclide to the radioactivity transformation, particle charging, and aggregation models, which can be combined with predictive atmospheric transport models.

CHAPTER 8

CONCLUSIONS AND RECOMMENDATIONS

In case of nuclear events such as a nuclear plant accident or a deliberate explosion of radiological devices, accurate prediction of atmospheric dispersion of radioactivity is essential for assessing human health and environmental risks caused by radiation. Neglecting effects of radioactive decay on various microphysical processes of atmospheric particles can significantly increase uncertainty in prediction results of dispersion of airborne radionuclides. Toward a better understanding of atmospheric dispersion of radionuclides, the main goal of this effort is to study the influence of radioactivity on particle-surface interactions and thereby to establish a theoretical framework that can couple knowledge of radiation physics and surface science with aerosol microphysics. For the accomplishment of the goal, theoretical and experimental investigations have been performed in this research. Findings of these investigations include:

- It has been typically assumed that electrostatic interactions of radioactive particles are negligible in the atmosphere because the particles can be easily discharged. It was shown in this study, however, that radioactive particles can be strongly charged with multiple elementary charges because of radioactivity-induced charging. Also, ionizing radiation caused by radioactivity may result in the charging of background aerosols, which can aggregate with radioactive particles. Thus, neglecting electrostatic interactions of radioactive particles can significantly increase uncertainty of predictive modeling studies of radioactivity transport.

- It was theoretically and experimentally shown that radioactivity-induced charge can be accumulated on surfaces of radioactive and nonradioactive materials. It was found that accumulated charges can be heterogeneously distributed because of the simultaneous occurrence of the two charging mechanisms: self-charging and diffusion charging. Radioactivity-induced charge can have effects on the interaction of various surfaces via generating electrostatic forces. For example, strong repulsive electrostatic forces can be generated between highly radioactive particles and, thus, aggregation rates of the radioactive particles are dissimilar to those of nonradioactive particles. These results reveal that radioactivity-induced charge can modify the electrostatic characteristics of radioactive surfaces and, thus, the behavior of radioactive particles may be largely different from that of nonradioactive particles.
- Three modeling approaches were developed to couple ionization of air and radioactivity-induced charging with particle aggregation, as well as taking into account mutual effects of particle charging and aggregation on the microphysical evolution of atmospheric particles. The developed three approaches had a wide range of complexity and can be easily incorporated into microphysical aerosol transport models of any scale. In addition, the three approaches can be applied to other investigations including particle measurement systems.
- The influence of radioactivity on charge/size distribution dynamics of radioactive particles was investigated using a comprehensive population balance model involving radioactivity-induced charging, aggregation, and electrostatic dispersion. It was found that the charge and size distributions of radioactive particles with initial charge can evolve dissimilarly over time because radioactivity-induced charging and electrostatic dispersion can

modify the charge distribution of particles, thereby affecting their size growth by aggregation.

- The charging and aggregation of multicomponent radioactive particles in homogeneous and heterogeneous populations were investigated using a coupled model of radioactive transformation, radioactivity-induced charging, and aggregation. It was found that the aggregation of multicomponent radioactive particles in homogeneous/heterogeneous populations can be hindered/facilitated because the particles can be strongly charged with multiple elementary charges and thus, strong electrostatic repulsive/attractive forces can be generated between the particles.

These findings suggest that the behavior of atmospheric particles containing radionuclides can be significantly different from that of typical atmospheric particles because radioactive decay of radionuclides can lead to the generation of strong electrostatic interactions of the particles. Hence, it can be concluded that to accurately predict atmospheric dispersion of radionuclides, the charging of radioactive particles should be taken into account in predictive models of radioactivity transport.

Based on the findings, the follow recommendations are given:

- Including radioactivity-induced charging, predictive studies of radioactivity transport are necessary to evaluate the charging effects on atmospheric dispersion of radionuclides and the corresponding impacts on health and environmental risks caused by radiation exposure. The systematic approaches presented in Chapter 5 can be readily incorporated into pre-existing aerosol circulation models involving aerosol microphysics such as the GISS-ModelE2-TOMAS. As an example study, the atmospheric dispersion of radionuclides released during the recent Fukushima

nuclear plant accident can be simulated because observations have been made at many places around the world since the nuclear event took place.

- Investigations into radioactivity-induced charging effects on other processes such as condensation and adsorption are essential. Condensation and adsorption, which are highly influenced by surface interactions, result in the acquisition of radioactivity by atmospheric particles. The influence of radioactivity charging on these processes, however, has rarely been examined. Such investigations can offer useful insight into the transformation of background aerosols into radioactive aerosols.
- Further investigations into self-charging of radioactive particles are highly recommended. The self-charging coefficient and radioactivity per particle are used to quantify the self-charging of radioactive particles. Most investigations, however, have been focused on the effects of radioactivity per particle on self-charging. Theoretical and experimental investigations into the self-charging coefficients of radioactive particles may be useful to better understand their dynamic and equilibrium charge. A possible investigation includes measurements of the self-charging coefficients of major radionuclides contained in typical atmospheric particles. A single particle levitation technique, which employs an electrodynamic balance to levitate individual particles, can be used for the measurements.
- Additional investigations into the charging effects on other collision mechanisms of radioactive particles are recommended, including fluid shear and differential sedimentation. The other collision mechanisms are important in investigating aggregation of large particles. The influence of radioactivity-induced charging on fluid shear and differential sedimentation can be assessed using trajectory analysis.
- Under humid conditions, uptake of water molecules by radioactive particles results in hygroscopic growth and deliquescence of the particles. Investigations

into the charging of radioactive particles in water are recommended. Measuring zeta potential of radioactive particles may be useful for such investigations.

- Investigations into ion nucleation in radiation fields are recommended. Ion-induced nucleation can lead to increase in the particle concentration, which can affect various microphysical processes of atmospheric particles. Because radioactive plumes spread out radioactivity in the atmosphere, numerous ion pairs can be created along the pathway of the plumes, but the effects have not been highlighted. Coupling the knowledge of radiation physics with thermodynamics of ion-induced nucleation may be helpful to the investigations.

APPENDIX A

SUPPORTING INFORMATION OF CHAPTER 4

Table A1. Cs-137 Uptake into Mounted AMP/ZrHP Microspheres at Steady State.

Coupon #	Averaged final count rate supernatant (cpm)	Difference in count rate (adsorbed ^{137}Cs activity)	% uptake	Contact Beta (mR/h)	Contact Gamma (mR/h)
1	Not measured	Not applicable	Not applicable	0	0
2	61786	4598	6.93	226	0.5
3	129659	9523	6.84	414	1
4	180590	16712	8.47	516	1
5	237549	22900	8.79	942	2
6	313565	19279	5.79	7563	1.7
7	10910	1184	9.79	3.8	<0.5

Table A2. Values of the parameters needed for the simulation.

Parameters	m_+ ($m^2/V/s$)	m_- ($m^2/V/s$)	α (m^3/s)	q ($\#/m^3$)	T (K)	A (J)
Values	1.14×10^{-4}	1.25×10^{-4}	1.6×10^{-12}	0	293	10^{-19}

Table A3. Ion-pairs produced per decay

Isotope	Decay type	E_{max} (MeV)	I	R_α (cm)
^{210}Po	Alpha	5.3	7.6×10^4	3.952
^{137}Cs	Beta	0.512	5.0×10^3	-
^{131}I	Beta	0.81	7.7×10^3	-

Table A4. Quantitative comparison of two solutions to experimental data

	Iterative solution (Clement and Harrison, 1992)	Approximate solution (Eq 4.2)
Root mean square error	0.0213	0.0195

$$V_A = -\frac{A}{6}\left[\frac{2r_i r_j}{s^2-(r_i+r_j)^2} + \frac{2r_i r_j}{r^2-(r_i-r_j)^2} + \ln\frac{s^2-(r_i+r_j)^2}{s^2-(r_i-r_j)^2}\right], \quad \text{(A1)}$$

$$V_R = \frac{z_i z_j e^2}{4\pi\varepsilon\varepsilon_0 s}, \quad \text{(A2)}$$

$$G^{-1} = 1 + \frac{2.6 r_i r_j}{(r_i+r_j)^2}\left(\frac{r_i r_j}{(r_i+r_j)(s-r_i-r_j)}\right)^{0.5} + \left(\frac{r_i r_j}{(r_i+r_j)(s-r_i-r_j)}\right), \quad \text{(A3)}$$

$$\frac{dC}{dt} = -KC, \quad \text{(A4)}$$

$$I_\alpha = \frac{E_0}{2Wi}, \quad \text{(A5)}$$

$$I_\beta = \frac{E_{\max}}{3Wi}, \quad \text{(A6)}$$

$$R_\alpha = (1.24E_0(MeV) - 2.62)\times 10^{-2}, \quad \text{(A7)}$$

$$\frac{N_j}{N_0} = \left(\frac{1}{\sqrt{2\pi}\sigma}\right)\exp\left(-\frac{(j-J)^2}{2\sigma^2}\right), \quad \text{(A8)}$$

$$\sigma = \left[\frac{1}{2\lambda(r)} + y(r)\right]^{0.5}, \quad \text{(A9)}$$

$$n_{k,t} = \frac{n_{k,0}(0.5t\beta n_{k,0})^{k-1}}{(1+0.5t\beta n_{k,0})^{k+1}}, \quad \text{(A10)}$$

In the equations above, μ is the fluid viscosity, s is the distance between the centers of the particles, A is the Hamaker constant, z is the number of electric charges of particles i and j, ε_0 is the permittivity of vacuum, ε is the dielectric constant of the medium, C is radioactivity, K is a first order constant, I is number of ion-pairs produced per decay of alpha- or beta-emission, E_0 is alpha particle energy, E_{max} is maximum beta particle energy, W_i mean energy required to form an ion pair (e.g. $W_{i,air}$ = 35 eV), R_α is the range of alpha particles, j is elementary charge, σ is standard deviation of charge distribution, t is the aggregation time, β is the collision frequency function, n_k is the number concentration of particles.

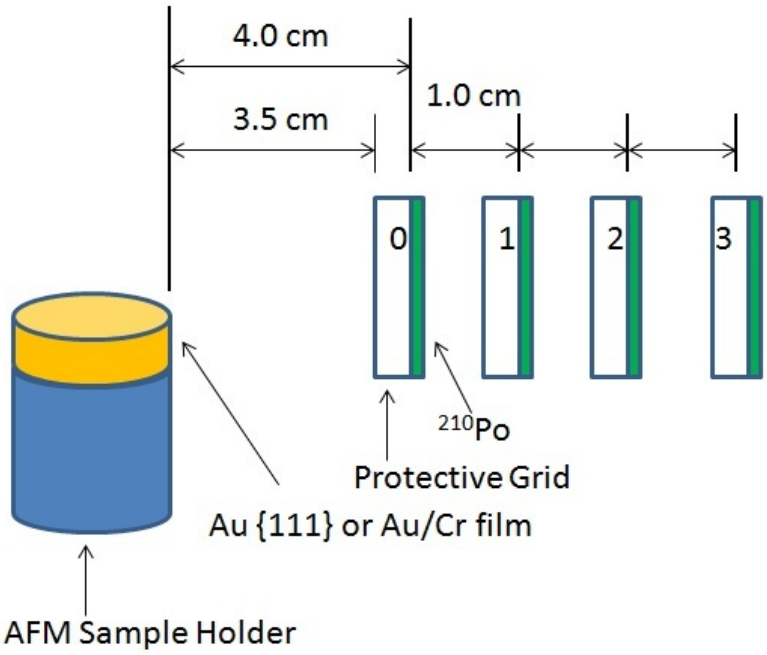

Figure A1. Experimental configuration showing the distance from the ^{210}Po radioactive source

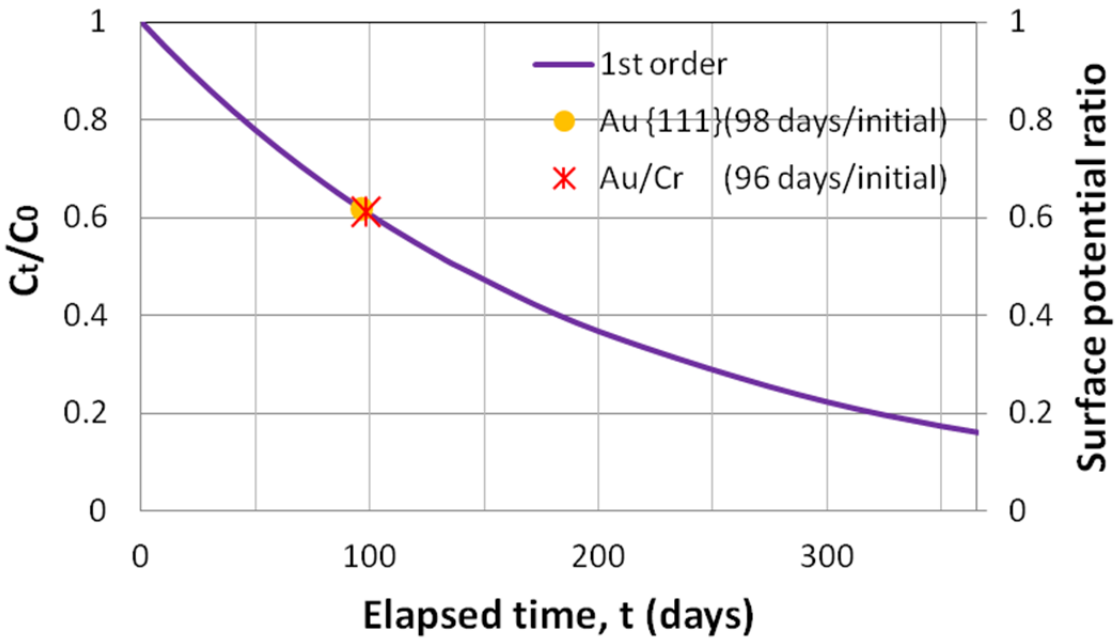

Figure A2. Surface potential of Au substrates and radioactivity of ^{210}Po.

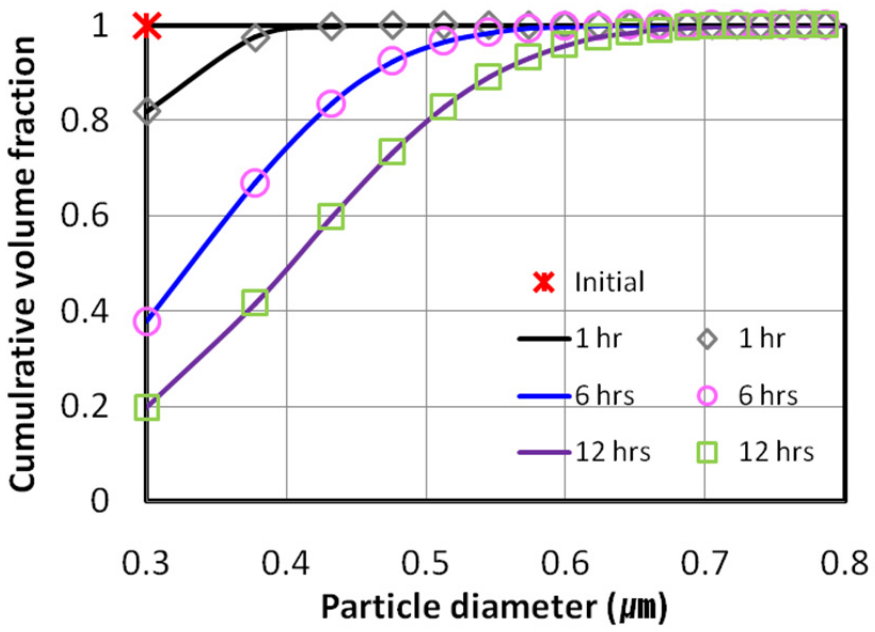

Figure A3. Comparisons of particle size distributions, plotted as cumulative volume fraction vs particle diameter, as obtained from the numerical solution (lines) of the population balance model and from the analytical solution (symbols) for initially monodisperse particle size distribution.

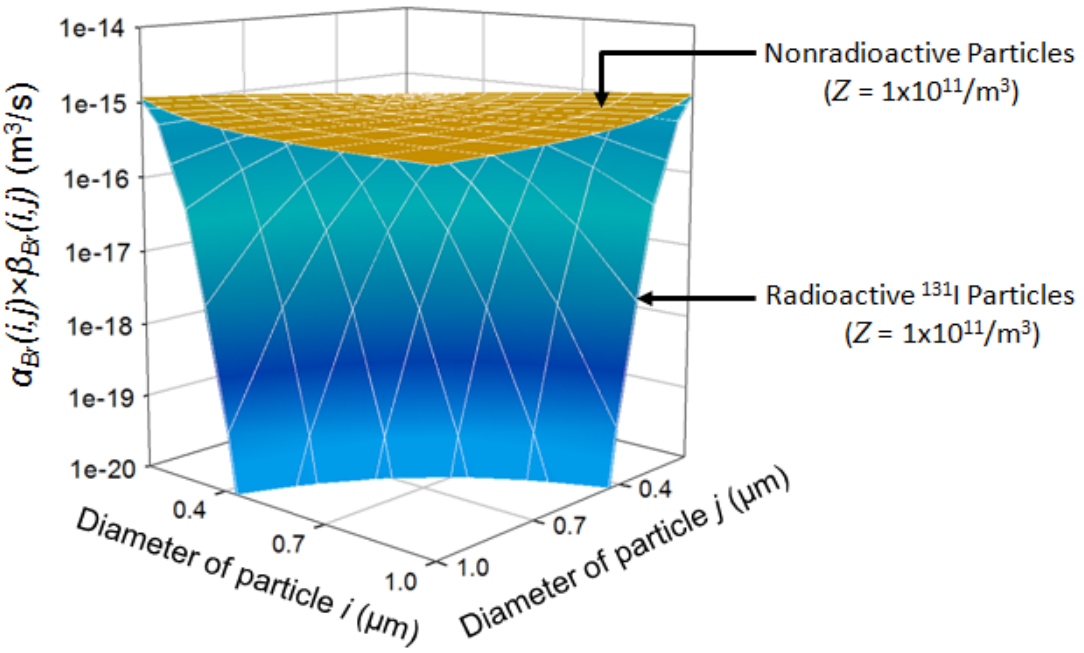

Figure A4. Aggregation frequency for (a) nonradioactive particles and (b) radioactive ^{131}I particles.

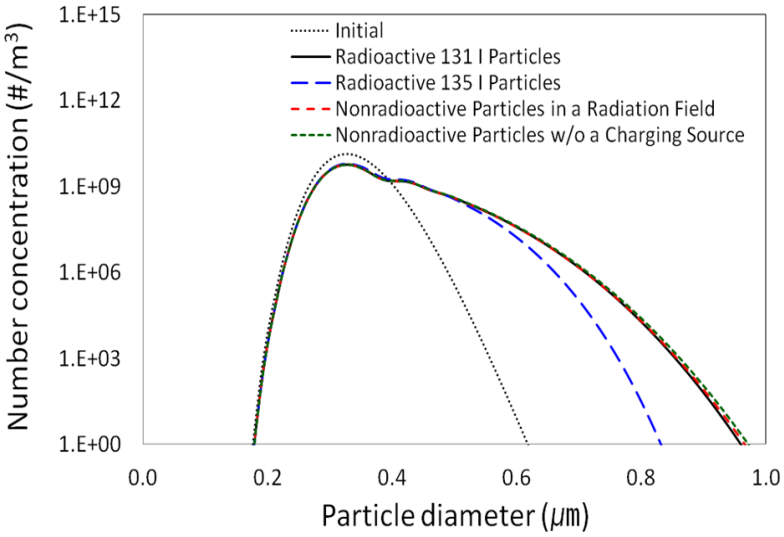

Figure A5. Aggregation of radioactive iodine particles, nonradioactive particles in a radiation field, and nonradioactive particles outside a radiation field for a log-normal initial distribution (t = 6 hrs; $N_t = 10^{11}\text{m}^{-3}$).

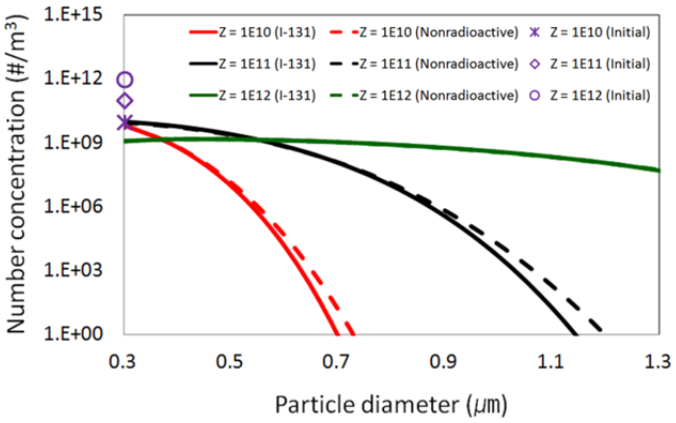

(a)

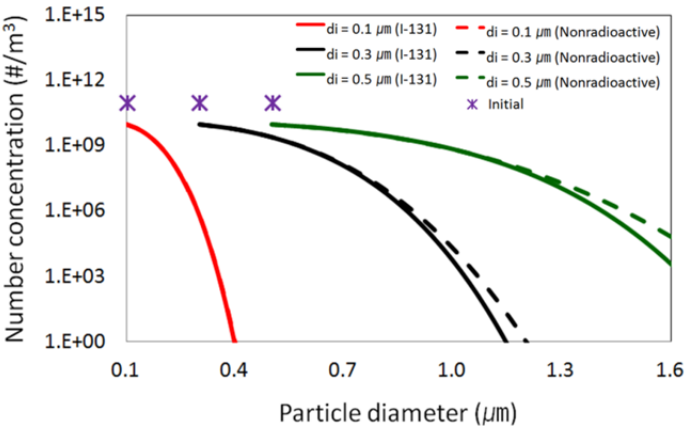

(b)

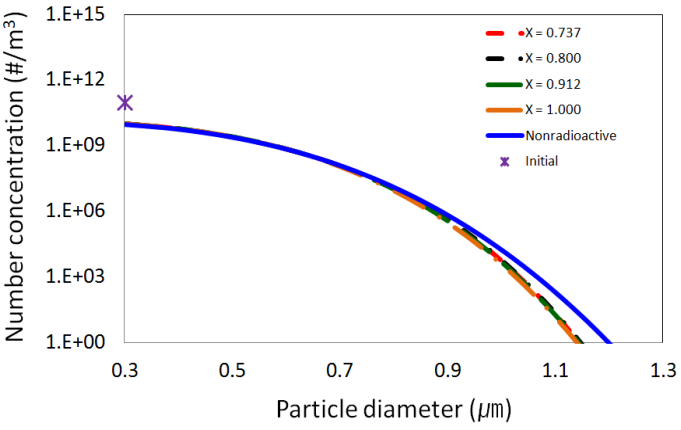

(c)

Figure A6. Effects of charging parameters on particle aggregation: (a) particle concentration (/m^3), (b) initial size, (c) ion asymmetric parameter. (t = 24 hrs; Monodispersed initial condition with standard values)

Text A1. Parameter selection for the sensitivity analysis

The initial particle size can influence λ and y through Eq 2. As a part of a reactor safety program, Mulpuru et al. (1992) investigated experimentally the characteristics of radioactive particles, which can be emitted during a postulated accident. The diameter of individual radioactive particles, generated from a hot nuclear fuel sample, was in a range of 0.1 to 0.3 μm and these particles were of spherical shape. Furthermore, monodispersed radioactive particles having a diameter of approximately 0.5 μm were used to investigate their potential inhalation hazard (Yeh et al., 1976). Thus, a sensitiviy analysis was carried out using particles having 0.1 to 0.5 μm diameter. The mean value of 0.3 μm was chosen as the standard.

The ion number concentration, which determines y, depends on the particle concentration Z. There have been several experimental studies to investigate the effects of radioactivity on the charging and aggregation of a particle population (Gensdarmes et al., 2001; Rosinski et al., 1962; Subramanian et al., 2012; Yeh et al., 1976). In these studies, a wider range of Z was used in the experiment (10^7 /m^3 to 2×10^7 /m^3 or 2×10^9 /m^3 to 10^{12} /m^3). Within a range of 10^{10} /m^3 to 10^{12} /m^3, Z can be similar to the background aerosol concentration. In the case of a nuclear event, background aerosols can easily interact with radionuclides or radioactive particles emitted from a radioactive source, and can also become radioactive. Thus, the values for Z used in this study were in the range of 10^{10} /m^3 to 10^{12} /m^3 and the mean value (10^{11} /m^3) was chosen as the standard.

The ion number concentration can also be influenced by the number of ion pairs produced per decay I. ^{131}I particles can emit beta particles having a high kinetic energy, which can dissociate the surrounding gas molecules along a linear path. The maximum kinetic energy of a single beta particle of ^{131}I is known to be 0.81 MeV, which corresponds to a maximum number of 7,700 ion pairs that can be produced per decay of ^{131}I (Table S4). However, the value for I can change as a function of the linear path

length of the single beta particle. The value of the parameter I of beta-emitting radioactive particles having 0.96 MeV was approximately 55 in a transport line (1.5 cm in diameter, 40 cm in length) (Yeh et al., 1976), while Eq (S11) gives a value of 9,100 for I. A value of 55 can be obtained by solving Eq (1) with the input data shown in (Reed et al., 1977; Yeh et al., 1976). The recent experiment of Gensdarmes et al. (2001) more clearly showed the effects of the linear path on I. In that experiment, the maximum value for I of the beta emitting particles having 0.51 MeV was 4,395 in a cylinder tank (40 cm in diameter, 30 cm in height), but it was reduced to 52 in tubes (0.6 cm in diameter, 80 cm in height). These experimental results suggest that ^{131}I particles can have various I values similar to or lower than 7,700. Thus, in this study, a sensitivity analysis was carried out with the maximum I value of ^{131}I and the values verified in the recent experiment (Gensdarmes et al., 2001) to analyze the effects of I on the radioactive particle aggregation.

The ion asymmetric parameter X can be defined as the ratio of positive and negative ion flux, but at steady state, it can be simplified to the ratio of the mobility of positive and negative ions (*4*). Under such condition, X can have the values: 0.737, 0.800, 0.912, and 1.000 (Adachi et al., 1985; Clement and Harrison, 1992; Clement et al., 1995; Gensdarmes et al., 2001; Reed et al., 1977; Subramanian et al., 2012; Yeh et al., 1976). A value of 0.912 provided by Clement et al. (1992) was chosen as the standard value.

All variables used for the sensitiviy analysis are now summarized in Table A5.

Table A5. Sensitivity analysis based on the major charging variables.

	$Z\ (m^{-3})$	I	$d_p\ (\mu m)$	X
Standard values	10^{11}	7,700	0.3	0.912
Ranges of variables	10^{10}/ 10^{11}/ 10^{12}	52/ 4,395/ 7,700	0.1/ 0.3/ 0.5	0.737/0.800/ 0.912/ 1.000

REFERENCES

Adachi, K., Kajino, M., Zaizen, Y., Igarashi, Y., 2013. Emission of spherical cesium-bearing particles from an early stage of the Fukushima nuclear accident. Sci. Rep. 3, 2554.

Adachi, M.; Kousaka, Y.; Okuyama, K. Unipolar and bipolar diffusion charging of ultrafine aerosol particles. J. Aerosol Sci. 1985, 16, 109-123.

Adachi, M., Okuyama, K., Kousaka, Y., 1981. Electrostatic coagulation of bipolarly charged aerosol particles. J. Chem. Eng. Jpn. 14, 467-473.

Alam, M.K., 1987. The Effect of van der Waals and Viscous Forces on Aerosol Coagulation. Aerosol Sci. Technol. 6, 41-52.

Alonso, M., Kousaka, Y., Nomura, T., Hashimoto, N., and Hashimoto, T., 1997. Bipolar charging and neutralization of nanometer-sized aerosol particles. J. Aerosol Sci. 28, 1479-1490.

Alonso, M., Hashimoto, T, Kousaka, Y., Higuchi, M., Nomura, T., 1998. Transient bipolar charging of a coagulating nanometer aerosol. J. Aerosol Sci., 29, 263-270.

Alonso, M., 1999. Simultaneous charging and Brownian coagulation of nanometre aerosol particles. J. Phys. A: Math. Gen., 32, 1313-1327.

ApSimon, H., Wilson, J. J. N., Simms, K. L., 1989. Analysis of the dispersal and deposition of radionuclides from Chernobly across Europe. Proc. R. Soc. A 425, 365-405.

Bragg, W. H., Kleeman, R., 1905. XXXIX. On the α particles of radium, and their loss of range in passing through various atoms and molecules. Philos. Mag. 10, 318-340.

Baltensperger, U., Gäggeler, H.W., Jost, D.T., Zinder, B., Haller, P., 1987. Chernobyl radioactivity in size-fractionated aerosol. J. Aerosol Sci. 18, 685-688

Barrett, J.C.; Clement, C.F.; Virdee, A.B.S., 2009. The removal of radioactive aerosols by electric fields. J. Aerosol Sci. 40, 185-192.

Burd, A. B., Moran, S.B., Jackson, G.A. 2000. A coupled adsorption–aggregation model of the POC/234Th ratio of marine particles. Deep-Sea Res. PT. I 47, 103-120.

Chesser, R.K., Bondarkov, M., Baker, R.J., Wickliffe, J.K., Rodgers, B.E., 2004. Reconstruction of radioactive plume characteristics along Chernobyl's Western trace. J. Environ. Radioactivity 71, 147-157.

Chin, C., Yiacoumi, S., Tsouris, C., 1998. Shear-induced flocculation of colloidal particles in stirred tanks. J. Colloid Interface Sci. 206, 532-545.

Clement, C.F., Clement, R.A., Harrison, R.G., 1995. Charge distributions and coagulation of radioactive aerosols. J. Aerosol Sci. 26, 1207-1225.

Clement, C.F., Harrison, R.G., 1992. The charging of radioactive aerosols. J. Aerosol Sci. 23, 481-504.

Cohen, B.S., Xiong, J.Q., Fang, C.-P., Li, W., 1998. Deposition of charged particles on lung airways. Health Phys. 74, 554-560.

Cooper, D.W., Reist, P.C., 1973. Neutralizing charged aerosols with radioactive sources. J. Colloid Interface Sci. 45, 17-26.

Cuddihy, R. G., Finch, G. L., Newton, G. J., Hahn, F. F., Mewhinney, J. A., Rothenberg, S. J., Powers, D. A., 1989. Characteristics of radioactive particles released from the Chernobyl nuclear reactor. Environ. Sci. Technol. 23, 89-95.

Devell, L., Tovedal, H., Bergström, U., Appelgren, A. l., Chyssler, J., Andersson, L., 1986. Initial observations of fallout from the reactor accident at Chernobyl. Nature 321, 192-193.

Fuchs, N.A.: The Mechanics of Aerosols; Dover Publications, 1989.

Fuchs, N. A., 1963. On the stationary charge distribution on aerosol particles in a bipolar ionic atmosphere. Geofis. Pura. Appl. 56, 185–193

Fortov, V. E., Nefedov, A. P., Vladimirov, V. I., Deputatova, L.V., Budnik, A.P., Khudyakov, A.V., Rykov, V. A., 2001. Dust grain charging in the nuclear-induced plasma. Phys. Lett. 284, 118-123.

Gauer, C., Jia, Z., Wu, H., Morbidelli, M., 2009. Aggregation Kinetics of Coalescing Polymer Colloids. Langmuir 25, 9703-9713

Gensdarmes, F., Boulaud, D., Renoux, A., 1998. Aerosol charging under gamma irradiation. J. Aerosol Sci. 29, S851-S852.

Gensdarmes, F., Boulaud, D., Renoux, A., 2001. Electrical charging of radioactive aerosols—Comparison of the Clement–Harrison models with new experiments. J. Aerosol Sci. 32, 1437-1458.

Greenfield, S. M., 1956. Ionization of radioactive particles in the free air. J. Geophys. Res. 61, 27-33.

Greenfield, S. M., 1957. Rain scavenging of radioactive particulate matter from the atmosphere. J. Atmos. Sci. 14, 115-125.

Gunn, R., 1954. Diffusion charging of atmospheric droplets by ions, and the resulting combination coefficients, J. Meteor., 11, 339-347.

Harris, D. L., 1955. Effects of radioactive debris from nuclear explosions on the electrical conductivity of the lower atmosphere. J. Geophys. Res. 60, 45-52.

Harrison, R. G., Carslaw, K. S., 2003. Ion-aerosol-cloud processes in the lower atmosphere. Rev. Geophys. 41, 1012.

Hiemenz, P. C., Rajagopalan, R.: Principles of Colloid and Surface Chemistry, revised and expanded; CRC Press, 1997.

Hoppel, W. A., Frick, G. M., 1986. Ion-aerosol attachment coefficients and the steady-state charge distribution on aerosols in a bipolar ion environment. Aerosol Sci. Technol. 5, 1-21.

Hoppel, W. A., 1985. Ion-aerosol attachment coefficients, ion depletion, and the charge distribution on aerosols, J. Geophys. Res., 90, 5917-5923.

Hu, X., Li, D., Huang, H., Shen, S., Bou-Zeid, E., 2014. Modeling and sensitivity analysis of transport and deposition of radionuclides from the Fukushima Daiichi accident. Atmos. Chem. Phys. 14, 11065-11092.

Huh, C.-A., Hsu, S.-C., Lin, C.-Y., 2012. Fukushima-derived fission nuclides monitored around Taiwan: Free tropospheric versus boundary layer transport, Earth Planet. Sci. Lett. 319–320, 9-14.

Huh, C.-A., Lin, C.-Y., Hsu, S.-C., 2013. Regional dispersal of Fukushima-derived fission nuclides by East-Asian monsoon: a synthesis and review, Aerosol Air Qual. Res. 13, 537–544.

Huizenga, H., Storchi, P. R. M., 1989. Numerical calculation of energy deposition by broad high-energy electron beams. Phys. Med. Biol. 34, 1371-1396.

International Commission on Radiation Units and Measurements (ICRU), 1984. Stopping powers for electrons and positrons, ICRU Report 37, ICRU, Bethesda, M. D.

Israelsson, S., Knudsen, E., 1986. Effects of radioactive fallout from a nuclear power plant accident on electrical parameters. J. Geophys. Res. 91, 11909-11910.

Israelsson, S., Schütte, T., Pisler, E., Lundquist, S., 1987. Increased occurrence of lightning flashes in Sweden during 1986. J. Geophys. Res. 92, 10996-10998.

Jacobson, M. Z., Turco, R. P., Jensen, E. J., Toon, O. B. 1994. Modeling coagulation among particles of different composition and size. Atmos. Environ. 28, 1327-1338.

Joffre, H., 1963. Les Problèmes physiques de la radioprotection; Institut national des sciences et techniques nucléaires, Paris, France.

Kaneyasu, N., Ohashi, H., Suzuki, F., Okuda, T., Ikemori, F., 2012. Sulfate aerosol as a potential transport medium of radiocesium from the Fukushima nuclear accident. Environ. Sci. Technol. 46, 5720-5726.

Kasper, G., 1981. Electrostatic dispersion of homopolar charged aerosols. J. Colloid Interface Sci. 81, 32-40.

Katata, G., Ota, M., Terada, H., Chino, M., Nagai, H., 2012. Atmospheric discharge and dispersion of radionuclides during the Fukushima Dai-ichi Nuclear Power Plant accident. Part I: Source term estimation and local-scale atmospheric dispersion in early phase of the accident. J. Environ. Radioactivity 109, 103-113.

Katz, L, Penfold, A. S., 1952. Range-energy relations for electrons and the determination of beta-ray end-point energies by absorption. Rev. Mod. Phys. 24, 28-44.

Kauppinen, E. I., Hillamo, R. E., Aaltonen, S. H., Sinkko, K. T. S., 1986. Radioactivity size distributions of ambient aerosols in Helsinki, Finland, during May 1986 after the Chernobyl accident: preliminary report. Environ. Sci. Technol. 20, 1257-1259.

Kim, Y.-H., Yiacoumi, S., Lee, I., McFarlane, J., Tsouris, C., 2014. Influence of radioactivity on surface charging and aggregation kinetics of particles in the atmosphere, Environ. Sci. Technol. 48, 182-189.

Kim, Y.-H., Yiacoumi, S., Tsouris, C., 2015a. Surface charge accumulation of particles containing radionuclides in open air, J. Environ. Radioactivity 143, 91-99.

Kim, Y.-H., Yiacoumi, S., Nenes, A., Tsouris, C., 2015b. Charging and coagulation of radioactive and nonradioactive particles in the atmosphere. Atmos. Chem. Phys. Disc. 15, 23795-23840.

Kristiansen, N. I., Stohl, A., Olivié, D. J. L., Croft, B., Søvde, O. A., Klein, H., Christoudias, T., Kunkel, D., Leadbetter, S. J., Lee, Y. H., Zhang, K., Tsigaridis, K., Bergman, T., Evangeliou, N., Wang, H., Ma, P.-L., Easter, R. C., Rasch, P. J., Liu, X., Pitari, G., Di Genova, G., Zhao, S. Y., Balkanski, Y., Bauer, S. E., Faluvegi, G. S., Kokkola, H., Martin, R. V., Pierce, J. R., Schulz, M., Shindell, D., Tost, H., Zhang, H., 2015. Evaluation of observed and modelled aerosol lifetimes using radioactive tracers of opportunity and an ensemble of 19 global models, Atmos. Chem. Phys. Discuss. 15, 24513-24585.

Kumar, S., Ramkrishna, D., 1996. On the solution of population balance equations by discretization—I. A fixed pivot technique, Chem. Eng. Sci. 51, 1311-1332.

Kweon, H., Yiacoumi, S., Lee, I., McFarlane, J., Tsouris, C., 2013. Influence of Surface Potential on the Adhesive Force of Radioactive Gold Surfaces. Langmuir 29, 11876-11883.

Kweon, H., Yiacoumi, S., Tsouris, C., 2015. The role of electrostatic charge in the adhesion of spherical particles onto planar surfaces in atmospheric systems. Colloid Surface A 481, 583-590.

Laakso, L, Mäkelä, J. M., Pirjola, L., Kulmala, M., 2002. Model studies on ion-induced nucleation in the atmosphere. J. Geophys. Res. 107, 4427.

Lujanienė, G., Aninkevičius, V., Lujanas, V., 2009. Artificial radionuclides in the atmosphere over Lithuania. J. Environ. Radioactiv. 100, 108-119.

Lee, H., Feichter, J., 1995. An intercomparison of wet precipitation scavenging schemes and the emission rates of 222Rn for the simulation of global transport and deposition of 210Pb. J. Geophys. Res.-Atmos. 100, 23253-23270.

Liu, B. Y., Pui, D. Y., 1974. Equilibrium bipolar charge distribution of aerosols. J. Colloid Interface Sci. 49, 305-312.

Mantel, J., 1972. The beta ray spectrum and the average beta energy of several isotopes of interest in medicine and biology. Int. J. Appl. Radiat. Is. 23, 407-413.

Marmier, P., Sheldon, E., 1969. Physics of Nuclei and Particles (Volume I), Academic Press, New York.

Martin, J. E., 2000. Physics for Radiation Protection, John Wiley & Sons, New York.

Matsoukas, T., 1997. The coagulation rate of charged aerosols in ionized gases. J. Colloid Interface Sci. 187, 474-483.

Mulpuru, S.R., Pellow, M.D., Cox, D.S., Hunt, C.E.L., Barrand, R.D., 1992. Characteristics of radioactive aerosols generated from a hot nuclear fuel sample. J. Aerosol Sci. 23, S827-S830.

Moral, L., Pacheco, A., 2003. Algebraic approach to the radioactive decay equations. Am. J. Phys. 71, 684-686.

Nikolopoulos, D., Vogiannis, E., 2007. Modelling radon progeny concentration variations in thermal spas. Sci. Total Environ. 373, 82-93.

Ooe, H., Seki, R., Ikeda, N., 1988. Particle-size distribution of fission products in airborne dust collected at Tsukuba from April to June 1986. J. Environ. Radioactivity 6, 219-223.

Oron, A., Seinfeld, J. H., 1989a. The dynamic behavior of charged aerosols: II. Numerical solution by the sectional method. J. Colloid Interface Sci. 133, 66-79.

Oron, A., Seinfeld, J. H., 1989b. The dynamic behavior of charged aerosols: III. Simultaneous charging and coagulation. J. Colloid Interface Sci. 133, 80-90.

Parache, V., Pourcelot, L., Roussel-Debet, S., Orjollet, D., Leblanc, F., Soria, C., Gurriaran, R., Renaud, P., Masson, O., 2011. Transfer of ^{131}I from Fukushima to the vegetation and milk in France. Environ. Sci. Technol. 45, 9998-10003.

Pöllänen, R., Valkama, I., Toivonen, H., 1997. Transport of radioactive particles from the Chernobyl accident. Atmos. Environ. 31, 3575-3590.

Pruppacher, H. R., Klett, J. D., Microphysics of Clouds and Precipitation, Kluwer Acad.: Norwell, Mass., 1997.

Reed, L.D., Jordan, H., Gieseke, J.A., 1997 Charging of radioactive aerosols. J. Aerosol Sci. 1977, 8, 457-463.

Rehfeld, S., Heimann, M., 1995. Three dimensional atmospheric transport simulation of the radioactive tracers 210Pb, 7Be, 10Be, and 90Sr. J. Geophys. Res.-Atmos. 100, 26141-26161.

Renard, J. B., Tripathi, S. N., Michael, M., Rawal, A., Berthet, G., Fullekrug, M., Harrison, R. G., Robert, C., Tagger, M., Gaubicher, B., 2013. In situ detection of electrified aerosols in the upper troposphere and in the stratosphere. Atmos. Chem. Phys. 13, 11187–11194.

Retalis, D., Pitta, A., 1989. Effects on electrical parameters at Athens, Greece by radioactive fallout from a nuclear power plant accident. J. Geophys. Res. 94, 13093-13097.

Rosinski, J., Werle, D.N., Agamoto, C.T., 1962. Coagulation and scavenging of radioactive aerosols. J. Colloid Sci. 17, 703-716.

Sawyer, C. N., McCarty, P. L., Parkin, G. F., Chemistry for environmental engineering, McGraw-Hill: New York, 1994.

Seinfeld, J.H., Pandis, S.N. Atmospheric Chemistry and Physics: From Air Pollution to Climate Change, John Wiley and Sons: New York, 1998.

Seltzer, S. M., Berger, M. J., 1982. Evaluation of the collision stopping power of elements and compounds for electrons and positrons. Int. J. Appl. Radiat. Is. 31, 1189-1218.

Sharma, K., Kim, Y.-H., Gabitto, J., Mayes, R., Yiacoumi, S., Bilheux, H., Walker, L., Dai, S., Tsouris, C., 2015, Transport of ions in mesoporous carbon electrodes during capacitive deionization of high-salinity solutions. Langmuir 31, 1038-1047.

Shaw, G. E., 1986. Size distribution of atmospheric aerosols at Ross Island. Antarct. J. U.S. 21, 241-242.

Spielman, L.A., 1970. Viscous interactions in Brownian coagulation. J. Colloid Interface Sci. 33, 562-571.

Subramanian, V., Kumar, A., Baskaran, R., Misra, J., Venkatraman, B., 2012. An experimental study on the charging of non-radioactive aerosols with and without the presence of gamma radiation, J. Aerosol Sci. 52, 98-108.

Taboada-Serrano, P., Chin, C., Yiacoumi, S., Tsouris, C., 2005. Modeling aggregation of colloidal particles. Curr. Opin. Colloid Interface Sci. 10, 123-132.

Tabata, T., Ito, R., Okabe, S., 1972. Generalized semiempirical equations for the extrapolated range of electrons. Nucl. Instrum. Methods 103, 85-91.

Takeda, M., Yamauchi, M., Makino, M., Owada, T., 2011. Initial effect of the Fukushima accident on atmospheric electricity. Geophys. Res. Lett. 38, L15811.

Tomé, W. A., Palta, J. R., 1998. On the calculation of mean restricted collision stopping powers. Med. Phys. 25, 758-772.

Trier, A., 1997. Submicron particles in an urban atmosphere: a study of optical size distributions—I. Atmos. Environ. 31, 909-914.

Tripathi, S., Harrison R. G., 2001. Scavenging of electrified radioactive aerosol. Atmos. Environ. 35, 5817-5821.

Tuomi, T. J. 1989. Ten year summary 1977–1986 of atmospheric electricity measured at Helsinki-Vantaa airport, Finland. Geophysica 25, 1-20.

Tsouris, C., Yiacoumi, S., Scott, T.C., 1995. Kinetics of heterogeneous magnetic flocculation using a bivariate population-balance equation. Chem. Eng. Commun. 137, 147-159.

Vale, H.M., McKenna, T.F. Solution of the population balance equation for two-component aggregation by an extended fixed pivot technique. Ind. Eng. Chem. Res. 2005, 44, 7885-7891.

Vanni, M., 2000. Approximate population balance equations for aggregation–breakage processes. J. Colloid Interface Sci., 221, 143-160.

Vemury, S., Janzen, C., Pratsinis, S.E., 1997. Coagulation of symmetric and asymmetric bipolar aerosols. J. Aerosol Sci. 28, 599-611.

Walker, M.E., McFarlane, J., Glasgow, D.C., Chung, E., Taboada-Serrano, P., Yiacoumi, S., Tsouris, C., 2010. Influence of radioactivity on surface interaction forces. J. Colloid Interface Sci. 350, 595-598.

Whitby, K. T., Liu, B.Y.H., Peterson, C.M., 1965. Charging and decay of monodispersed aerosols in the presence of unipolar ion sources. J. Colloid Interface Sci. 20, 585-601.

Whyte, G., 1963. Energy per ion pair for charged particles in gases. Radiat. Res., 18, 265-271.

Wiedensohler, A., Fissan, H.J., 1991. Bipolar charge distributions of aerosol particles in high-purity argon and nitrogen. Aerosol Sci. Technol. 14, 358-364.

Yair, Y., Levin, Z., 1995. Charging of polydispersed aerosol particles by attachment of atmospheric ions. J. Geophys. Res.-Atmos. 94, 13085-13091.

Yamauchi, M., Takeda, M., Makino, M., Owada, T., Miyagi, I., 2012. Settlement process of radioactive dust to the ground inferred from the atmospheric electric field measurement. Ann. Geophys. 30, 49–56.

Yeh, H. C., Newton, G. J., Raabe, O. G., Boor, D. R., 1976. Self-charging of ^{198}Au-labeled monodisperse gold aerosols studied with a miniature electrical mobility spectrometer. J. Aerosol Sci. 7, 245-253.

Yeh, H.C., Newton, G.J., Teague, S.V., 1978. Charge distribution on plutonium-containing aerosols produced in mixed-oxide reactor fuel fabrication and the laboratory. Health Phys. 35, 500-503.

Yiacoumi, S., Rountree, D.A., Tsouris, C., 1996. Mechanism of particle flocculation by magnetic seeding. J. Colloid Interface Sci. 184, 477-488.

Yoshenko, V.I., Kashparov, V.A., Protsak, V.P., Lundin, S.M., Levchuk, S.E., Kadygrib, A.M., Zvarich, S.I., Khomutinin, X.V., Maloshtan, I.M., Lanshin, V.P., Kovtun, M.V., Tschiervsch, J., 2006a. Resuspension and redistribution of radionucleotides during grassland and forest fires in the Chernobyl exclusion zone. Part I: fire experiments. J. Environ. Radioactivity 86, 143-163.

Yoshenko, V.I., Kashparov, V.A., Levchuk, S.E., Glukhovskiy, A.S., Khomutni, Y.V., Protsak, V.P., Lundin, S.M., Tschiersch, J., 2006b. Resuspension and redistribution of radionucleotides during grassland and forest fires in the Chernobyl exclusion zone. Part II: modeling the transport process. J. Environ. Radioactivity 87, 260-278.

Zebel, G., 1958. Zur theorie des verhaltens elektrisch geladener aerosole, Colloid Polym. Sci., 157, 37-50.

VITA

YONG-HA KIM

Yong-ha Kim was born in Jeju, Republic of Korea. He completed his mandatory military service at the Republic of Korea Army, Korea in 2003. He received a Bachelor of Science in Civil and Environmental Engineering from Jeju National University, Jeju, Korea in 2007, and a Master of Science in Civil and Environmental Engineering from Seoul National University, Seoul, Korea in 2009. He completed his Ph.D. courses in Civil and Environmental Engineering from Seoul National University, Seoul, Korea in 2011, before coming to Georgia Tech to pursue a doctorate in Environmental Engineering. In spring 2012, he joined the colloids and interfacial science group of Dr. Yiacoumi and defended his Ph.D. thesis on December 4, 2015.